1991

Potential energy surfaces governing chemical reactions involving carbon, oxygen and hydrogen

Sotiris S. Xantheas
Iowa State University

Recommended Citation

Xantheas, Sotiris S., "Potential energy surfaces governing chemical reactions involving carbon, oxygen and hydrogen " (1991). *Retrospective Theses and Dissertations*. 9602.
https://lib.dr.iastate.edu/rtd/9602

INFORMATION TO USERS

This manuscript has been reproduced from the microfilm master. UMI films the text directly from the original or copy submitted. Thus, some thesis and dissertation copies are in typewriter face, while others may be from any type of computer printer.

The quality of this reproduction is dependent upon the quality of the copy submitted. Broken or indistinct print, colored or poor quality illustrations and photographs, print bleedthrough, substandard margins, and improper alignment can adversely affect reproduction.

In the unlikely event that the author did not send UMI a complete manuscript and there are missing pages, these will be noted. Also, if unauthorized copyright material had to be removed, a note will indicate the deletion.

Oversize materials (e.g., maps, drawings, charts) are reproduced by sectioning the original, beginning at the upper left-hand corner and continuing from left to right in equal sections with small overlaps. Each original is also photographed in one exposure and is included in reduced form at the back of the book.

Photographs included in the original manuscript have been reproduced xerographically in this copy. Higher quality 6" x 9" black and white photographic prints are available for any photographs or illustrations appearing in this copy for an additional charge. Contact UMI directly to order.

UMI

University Microfilms International
A Bell & Howell Information Company
300 North Zeeb Road, Ann Arbor, MI 48106-1346 USA
313/761-4700 800/521-0600

Order Number 9126270

Potential energy surfaces governing chemical reactions involving carbon, oxygen and hydrogen

Xantheas, Sotiris S., Ph.D.

Iowa State University, 1991

U·M·I
300 N. Zeeb Rd.
Ann Arbor, MI 48106

Potential Energy Surfaces Governing Chemical Reactions Involving Carbon, Oxygen and Hydrogen

by

Sotiris S. Xantheas

A Dissertation Submitted to the
Graduate Faculty in Partial Fulfillment of the
Requirements for the Degree of
DOCTOR OF PHILOSOPHY
Department: Chemistry
Major: Physical Chemistry

Approved:

Signature was redacted for privacy.

In Charge of Major Work

Signature was redacted for privacy.

For the Major Department

Signature was redacted for privacy.

For the Graduate College

Iowa State University
Ames, Iowa
1991

TABLE OF CONTENTS

Page

I. INTRODUCTION 1

II. POTENTIAL ENERGY SURFACE OF THE GROUND STATE OF O_3 9

A. Introduction 9

B. Experimental Data and Previous Theoretical Calculations 10

C. Method of Calculation 13

D. The Lowest Singlet States in C_{2v} 14

E. The C_{2v} Potential Energy Surface for the $^1A_1$ State 17

1. The ring minimum 17
2. Location of the transition state for the ring opening 18
3. The intersection between the 1-^1A_1 and 2-^1A_1 surfaces 23

F. Exploration of Parts of the Complete Ground State $^1A'$ PES 36

1. Usefulness of the $^1A'$ ground state PES 36
2. The panel for ϕ=116.3° 38

G. Conclusions 40

III. POTENTIAL ENERGY SURFACE OF THE GROUND STATE OF CO_2 43

A. Introduction 43

B. Method of Calculation 44

C. Mapping of the Complete Ground State $^1A'$ PES 45

D. The Lowest Singlet States in C_{2v} 47

E. The C_{2v} Potential Energy Surface for the $^1A_1$ State 50

1. The ring minimum 50
2. PES governing the ring opening process 54
3. Location of the ring opening transition state 56

F. Exploration of the Complete Ground State PES $E(\phi,R_1,R_2)$ 58

1. Introduction 58
2. The panel for ϕ=94° 61
3. The panel for ϕ=180°: collinear approach of O(^{1}D) to CO($^1\Sigma^+$) 66
4. The panel for ϕ=0°: collinear C(^{3}P)+O$_2$($^3\Sigma_g^-$) → CO($^1\Sigma^+$)+O(^{1}D) 70

G. Conclusions 72

IV. THE RING OPENING OF CYCLOPROPYLIDENE TO ALLENE 74

A. Key Regions of the Singlet Ring Opening Surface 74

1. Introduction 74
2. Method of calculation 78
   2.1. Scope of calculations 78
   2.2. Basis sets 79
   2.3. Configuration spaces 81
3. Critical regions 83
   3.1. The ring opening transition state 83
   3.2. The other critical points 90
4. Reaction paths 98
   4.1. The steepest descent: qualitatively 98
   4.2. The steepest descent: quantitatively 102
      From R to TS 102
      From TS to CR 104
      From CR to TS* 107
      From TS* to A 107
      From I/CR to P/P' 107
5. The intersecting coordinate subspace (ICS) 108
   5.1. Dimensionality 108
   5.2. Linear approximation near CR 110
   5.3. Determination of the linear approximation 113
   5.4. Steepest descent lines near CR 114
   5.5. Intersecting coordinate subspace & reduced energy surface 115
6. The free internal rotation of the CH$_2$ groups 119

B. Ab-Initio Interpretation of the Electronic Rearrangements in Terms of Quasiatomic Orbitals 123

1. Introduction 123
2. Method of analysis 125
   2.1. Localized FORS MO's as molecule-adapted deformed minimal basis-set atomic orbitals: quasi-atomic orbitals 125
   2.2. Density and population analysis of a FORS wavefunction 127
   2.3. Configurational analysis of a FORS wavefunction 132
   2.4. The localization process 134
3. The ring opening barrier 135
   3.1. Quasi-atomic FORS MO's 135
      Reactant 136
      Transition state 138

3.2. Population and bond order analysis 139
Reactant 139
Transition state 144
3.3. FORS configuration analysis 148
Reactant 149
Transition state 151
4. The allene isomerization barrier 152
4.1. Staggered linear allene 153
4.2. Bent planar allene (ϕ=133.3°) 158
4.3. Symmetry considerations, conical intersection between the two transition states 164
5. The free internal cogwheel motion 165
5.1. Quasi-atomic FORS MO's 166
(δ_1, δ_2) = (90° ,0°) 166
(δ_1 = δ_2 = 45°) 168
(δ_1, δ_2) = (0° ,90°) 171
5.2. Analysis for (δ_1, δ_2)=(90° ,0°) and (δ_1, δ_2)=(0° ,90°) 171
Population and bond order analysis 171
Configurational analysis 181
5.3. Analysis for δ_1=δ_2=45° 182
Population and bond order analysis 182
Configurational analysis 185
6. The population and configuration analysis for the extended basis set calculations 186
6.1. Quasiatomic character of localized MO's 187
6.2. Population analysis 189
6.3. Configurational analysis 193
7. Summary and Conclusions 193

V. REFERENCES 197

VI. ACKNOWLEDGEMENTS 201

I. INTRODUCTION

Computational Chemistry has evolved over the last few years into a powerful tool which can accurately describe both atomic and molecular properties in very close agreement with experimental observations. Although the basic ideas of quantum mechanics were set in the beginning of this century, definite difficulties in their application to real systems prevented theorists from making early computational breakthroughs. This problem was recognized by Dirac (1929) who wrote: "The underlying physical laws necessary for the mathematical theory of the whole of chemistry are thus completely known, and the difficulty is only that the exact application of these laws leads to equations much too complicated to be soluble". The inability to solve the exact equations analytically yielded a plethora of approximate solutions. These are due to the fact that in order for the quantum mechanical ideas to be applied to real systems various approximations need to be employed which in turn introduce errors to the values of the computed physical quantities. Furthermore the crudity of these approximations and as a consequence the magnitude of the errors they introduce increase rapidly with the size of the system.

The approximations used in molecular modelling are tested in cases where experimental data are available - usually compared against spectroscopic measurements or X-ray diffraction studies - at nuclear configurations describing stable and/or metastable species of real molecules. By comparing the experimental data with the theoretical predictions, theoreticians were able to build over the years a level of theory which although is far from being simple and understandable by someone without explicit knowledge of advanced applied mathematical techniques, has succeeded in providing the theoretical background needed to give some insight into important chemical concepts such as molecular bonding, reactivity, reaction mechanisms as well as equilibrium geometries and amounts of energy needed or released during various chemical reactions.

By testing the validity of the theoretical approximations in cases where experimental data are available (i.e. ground states of small molecules) one can furthermore employ them in a predictive manner in order to speculate about species lacking direct experimental verification (i.e. short-life intermediates). The latter consist of structures for transition states or other metastable species occurring during chemical reactions, yielding therefore energy barriers, reaction paths, rates as well as the energy contents of various chemical processes. In order to achieve these goals it is desirable to be able to visualize the way the nuclei move around during a chemical reaction as well as the energy content associated with these nuclear motions.

One of the most important approximations used in electronic structure calculations which has almost universal validity is the one proposed by Born and Oppenheimer (1927). It states that due to the fact that the electrons are much lighter than the nuclei, the latter can be consider standing still. Therefore it is possible to uncouple the theoretical treatment of the electronic and nuclear motions. The electronic motions are obtained by calculating the electronic energy for various fixed nuclear coordinates q_1, q_2,...,q_N and adding the electrostatic nuclear repulsion energy. For a polyatomic molecule consisting of N atoms the electronic energy is represented by a hypersurface in N dimensions:

$$E_{elec.}-E\,(q_1,q_2,\ldots,q_N) \qquad (1.1)$$

This hypersurface is known as the potential energy surface (PES) of the system. Once the PES is known the nuclear motions can be determined either through vibrational (small displacements) or dynamics (large displacements) calculations. Furthermore the topology of the potential energy hypersurface unveils useful information concerning the molecular system. Different points on a PES represent different nuclear configurations corresponding to different conformations of the same molecular species. The points of interest on a PES (critical points) are these where the first derivative of the energy (gradient) is zero with respect to all coordinates:

$$g_i(q_0)-\left(\frac{\partial E}{\partial q_i}\right)_{q-q_0}-0 \qquad (1.2)$$

Further classification of the critical points is achieved by examining the eigenvalues of the matrix of second derivatives (hessian) at these points:

$$H_{ij}(q_0)-\left(\frac{\partial^2 E}{\partial q_i \partial q_j}\right)_{q-q_0} \qquad (1.3)$$

Critical points where all eigenvalues of the hessian are positive are classified as minima on a PES and correspond to stable or metastable molecules. For example the C_{2v} ground state geometry of H_2O corresponds to a minimum on a 2-dimensional surface of the energy with respect to the nuclear coordinates. The coordinates of this minimum correspond to an H-O-H angle of 104.5° and an O-H bond length of 0.957 Å. The points where the hessian has only 1 negative eigenvalue can be visualized as "mountain passes" on a topographic map. Starting at these points it is always possible to follow a steepest descent path along which the gradient of the energy is maximum on either side of the direction to which the negative eigenvalue of the hessian points and end up in a minimum. The path connecting two minima on a PES almost always passes through a point where the hessian has one negative eigenvalue (saddle point) and at that point the energy has the maximum value with respect to all other points of the path. A chemical reaction can then be visualized as the nuclear rearrangements happening when following a path on a PES from one minimum (corresponding to the reactants) to the other (corresponding to the products). The endo/exothermicity of the reaction is then the energy difference between the two minima corresponding to the reactants and products. Among all saddle points, that might connect two minima on a PES through different paths, the one having the lowest energy is called the transition state of the reaction. The energy difference between the transition state and the reactant minimum is the barrier or activation energy needed for the system in order to "climb" from the reactant minimum to the "mountain pass". Paths on a PES connecting a minimum with many different ones correspond to different reactions and therefore have different transition states. The relative magnitudes of the different barriers corresponding to different reactions starting from the same minimum determine in many cases the route along which a reaction will proceed among the many choices it might have. Finally the points on a PES at which the hessian has more than 2 negative eigenvalues correspond to local maxima having a high energy content and are of no particular interest since they correspond to very unstable and thus very unlikely nuclear conformations.

In a polyatomic molecule of N atoms the energy is, within the Born-Oppenheimer approximation excluding translations and rotations, a function of 3N-6 (3N-5 for linear species) internal coordinates (i.e. bond lengths and/or bond angles). The computation of accurate potential energy surfaces is therefore a laborious task. This is mainly the reason that in the past only very small regions of PESs around the minima corresponding to stable species were known. The rest of the PES was computed using semi-empirical methods which contained a lot of uncertainties. A computational method in order to be appropriate for computing PESs should meet the following standards: describe all species on equal basis as much as possible, account for the fact that the orbitals change both in character and occupation numbers and accurately simulate bond formation(s) and breaking(s). Furthermore it should recover most of the electronic correlation energy by mixing of various configurations. It is therefore apparent that in order to be able to accurately describe the nuclear rearrangements and their associated energetic effects occurring during a chemical reaction the employment of methods beyond SCF is desirable. To this end a multiconfigurational wavefunction represents a very accurate first step. In this approximation the Multi Configuration Self Consistent Field (MCSCF) wavefunction Ψ is written as a sum of Symmetry Adapted Antisymmetrized Products (SAAPs) $\Phi_{\kappa t}$:

$$\Psi_{\kappa t} = \sum_{\kappa,t} C_{\kappa t}\, \Phi_{\kappa t}{}^{SM} \tag{1.4}$$

The SAAPs are themselves N electron wavefunctions:

$$\Phi_{\kappa t}^{SM}(space,spin) = N_{\kappa} A(U_{\kappa}(space)\Theta_{t}^{SM}(spin)) \tag{1.5}$$

where	$\Theta_t{}^{SM}$	are spin eigenfunctions
	S, M	are the eigenvalues of S^2 and S_z respectively
	U_κ	is a product of configuration generating orbitals
	A	is the antisymmetrizer
	N_κ	is the normalization constant

Furthermore the Full Optimized Reaction Space (FORS) model introduced by Ruedenberg and Sundberg (1976) and further developed by Ruedenberg, Schmidt, Gilbert and Elbert (1982) can be implemented within the MCSCF framework to determine the best wavefunction obtained by a superposition of all possible configurations generated from a formal minimal basis of the orbitals which change throughout the chemical reaction.

Triatomic molecules have drawn considerable attention in the past because they are the smallest molecular systems for which there exist a non-trivial (i.e. with dimension higher than one) potential energy surface. The lowest symmetry they possess is C_s (a plane containing all 3 atoms) and their potential energy is a function of 3 internal coordinates (bond lengths or angles). In particular for the AB_2-type triatomics (i.e. H_2O, CO_2 etc.) there exists a 2-dimensional subspace (plane) of the full 3-dimensional surface with higher symmetry (C_{2v}) representing nuclear conformations having equal $A\text{-}B_\alpha$ and $A\text{-}B_\beta$ bond lengths. The possibility of existence of double minima on the potential energy surfaces of AB_2-type molecules was first suggested by Hayes and Pfeiffer (1968) through the use of Walsh-type diagrams. The scope of this study is to investigate the complete ground state potential energy surfaces of O_3 and CO_2 since the understanding of the PESs of small systems is prerequisite for understanding the corresponding surfaces of polyatomic systems having many more nuclear coordinates.

The ozone molecule, O_3, and its reactions are important because of the potential health hazards which can result from ozone excess in the breathing air of large cities and from ozone deficiency in the upper atmosphere. In Chapter II the adiabatic energy surfaces of the lowest singlet states of the molecule and its dissociation products together with a complete investigation of the ground state PES are presented. In the course of the investigation of the ground state PES in C_{2v} some complicated features to which little attention has been paid before are discovered. These include the discovery of a ring minimum on the ground state potential energy surface and a conical intersection between the 1-^1A_1 and 2-^1A_1 potential energy surfaces in the vicinity of the ring opening transition state.

Carbon dioxide and its reactions play important roles in atmospheric chemistry, in combustion chemistry and in the photochemical cycle connecting plants and animals. Most of these reactions depend upon the energy states of the system. Many experimental and a few theoretical studies notwithstanding, past knowledge about them has been essentially limited to narrow regions around the linear ground state equilibrium geometry. In Chapter III reliable global information on the CO_2 ground state potential energy surface is presented. A carbene-type metastable species corresponding to a ring structure is found on the ground state potential energy surface. Furthermore various dissociation channels are also investigated.

In Chapter IV the mechanism of the ring opening of singlet cyclopropylidene to allene is investigated. This reaction represents a prototype of bond fission of a cyclic carbene due to ring strain. Because of the consequential roles played by carbenes as well as by strained rings as reaction intermediates, this isomerization has fundamental implications for many organic reactions, including combustion phenomena. Although this molecule has 7 atoms it is treated as a ring of 3 carbons and the potential energy surface is obtained as a function of the C-C-C ring opening angle ϕ and the two $-CH_2$ rotation angles δ_1 and δ_2 while the remaining 12 internal coordinates are relaxed by energy minimization for each (ϕ,δ_1,δ_2) triple.

II. POTENTIAL ENERGY SURFACE OF THE GROUND STATE OF O_3

A. Introduction

The concept of the adiabatic potential energy surface defined within the Born-Oppenheimer approximation is of great importance in the understanding of the various reaction paths connecting the reactants with the products as well as in identifying any reactive intermediates and alternative routes through which a chemical reaction can proceed. The reliable determination of the energy separation of different potential energy surfaces associated with different electronic states of the molecular system is one of the cornerstones of molecular spectroscopy and photochemistry since it determines whether the molecules can "jump" from a higher electronic state to a lower one while at the same time transforming electronic energy into light. The accessibility of the higher electronic state for electronic transitions from the ground state is furthermore determined by various selection rules pertaining to the different symmetries of the electronic states as well as the energy separation between them.

The ground state potential energy surface of O_3 is of particular interest due to the fact that the ground state of O_3 dissociates to ground-state products according to the scheme:

$$O_3(\tilde{X},{}^1A_1) \rightarrow O_2(X,{}^3\Sigma_g^-) + O\,({}^3P) \qquad (2.1)$$

A preliminary study of the ground state potential energy surface by Murrell et. al. (1976) using semiempirical many-body expansions for the potential energy surface produced qualitative agreement with the experimental data for the ground state geometry of O_3. By imposing symmetry on the potential function the same authors were able to reach qualitatively correct results. In the present treatment of the ground state PES no symmetry constraints are imposed to the wavefunction and the quantitatively correct geometry of the ground state comes as a natural consequence of the level of the ab-initio theory.

B. Experimental data and previous theoretical calculations

The importance of ozone in life and in particular its presence in the upper atmosphere has motivated a lot of previous experimental and theoretical studies, concerning the structure of the ground and several excited states as well as its photochemistry and dissociation process. Experimental evidence (cf. Herzberg 1966, p. 604) suggests that the ground state has a C_{2v} structure with an O-O-O angle of 116.8° and an O-O bond length of 1.278 Å. Its electronic structure corresponds to a Hartree-Fock singlet configuration:

$$(1a_1)^2(1b_2)^2(2a_1)^2(3a_1)^2(2b_2)^2(4a_1)^2(5a_1)^2(3b_2)^2(1b_1)^2(4b_2)^2(6a_1)^2(1a_2)^2$$

The fact that ozone is extremely reactive and has a very low stability with respect to dissociation towards O_2 + O in their ground electronic states does not fit in well with its symmetric bent structure and the presence of double bonds. It has therefore been suggested (cf. Pauling, 1960) that alternative forms corresponding to metastable species may exist. Pulse radiolysis experiments of O_2 by Hochanadel, Ghormley and Boyle (1968) suggested the existence of a bound excited state which is stable to partial dissociation. Riley and Cahill (1970) measured the half-life of this species to be 5 μsec but they raised some questions on the issue of whether this was vibrationally excited ozone as it was previously thought. Optical absorption measurements during pulse radiolysis of oxygen gas experiments by Bevan and Johnson (1973) established the presence of two ozone precursors O_3^{α} and O_3^{β}, having absorption maxima at 315 and 285 nm respectively, which were also considered at that time to be vibrationally excited ozone. Rosenberg and Trainor (1974) identified the O_3^{β} species as vibrationally excited O_3 whereas Burton and Harvey (1977) suggested that the O_3^{α} precursor which shows absorption at 315 nm and has a lifetime of 5 μsec might correspond to a metastable species having D_{3h} symmetry. In order to prove the above assumption it is necessary to compute the energy difference between the two minima and furthermore to establish the position of the D_{3h} species with respect to the $O_2 + O$ dissociation limit which is experimentally determined by Jones (1985) to lie 26.1 kcal/mol above the C_{2v} ground state. The energy separation between the C_{2v} and D_{3h} minima has been the subject of many theoretical calculations in the past most of which yielded conflicting results. Although it is unanimously agreed that the D_{3h} minimum lies above the C_{2v} ground state, the energy separation between the two minima is still the subject of debate. Wright (1973) was the only one to suggest that the ring state lies 6.2 kcal/mol below the ground state as a result of a two configuration minimal basis set calculation. Ab initio calculations with double zeta quality basis sets by Hay and Goddard (1972) and by Hay, Dunning and Goddard (1973) place the ring minimum 27.6

kcal/mole and 34.5 kcal/mole above the open structure respectively. Shih, Buenker and Peyerimhoff (1974) computed a value of 16 kcal/mole in the SCF-CI level, Hay, Dunning and Goddard (1975) a value of 32.2 kcal/mole using GVB-CI wavefunctions while Harding and Goddard (1977) estimated the energy difference to be 27.3 kcal/mole in the GVB-POL-CI approximation. Using singles and doubles configuration interaction (CISD) wavefunctions Lucchese and Schaefer (1977) predicted a value of 17.8 kcal/mole whereas Hay and Dunning (1977) gave a value of 28.0 kcal/mole in the generalized valence bond plus singles and doubles GVB+(1+2) level. Additional two-reference CISD wavefunction calculations by Karlström, Engström and Jönsson (1978) based on multiconfiguration (MCSCF) orbitals yielded a value of 28.7 kcal/mole. Burton (1979) used the PNO-CI and CEPA electron correlation methods with triple quality plus polarization (TZP) basis set to calculate a value of 12.0 kcal/mole. Wilson and Hopper (1981) report a value of 38.9 kcal/mole using a 76 configuration MCSCF/CI wavefunction which however predicts a ring state with a near equilateral triangle geometry. Moreover Jones (1985) has calculated the energy difference to be 32.3 kcal/mole using density functional methods. The most recent studies by Moscardo, Andarias and San-Fabian (1988) in the CIPSI level place the ring structure 21.1 kcal/mole above the ground state whereas Lee (1990) reports a value of 28.7 kcal/mole in the coupled cluster including single, double and a perturbational estimate of triple excitations CCSD(T) level of theory including the zero-point vibrational energy and using a large [5s4p3d2f1d] ANO basis set. The last calculation which is probably the most accurate to date indicates that the ring minimum lies above the O_2 + O dissociation limit. The discrepancy between the previous calculations is mainly due to the arbitrariness of the selection of the important configurations in building up the MCSCF wavefunction.

C. Method of calculation

For the reliable determination of potential energy surfaces an MCSCF approach with an extended basis set is desired. This is due to the fact that different parts of the potential energy surface represent different bonding situations which require both redistribution of the electrons among the active molecular orbitals as well as reoptimization of the molecular orbitals themselves. The active space should be selected in a way that all important configurations at every part of the potential energy surface should be included in the wavefunction. The molecular orbitals should also be described by an extended basis set and additional polarization functions should be included in order to be able to handle bond formations and breakings. However, if large parts of the potential energy surface are to be explored, a compromise should be made as regards the size of the basis set. Furthermore for areas of the potential energy surface neighboring intersections of two potential energy surfaces of the same symmetry special attention should be given in the simultaneous optimization of the orbitals for both states by a state averaging calculation.

In O_3 there are 24 electrons and 15 molecular orbitals. The FORS space is constructed by keeping the 1s orbitals of the three Oxygen atoms doubly occupied and allowing the rest 18 electrons to be distributed in the 12 active orbitals creating therefore a full optimized valence space. The number of configurations for the four lowest lying singlet states of O_3

in C_{2v} is 4067, 3893, 3962 and 3858 for the $^1A_1$, $^1A_2$, $^1B_1$ and $^1B_2$ states respectively. We have used a Dunning-Hay (1977) basis set consisting of the segmented contractions (9s5p1d/3s2p1d) which yields a total of 45 basis functions. For the d-type polarization function the exponent ζ_0=0.85 is used (cf. Dunning and Hay, 1977). All geometry optimizing calculations are performed using the GAMESS program by Dupuis et. al. (1980) while all state averaging calculations are performed with the MOLRPO program of Werner and Knowles (1988).

D. The lowest singlet states in C_{2v}

The potential energy curves of O_3 corresponding to the $^1A_1$, $^1A_2$, $^1B_1$ and $^1B_2$ states in C_{2v} are shown in Figure 2.1. The energy is plotted as a function of the O-O-O angle ϕ for each value of which the O-O bond lengths are optimized. The internal coordinates of the C_{2v} minima for the various singlet states of O_3 are shown in Table 2.1. The ground state of O_3 has C_{2v} symmetry with an O-O-O angle of 116.31° and an O-O bond length of 1.299 Å. It lies 30.2 kcal/mole lower than another minimum on the $^1A_1$ ground state PES which corresponds to an equilateral geometry structure having D_{3h} symmetry. It is worth pointing out that only the two ground state $^1A_1$ minima at ϕ=60° and 116.31° are true minima upon asymmetric distortions when the symmetry is lowered to C_s. The hessian matrix at the points corresponding to the minima of the $^1A_2$, $^1B_1$ and $^1B_2$ has one negative eigenvalue along the C_{2v} breaking normal mode, indicating that these structures correspond to transition states on the complete C_s potential energy surface.

Table 2.1. Minima on the O_3 surface for the various C_{2v} states

State	ϕ°	R (Å)	E (hartree)	ΔE^a (kcal/mol)
$^1A_1$	116.31	1.299	-224.5523175	0.0
	60.00	1.470	-224.5041628	30.2
$^1A_2$	99.58	1.379	-224.4960172	35.2
$^1B_1$	111.92	1.482	-224.3875970	103.4
$^1B_2$	117.50	1.482	-224.4789770	46.0
	46.27	1.785	-224.4074403	90.9

[a]: with respect to the ground state minimum.

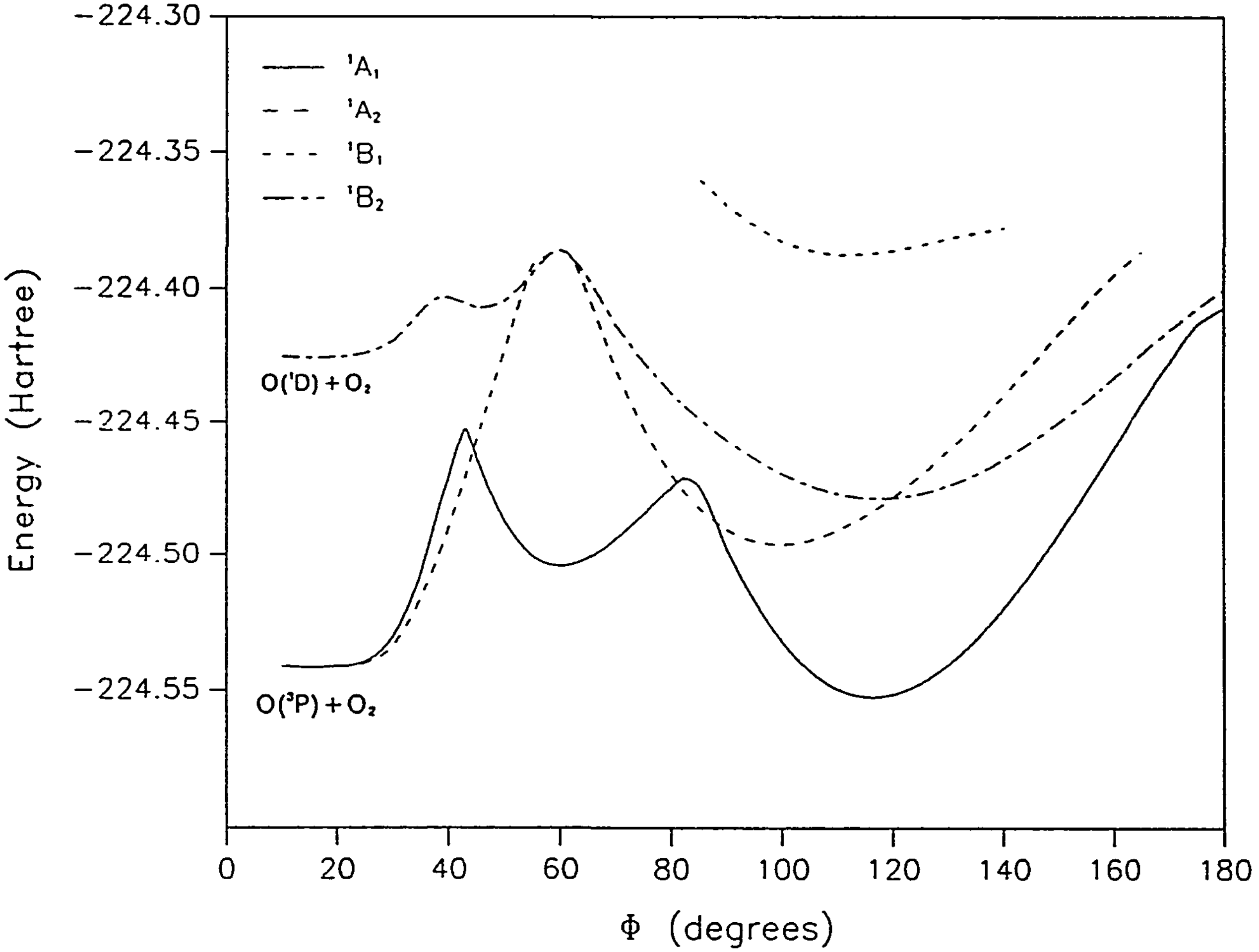

Figure 2.1. Energies of the lowest $^1A_1$, $^1A_2$, $^1B_1$ and $^1B_2$ states of O_3 in C_{2v} as a function of the O-O-O angle ϕ when the O-O distances are optimized for each ϕ

E. The C_{2v} potential energy surface for the $^1A_1$ state

1. The ring minimum

As it can be seen from Table 2.1 the ring minimum of O_3 has D_{3h} symmetry having an O-O-O angle of 60° and an O-O bond length of 1.470 Å. The electronic configuration of the ring structure corresponds to a Hartree-Fock singlet configuration:

$$(1a_1)^2(1b_2)^2(2a_1)^2(3a_1)^2(2b_2)^2(4a_1)^2(5a_1)^2(3b_2)^2(1b_1)^2(6a_1)^2(1a_2)^2(2b_1)^2$$

Its difference from the open structure, which corresponds to a $\sigma^{14}\pi^4$ system where the π electrons occupy a bonding and a non-bonding molecular orbital, is a transfer of two electrons from the σ to the π molecular orbitals. The ring structure therefore corresponds to a $\sigma^{12}\pi^6$ system in which there is an additional anti-bonding π-molecular orbital occupied. The determination of its optimized geometry is performed in C_s symmetry and the higher symmetry elements come as a natural consequence of the ab-initio level of theory. The ring structure is a real minimum on the C_s potential energy surface since the hessian matrix evaluated at this point has 3 positive eigenvalues which correspond to the harmonic frequencies of the normal vibrational modes. There are 2 degenerate ones corresponding to the e′ and one corresponding to the totally symmetric a_1' mode. Their values calculated in the full valence space FORS MCSCF level are 750 and 1046 cm^{-1} respectively in fair agreement with Lee's (1990) reported values of 795 and 1114 cm^{-1} in the CCSD(T) approximation with a [5s4p3d2f] ANO basis set. The analogous computed harmonic frequencies for the C_{2v} ground state minimum are 685, 1044 and 1093 cm^{-1} vs. Herzberg's (1966, p.604) 705, 1042 and 1110 cm^{-1} experimental values and Lee's (1990) 718, 1053 and 1153 cm^{-1}.

These harmonic frequencies yield a value of 4.03 and 3.63 kcal/mol for the zero-point vibrational energy at the open and ring minima respectively. By including this correction the energy separation between the two minima becomes 29.8 kcal/mol which is within chemical accuracy with Lee's (1990) value of 28.7 kcal/mol. It is therefore at this point concluded that the ring minimum lies above the O_2 + O dissociation limit which is 26.1 kcal/mol above the ground state.

2. Location of the transition state for ring opening

For some time it was erroneously thought that the ring structure of O_3 does not lie on the ground state potential energy surface but on a surface corresponding to an excited state of the same symmetry with the ground state denoted as 2-^1A_1. The fact that the SCF configuration is different at the two minima was the reason for this misconception. However along the path that connects the ring with the open minimum, a part of which is shown in Figure 2.1, there is a continous change in the character of the MCSCF wavefunction the ring configuration being the dominant one at one end whereas the open configuration dominates at the other. This path lies exclusively on the ground state potential energy surface.

The accessibility of the ground state from the ring minimum depends on one hand on the energy separation between them, a quantity which is accurately determined to be 29.8 kcal/mol in Section II.E.1, and on the other hand on the barrier between the two minima. Furthermore the mechanism of the ring opening (i.e. the way that the nuclei move around in order for the geometry to change from the ring to the open structure) is governed by the ground state potential energy surface. As a first guess one might assume that the ring opening occurs by increasing the O-O-O angle from 60° to 116.31° by keeping the O-O bond lengths equal at all times while at the same time adjusting them to the value that minimizes the energy for each ϕ. Therefore by assuming C_{2v} symmetry the energy is a function of 2 coordinates (i.e. the O-O-O angle ϕ and the O-O bond length R). Contours of the energy of the ground state $^1A_1$ potential energy surface are shown in Figure 2.2. The coordinates X and Y against which the energy is plotted are related to ϕ and R according to:

$$X = R \sin(\phi/2) \quad \text{and} \quad Y = R \cos(\phi/2)$$

The choice of this coordinate system serves the following practical purpose: by placing the central oxygen atom at the origin, any point on the PES indicates the position of the second oxygen at one end whereas the position of the third oxygen at the other end is symmetric with respect to the Y axis. About 130 points are calculated in order to create the 2-dimensional grid used to draw the energy contours with an increment of 10 millihartree. For each point a full valence space FORS MCSCF calculation is performed with a wavefunction which has 4067 configurations. On this PES the ring mimimum is denoted by "R" and the open minimum by "O". In between the two minima there exists a saddle point, denoted by "S^*", which corresponds to the transition state of the ring opening upon preservation of C_{2v} symmetry. The geometry of the transition state and the barrier of the ring opening has not been accurately determined before appart from a qualitative estimation by Shih, Buenker and Peyerimhoff (1974). They report a barrier of 17.6 kcal/mol with respect to the ring minimum and a

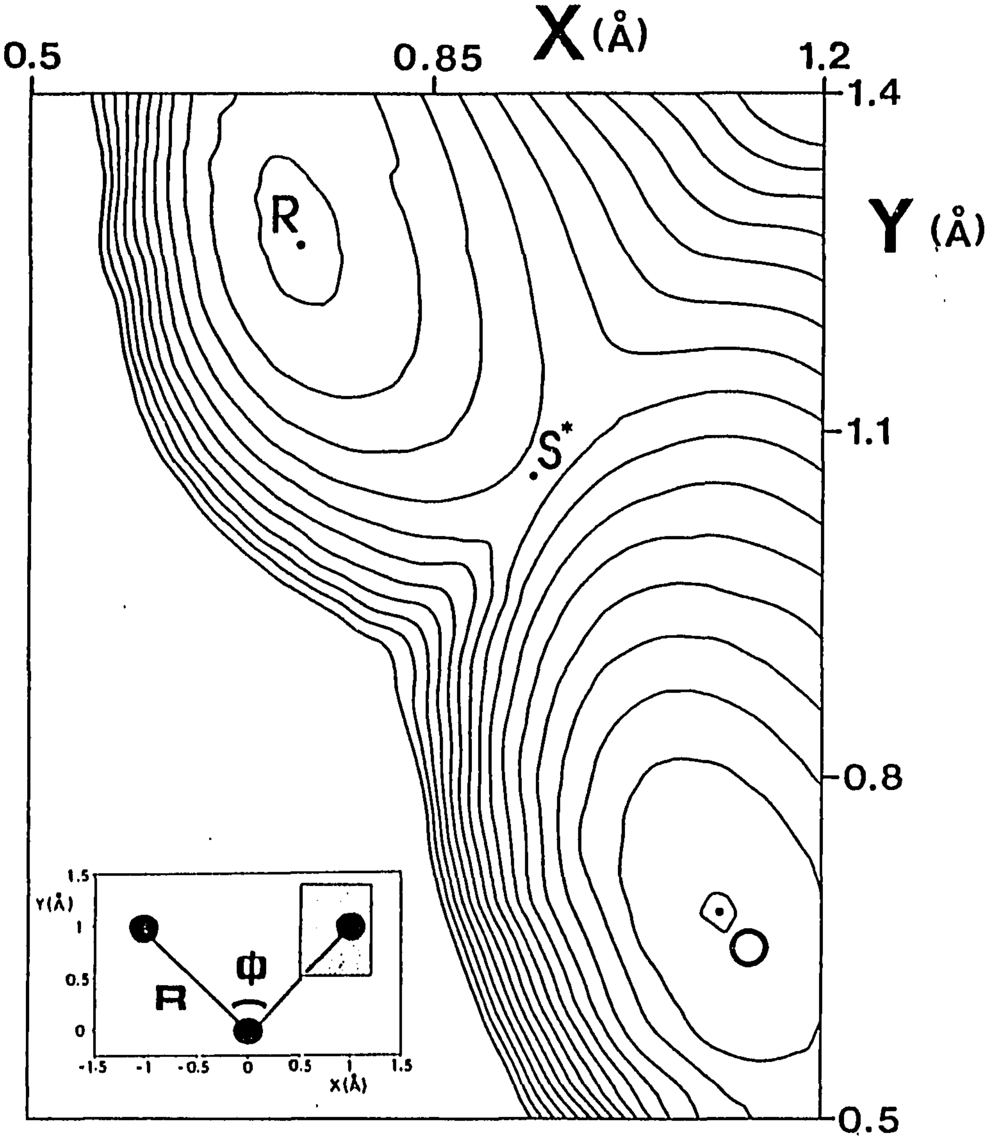

Figure 2.2. Ground state $^1A_1$ potential energy surface in the full valence space FORS-MCSCF (4067 CSFs) approximation corresponding to the C_{2v} constrained ring opening of triangular O_3. Increment: 10 mhartree. R: ring minimum, O: open minimum, S^*: saddle point.

structure for the transition state having C_{2v} symmetry and internal coordinates $\phi = 85^\circ$ and $R = 1.418$ Å. However they did not investigate whether the C_{2v} saddle point is the real transition state in the $^1A'$ surface. In order for a structure to resemble a true transition state in the global ground state $^1A'$ potential energy surface the hessian matrix evaluated at this point should have only one negative eigenvalue. Since the hessian at the C_{2v} transition state has already one negative eigenvalue the curvature of the PES away from C_{2v} symmetry (i.e. along the symmetry breaking mode corresponding to asymmetric distortions) should be investigated. Figure 2.3 shows a blow-up of the C_{2v} ground state PES around the point S^* where the energy contours are drawn with an increment of 0.1 millihartree. The surveilance of the area around S^* yields the following observations: The upper left part of the surface exhibits a different slope than the lower right part. This is due to the fact that in the former part the wavefunction has predominantly the character of the ring structure whereas in the latter part the configuration corresponding to the open part is dominating. The two parts are connected through a ridge across which the wavefunction changes character from the one configuration to the other very rapidly. Following similar arguments the wavefunction on the PES corresponding to the first excited state 2-^1A_1 should exhibit a similar behavior but with inverse character: at geometries corresponding to small O-O-O angles its dominant configuration should resemble the one of the open structure and vice versa. On the PES for the first excited 2-^1A_1 state there presumably exists a valley across which the wavefunction of the excited state rapidly changes character from the open to the ring structure. The C_{2v} transition state S^* on the ground state

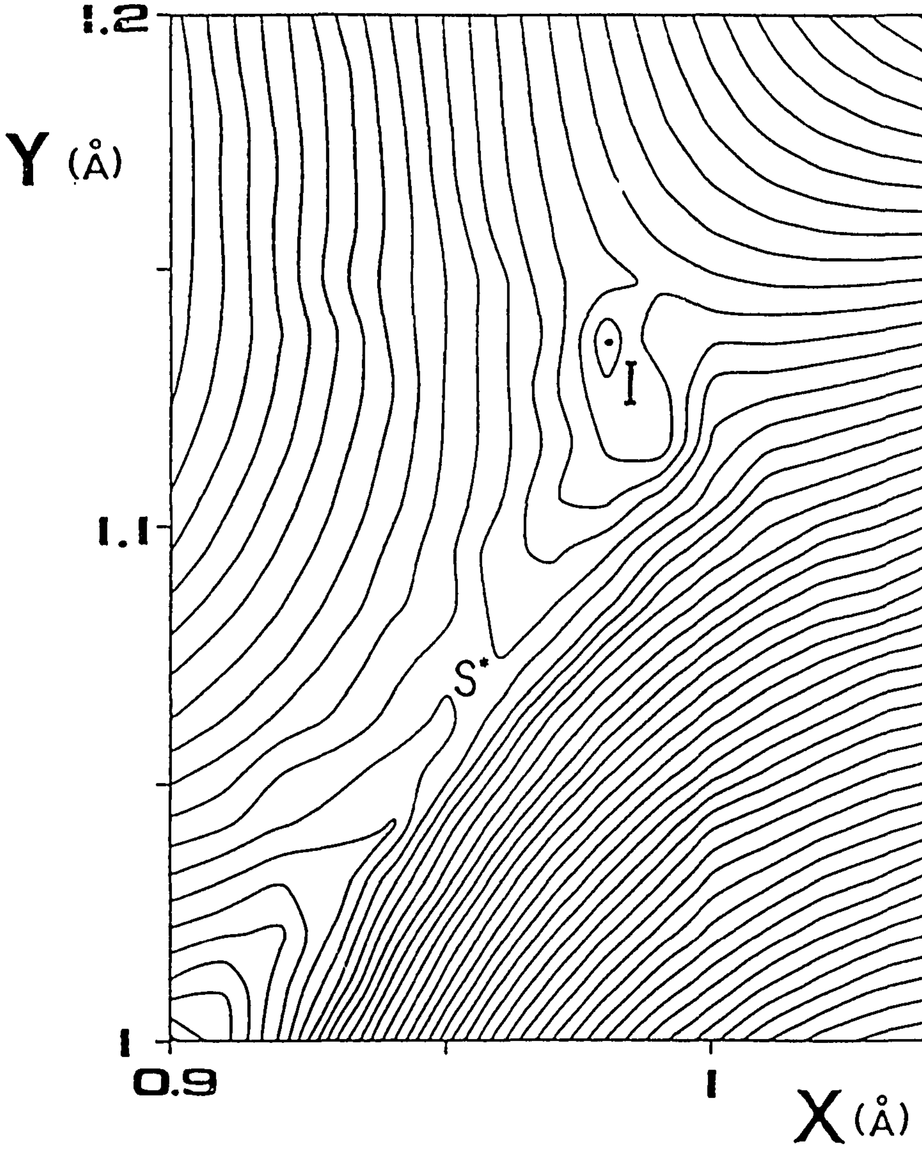

Figure 2.3. Ground state PES near the ring opening transition state.

Increment: 0.01 mhartree. S: saddle point, I: intersection surface lies on the ridge and very close to it there exists a local maximum denoted as "I" on Figure 2.3. The presence of this unusual point and the topology around it suggests that there is a possibility that the two PES corresponding to the two low lying states 1-^1A_1 and 2-^1A_2 come very close together along this ridge and might touch each other at the point I. In order to investigate this possibility and to accurately determine the geometry and the energy of the C_{2v} transition state, both states should be calculated in the vicinity of the ridge. Furthermore since after locating the C_{2v} transition state the curvature of the ground state PES away from C_{2v} symmetry is going to be investigated in order to determine whether the C_{2v} transition state is the real transition state in C_s, the topology of the manifolds along which PES intersect each other should also be examined.

3. The intersection between the 1-^1A_1 and 2-^1A_1 surfaces

It is sometimes common that at the points on the potential energy surface which correspond to the reactant and product of a chemical reaction there exist higher symmetry elements than the ones present at points corresponding to intermediate geometries (i.e. along the reaction path). It is also possible that the molecular geometries for parts of the reaction path transform according to different irreducible representations of the same symmetry point group. This happens when they lie on potential energy surfaces corresponding to different electronic states that intersect each other. Hund (1927) was the first one to recognize that at the point(s) where two potential energy surfaces intersect each other the wavefunction is degenerate. Von Neumann and Wigner (1929) and Teller (1937) have given the mathematical proof of Hund's qualitative argument. Following Teller's

(1937) formalism let us suppose that all but two of the solutions of the electronic wavefunction have been determined and ϕ_1, ϕ_2 are two functions which together with the solutions of the electronic wavefunction form a complete orthonormal set. The two remaining solutions of the electronic wavefunction can then be written as:

$$\Psi = c_1\phi_1 + c_2\phi_2 \tag{2.2}$$

where c_1 and c_2 are constants. The energies of these two electronic states are:

$$E_\pm = \frac{1}{2}(H_{11}+H_{22}) \pm \frac{1}{2}\sqrt{(H_{11}-H_{22})^2+4H_{12}^2} \tag{2.3}$$

where

$$H_{\mu\nu} = \langle\phi_\mu|\hat{H}\ |\phi_\nu\rangle = \int\phi_\mu^*\hat{H}\ \phi_\nu d\tau \tag{2.4}$$

It is obvious that for degenerate solutions ($E_+=E_-$) <u>two</u> conditions should be met, namely:

$$H_{11} = H_{22} \quad , \quad H_{12} = 0 \tag{2.5}$$

The above two conditions are independent of each other as it was originally suggested by Teller (1937) and proved beyond any doubt by Longuet-Higgins (1975). This cleared a confusion which was created by a series of papers by Naqvi and Brown (1972), Naqvi (1972) and Hoytink (1975) claiming that there is only one independent condition that should be satisfied in order for the two potential energy surfaces to cross.

In a molecule of N atoms the energy is within the Born-Oppenheimer approximation a function of the 3N-6 internal coordinates (i.e. the internuclear distances):

$$U = U(r_1, r_2, \ldots, r_{3N-6}) \tag{2.6}$$

This is generally a hypersurface in 3N-5 dimensions. Intersections of these hypersurfaces can occur in manifolds of varying numbers of dimensions ranging from 0 (intersection at a point) to 3N-7 (since there are two independent conditions). Further determination of the dimensionality of the manifolds along which potential energy hypersurfaces of the same spin intersect each other can be achieved by considering the following two cases as regards the symmetry of the two intersecting surfaces:

(i) Different symmetries: provided that spin-orbit terms are absent from the Hamiltonian, H_{12} is identically zero which leaves only one condition, namely $H_{11} = H_{22}$, which should be satisfied in order for two potential energy surfaces of different symmetries to cross. In a diatomic molecule there is only one degree of freedom (the internuclear distance R_{AB}) and by varying this parameter it is possible to locate a point in which two potential energy curves having different symmetries can cross. For a polyatomic molecule there are in general 3N-6 degrees of freedom, therefore the hypersurfaces associated with electronic states of different symmetries can cross in manifolds of dimensions ranging from 0 to 3N-7.

(ii) Same symmetries: in this case both conditions in equation (2.9) should be met in order for the two hypersurfaces to intersect. In a diatomic molecule this is not possible in general due to the fact that there is only one degree of freedom. Therefore diatomic potential energy curves of the same symmetry avoid rather than cross each other, a fact which is known as the non-crossing rule. This does not exclude however the possibility of an "accidental crossing" such as in the LCAO-SCF treatment of HeH^{2+} by George and Morokuma (1973), or when there are other circumstances which allow the crossing of electronic terms having the same symetry such in the non-relativistic H_2^+ (cf. Landau and Lifshitz, 1965). The above cases do not violate the non-crossing rule and can be considered as consequences of the rule rather than reasons for doubting it as it was pointed out by Mead (1979). In fact it is believed that if such a case is treated on a more accurate level of theory then the two curves will avoid each other rather than cross as it is happening in the relativistic treatment of H_2^+. On the other hand in a polyatomic molecule of N atoms the presence of more degrees of freedom allows in principle two potential energy hypersurfaces of the same symmetry to cross in manifolds of dimensions from 0 to 3N-8. However, due to the higher dimensionality it is more difficult to detect intersections of potential energy hypersurfaces of polyatomic molecules. This fact has created the illusion that PES of the same symmetry always avoid each other even for polyatomic molecules despite Longuet-Higgins'

(1975) example of crossing of two electronic states having the same symmetry for a system of 3 dissimilar atoms in their ^2S ground states (i.e. Li, Na, K). However this was the only model to date and there have not been known so far any cases of real molecules that exhibit this phenomenon.

In the present case the energy of the global ground state $^1A'$ potential energy surface is a function of 3 coordinates (i.e. 3 angles or three bond lengths). Furthermore by assuming C_{2v} symmetry we impose an additional constraint to the system by keeping the two O-O bond lengths equal. The dimensionality of both 1-^1A_1 and 2-^1A_1 potential energy surfaces is then reduced to two, the energy being a function of the coordinates X, Y (or their equivalent ϕ, R). Furthermore since they have the same symmetry (a_1) there are two conditions, namely $H_{11} = H_{22}$ and $H_{12} = 0$ that should be satisfied in order for the two surfaces to cross. The quantities H_{11}, H_{22} and H_{12} of the system of these two equations depend on the two coordinates X, Y (or ϕ, R) of the surface in a rather complicated manner in general. In such a case the manifold of intersection of the two surfaces - if any - is of dimension 0 (i.e a point). The coordinates X_c, Y_c (or ϕ_c, R_c) of such a point should satisfy the system of equations (2.10). It should also be noted that it is possible in general that there exist more than one of these points at which the two surfaces touch each other. This is because the system of two equations (2.10) can have more than one set of solutions. This possibility is highly unusual due to the fact that the quantities H_{11}, H_{22} and H_{12} are in principle smooth functions of the coordinates X and Y but should not be excluded as impossible. In any case we are going to investigate if at the point denoted as "I" in Figure 2.3 there is a crossing of the two $^1A_1$ surfaces since this point is related to important features of the ring opening reaction surface being so close to the C_{2v} transition state.

Figure 2.4 shows the energies of the two lowest $^1A_1$ surfaces as a function of ϕ for various cuts of the surfaces corresponding to different values of R. The energies of both states are obtained as a result of a state averaging calculation in which the two states are given equal weights. The value of R for which the energies are calculated as a function of ϕ are indicated below the curves. The numbers above the curves show the energy separation between the two states in μhartree. In the domain 1.47 Å $\leq$ R $\leq$ 1.48 Å the two states come together as close as 35 μh and away from that area their separation increases. Therefore the intersection point - if any - should lie in the above domain whereas the C_{2v} transition state occurs when the maximum on the lower state potential energy curves passes through its minimum value in the domain 1.43 Å $\leq$ R $\leq$ 1.45 Å.

Before attempting to locate the intersection point it is necessary to definitively prove that it exists and make sure that the two surfaces do not really avoid each other at the last minute. For this purpose the following topological theorem which serves as a test for intersections and was proposed by Longuet-Higgins (1975) is used: Let S be any simply connected surface in nuclear configuration space, bounded by a closed loop L. Then if $\Psi(q;Q)$ changes sign when transported adiabatically around L, there must be at least one point on S at which $\Psi(q;Q)$ is discontinuous, implying that the potential energy surface intersects that of another electronic state.

Two loops along the ridge on the ground state potential energy

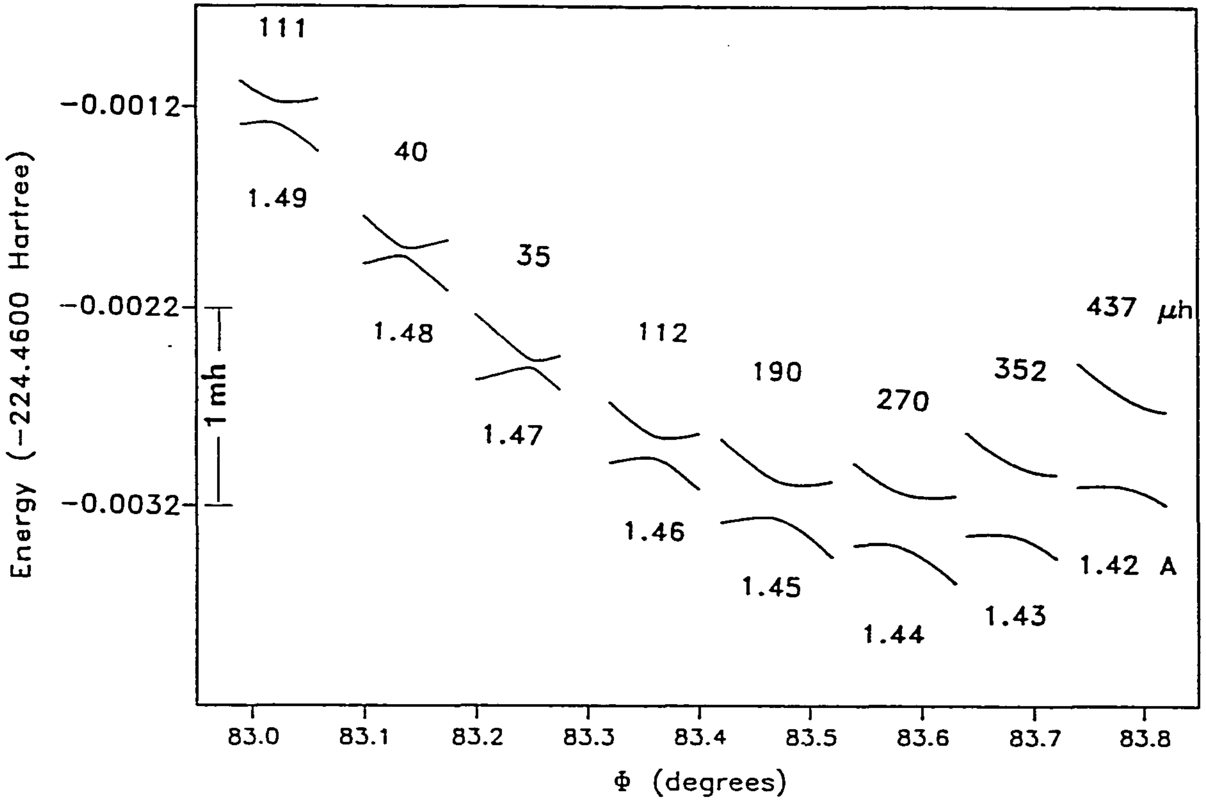

Figure 2.4. Energies of the two lowest $^1A_1$ surfaces on various passes across the ground state PES ridge of O_3 near the transition state. The energy separation of the two states is indicated above the curves in μhartree. Each set of curves corresponds to a different R value which is indicated (in Å) below them

surface of O_3 are chosen: one enclosing the intersection point "I", the other not enclosing it. Their position on the (X,Y) coordinate frame is shown in Figure 2.5. The relative positions of the ϕ=constant and R=constant lines on this frame are also indicated. The shadowed area corresponds to the ridge on the PES across which the wavefunction rapidly changes character from the ring to the open structure. A total of 51 points are computed on the loop enclosing the intersection. Most of them lie on the directon across the ridge since a continuous monitoring of the sign of the wavefunction in this direction is desired. In the direction parallel to the ridge only a few points are computed since in this area the wavefunction has the character of the ring or the open structure on either side of the ridge respectively. On the loop not enclosing the intersection a total of 8 points are calculated. The computed MCSCF wavefunction has four dominant terms all of them corresponding to configurations having doubly occupied molecular orbitals: two for the ring and another two for the open structure. Their relative magnitudes for the loop enclosing the intersection are plotted in Figure 2.6 against the distance along the path starting from point 1. It is worth noticing that moving around the loop on one revolution all 4 coefficients change sign. The relative sign of the CI coefficients is determined as follows: the change of sign in the dominant CI coefficient for the ring structure between points 36 and 40 in Figure 2.6 is directed by the constant positive value of the dominant CI coefficient for the open structure in this region. Upon two revolutions the sign of the wavefunction returns to its original value. The analogous plot for the loop not enclosing the intersection point "I" is shown in Figure 2.7. All CI coefficients in this case return to their original sign

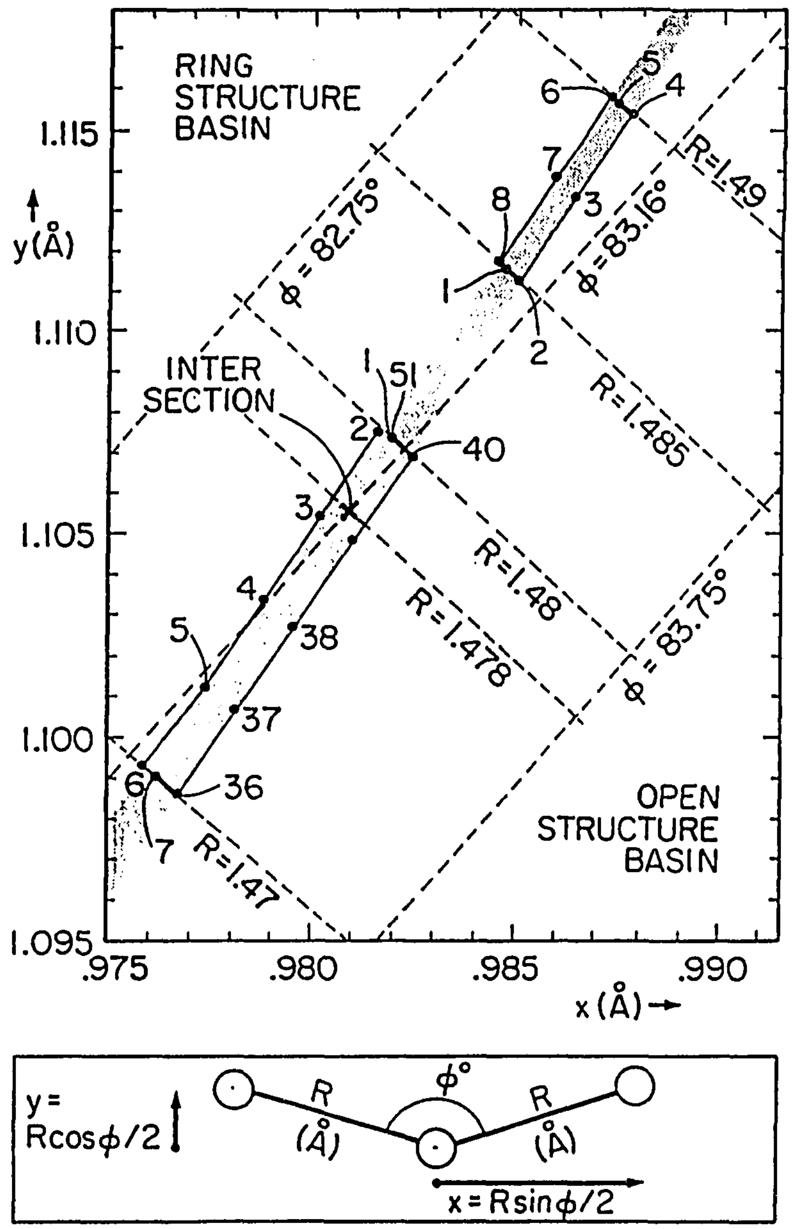

Figure 2.5. Two loops crossing the O_3 ridge: One enclosing the intersection, the other not enclosing the intersection

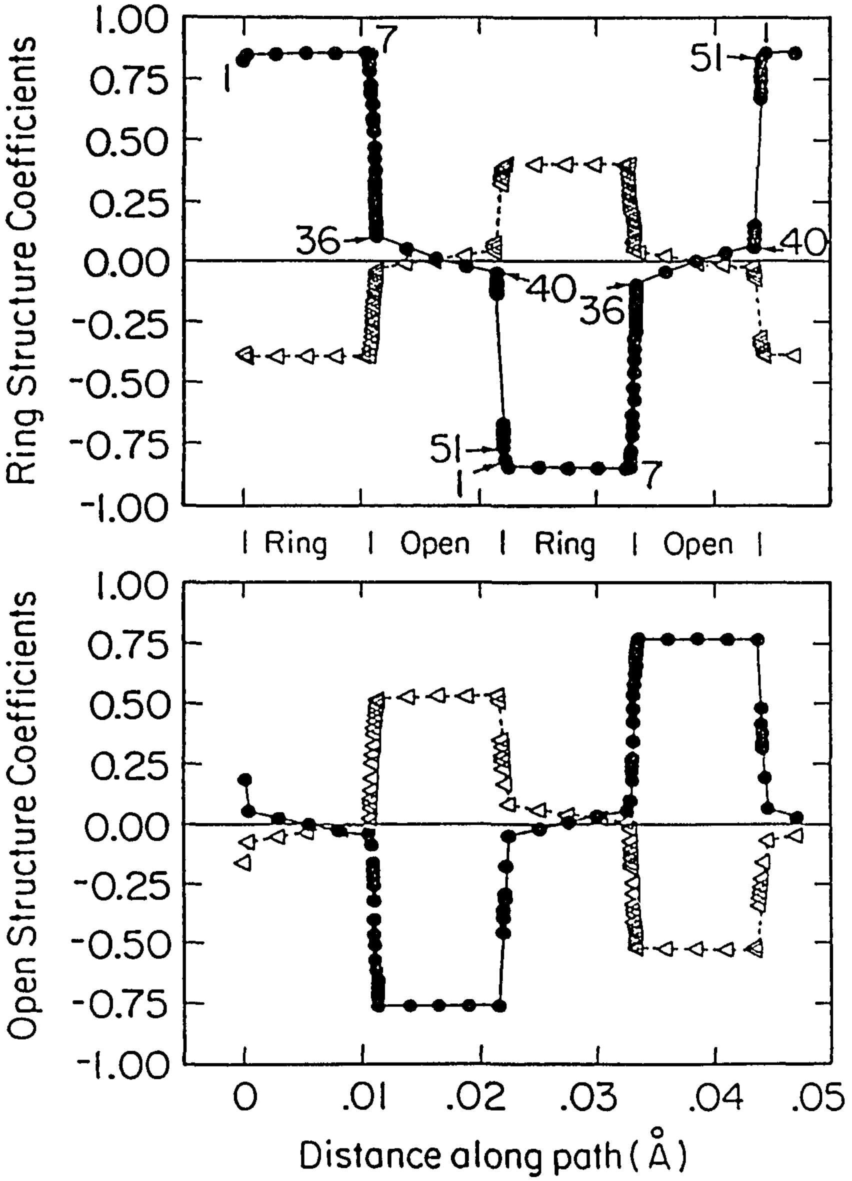

Figure 2.6. Dominant CI coefficients along path including the conical intersection (two revolutions)

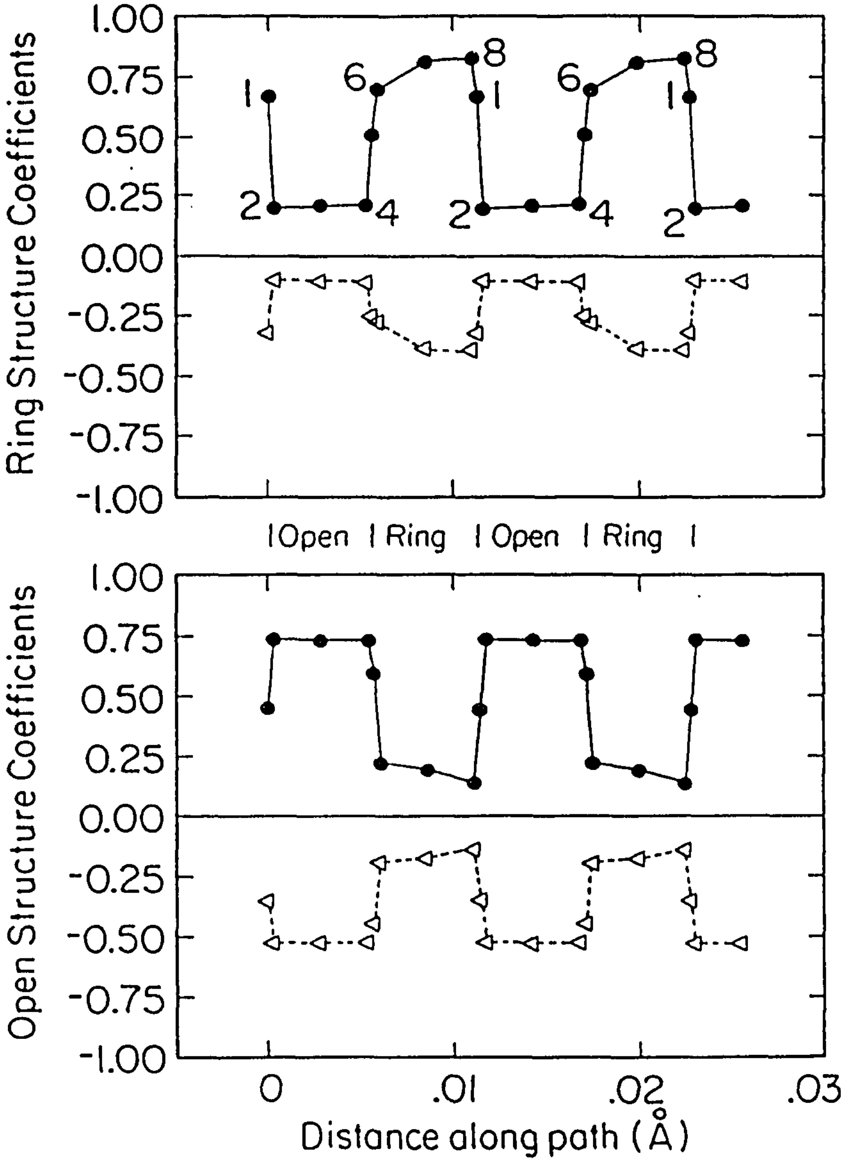

Figure 2.7. Dominant CI coefficients along path not including the conical intersection (two revolutions)

moving one revolution around the loop. The fact that the dominant CI coefficient for the ring structure does not change sign between points 2 and 4 is again directed by the positive constant value of the dominant CI coefficient for the open structure in this area. It is therefore at this point definitively proved that there exists a point where the 1-$^1A_1$ and 2-$^1A_1$ potential energy surfaces touch each other. This point lies inside the loop whose boundaries are indicated by the points 1 to 51 in Figure 2.5. Its exact location is yet to be determined.

The fact that the intersection point lies very close to the C_{2v} transition state poses the difficulty that a regular quadratic polynomial of the coordinates X and Y (or ϕ and R) does not suffice for locating both the intersection and the transition state by means of a least mean squares fit. This is because the energy of the lower surface E_- given by equation (2.3) contains the square root of the sum of the squares of the elements H_{11}, H_{22} and H_{12} which can be considered to vary linearly with the coordinates X and Y (or ϕ and R correspondingly) in the neighbourhood of the intersection point. On the other hand around the transition state the energy of the lower state varies as a quadratic function of these coordinates. The energy of about 55 points in the domain $83.3° \leq \phi \leq 83.8°$ and 1.42 Å $\leq R \leq 1.46$ Å is fitted to a regular quadratic polynomial by a least mean square fit to locate the transition state. The standard deviation of the fit is 1.37%. For the location of the intersection point the square of the energy difference between the two states is fitted to a regular quadratic polynomial in the domain: 1.46 Å $\leq R \leq 1.49$ Å and $83.0° \leq \Phi \leq 83.4°$. The number of points used in this fit is 50 and the standard deviation 1.76%. The two fits yielded the following values for the internal coordinates of the transition state and the intersection point respectively:

Transition state : $\phi^* = 83.574°$, $R^* = 1.438$ Å

Intersection point : $\phi^i = 83.180°$, $R^i = 1.476$ Å

In order to investigate whether the C_{2v} saddle point is the real transition state for the ring opening it is necessary to obtain the sign of the eigenvalue of the hessian along the symmetry breaking mode pointing at a direction away from the C_{2v} surface. For this purpose the energy is computed at a geometry having internal coordianates $\phi = \phi^* = 83.574°$, $R_1 = R^*+0.01 = 1.448$ Å and $R_2 = R^*-0.01 = 1.428$ Å. The 2 state-averaged MCSCF energy of the fitted transition state in C_{2v} is $E^* = -224.46339315$ which is 5 μhartree higher than the corresponding value of the energy computed by optimizing only the lower state (i.e., without state avaraging). Upon asymmetric distortions of the two O-O bond lengths the symmetry of the system is lowered from C_{2v} to C_s and the two potential energy surfaces which had a_1 symmetry in C_{2v} now transform according to the a′ irreducible representation of the C_s point group. The two (1-^{1}A′ and 2-^{1}A′) state-averaged MCSCF energy of the new point with asymmetric bond lengths is -224.463320356 (above E^*) indicating that the curvature of the potential energy surface and therefore the corresponding eigenvalue of the hessian is positive along the symmetry breaking mode. This means that the fitted structure for the C_{2v} saddle point is the true transition state for the ring opening on the full ^{1}A′ ground state potential energy surface.

The next topic to be addressed is whether the ring opening reaction path, its projection on the C_{2v} surface shown in Figure 2.1 as a function of ϕ for each value of which R is optimized, lies exclusively on the C_{2v} ground state $^1A_1$ PES. In order for this to be true it is necessary that the curvature of the PES is positive along the symmetry breaking mode going away from the C_{2v} geometry which minimizes the energy for each ϕ. Additional MCSCF evaluations of the energy on the $^1A'$ ground state potential energy surface for the values of $\phi = 65^\circ, 70^\circ, 80^\circ, 85^\circ, 90^\circ, 95^\circ, 100^\circ$ and 110° with R asymmetrically varied by ±0.01 Å from the corresponding value that minimizes the C_{2v} energy for each of the above values of ϕ are performed. In all cases the energy of the asymmetrically distorted C_s geometry is higher than the corresponding minimum energy on the C_{2v} surface having the same ϕ. This indicates that the C_{2v} minimum energy path lies at the bottom of a valley in the complete $^1A'$ ground state PES. It is therefore concluded that the ring opening proceeds via a C_{2v} preserving path.

F. Exploration of parts of the complete ground state $^1A'$ PES

1. Usefulness of the $^1A'$ ground state PES

As it was mentioned earlier the complete ground state $^1A'$ PES is a hypersurface in 4 dimensions since the energy is a function of 3 internal coordinates: $E = E(\phi, R_1, R_2)$. It was also established that all important features of the ground state PES which involve the ring and open structures, the transiton state for the ring opening as well as the path connecting these two minima all lie on the C_{2v} subspace defined by the constraint $R_1 = R_2$. However this C_{2v} subspace is not sufficient for a complete description of the O_3 dissociation process since it can only account for a dissociation channel along the C_{2v} preserving mode. This channel proceeds, starting from the open structure, on the bottom of a valley along which the O-O-O angle ϕ is continuously decreasing and the O-O bond lengths are adjusted simultaneously. It has to overcome a barrier of 53 kcal/mole in order to reach the ring minimum releasing at the same time 23 kcal/mole. From the ring minimum this particular dissociation channel proceeds over a barrier of 32 kcal/mole on a path along which the central oxygen is pulled away ending up as $O(^3P)$ while the two end oxygens come close together to form O_2. The exothermicity from the ring minimum to the dissociation products is 23.5 kcal/mole. This is a very unlikely situation due to the existence of large barriers along the path shown in Figure 2.1.

An alternative route for dissociation of O_3 is along the C_{2v} symmetry breaking mode starting at the open minimum. Following this path one of the end oxygens approaches the central atom in order to form O_2 while the other end oxygen departs ending up to $O(^3P)$. The barrier along this path is most probably smaller than the one required for the C_{2v} preserving dissociation in which case the latter dissociation channel is favorable. It is also of interest to investigate the fashion in which the angle ϕ changes along the C_s dissociation channel. However in order to do so various parts of the ground state $^1A'$ PES should be investigated a fact which requires the energy evaluation at many more nuclear conformations. One additional computational difficulty lies in the fact that the wavefunction should resemble the overall symmetry of the complete PES (a' in C_s) therefore requiring additional terms to a total of 8029 configurations.

2. The panel for ϕ=116.31°

One way of depicting the complete 4-dimensional ground state $^1A'$ PES is through various 3-dimensional cuts (panels) on which the energy is plotted as a function of any two internal coordinates while the third one is kept constant. By choosing ϕ as the coordinate which is held constant one obtains the stretching potentials for nuclear motion as a function of R_1 and R_2 for each value of ϕ. The stretching potential as a function of R_1 and R_2 for $\phi = 116.31°$ is shown in Figure 2.9. The potential rises from a shallow well (corresponding to the ground state minimum of O_3) smoothly to an atom-plus-diatomic channel along the valley corresponding to $O_2 + O$. An interesting feature of this potential not found in an analogous plot by Wilson and Hopper (1981) is that there exists a transition state along the dissociation channel for $\phi = 116.31°$. Its internal coordinates are $R_1 = 1.233$ Å and $R_2 = 1.759$ Å and its energy $E = -224.5282606$ hartree. The barrier of the dissociation process, keeping ϕ fixed at 116.31°, is therefore 15.1 kcal/mol which is below the barrier needed for C_{2v} preserving dissociation. It is therefore at this point concluded that dissociation is favored along a C_s path rather along a C_{2v} path.

The next step is to locate the real transition state of the dissociation along the C_s path in the $^1A'$ surface. The gradient of the energy at the saddle point on the $\phi = 116.31°$ panel has zero components as regards the R_1 and R_2 internal coordinates but a non-zero component as regards the bending angle ϕ, indicating that it is not a stationary point on the complete ground state PES. Furthermore the hessian of the energy computed at this point has only one negative eigenvalue indicating that it lies on the downhill reaction path from the true transition state.

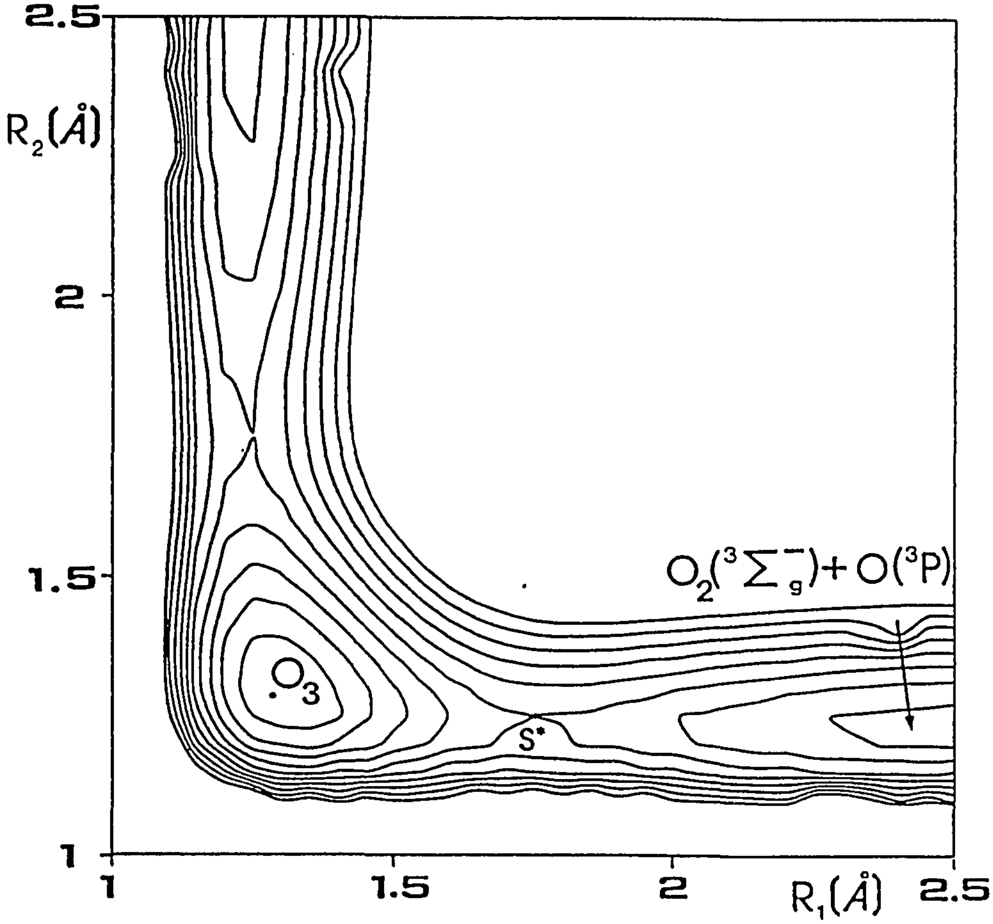

Figure 2.8. Energy as afunction of the O-O bond lengths R_1, R_2 for ϕ=116.31°. Increment: 5 mhartree

A transition state search going uphill on the direction of the negative eigenvalue of the hessian from the saddle point at the $\phi = 116.31°$ panel yielded a structure having internal coordinates $\phi = 114.90°$, $R_1 = 1.234$ Å $R_2 = 1.759$ Å and zero-gradient. Furthermore the hessian of the energy computed at this point has 2 positive (63.3 and 422.5 cm^{-1}) and one negative (96.3 cm^{-1}) eigenvalues indicating that this is the true transition state on the complete ground state $^1A'$ surface for the dissociation process along a C_s path. The barrier for the O_3 dissociation is calculated to be 11.73 kcal/mol including the harmonic zero point energies of the open minimum and the O_3 dissociation transition state which are 4.03 and 0.7 kcal/mol respectively.

G. Conclusions

A thourough examination of the ground state potential energy surface of O_3 in the full valence space FORS MCSCF approximation using a wavefunction with as many as 4067 terms has revealed the existence of a ring species having D_{3h} symmetry. This minimum has a O-O-O angle of 60° and a O-O bond length of 1.470 Å and lies 29.8 kcal/mol above the C_{2v} ground state which has an angle of 116.31° and a bond length of 1.299 Å. More importantly it lies above the O_3 dissociation limit which is 26.1 kcal/mol (experimental value). The ring opening occurs along a path lying exclusively on the ground state $^1A_1$ PES therefore having C_{2v} symmetry. The transition state for the ring opening has an angle of 83.6° and a bond length of 1.440 Å lying 26.0 kcal/mol above the ring minimum. In the neighbourhood of the transition state there exists a conical intersection of the potential energy surfaces corresponding to the 1-$^1A_1$ and 2-$^1A_1$ states. Its presence has been definitively proved by minitoring the sign of the MCSCF wavefunction on a closed loop around it. This is the first time that a conical intersection of two states having the same symmetry has been observed in a real polyatomic system. Furthermore the transition state for O_3 dissociation is located on the ground state $^1A'$ potential energy surface in the full valence space FORS MCSCF approximation (8029 configurations). It corresponds to a structure having a O-O-O angle ϕ=114.90° and asymmetric bond lengths R_1 = 1.234 Å and R_2 = 1.759 Å. The barrier for O_3 dissociation to O_2 + O in their ground states along the symmetry breaking mode is calculated to be 11.73 kcal/mol favoring the dissociaton along a C_s rather a C_{2v} channel. Table 2.2 lists the internal coordinates, the energies and the assignment of all critical points on the ground state $^1A'$ potential energy surface of O_3.

Table 2.2. Critical points on the ground state $^1A'$ PES of O_3.

ϕ°	R_1 (Å)	R_2 (Å)	E (hartree)	Assignment	ΔE^a (Kcal/mol)
116.31	1.299	1.299	-224.5523175	Open minimum	0.00
60.00	1.470	1.470	-224.5041628	Ring minimum	29.82[b]
83.57	1.438	1.438	-224.4633832	Ring opening T.S.	55.8
116.31	1.233	1.759	-224.5282606	Saddle point	15.10
114.90	1.234	1.759	-224.5283207	T.S. for O_3 dissociation	11.73[b]
83.18	1.476	1.476		Intersection of 1-$^1A_1$ and 2-$^1A_1$ PES	

---

[a]: with respect to the C_{2v} open minimum.

[b]: including harmonic zero point energies.

III. POTENTIAL ENERGY SURFACE OF THE GROUND STATE OF CO_2

A. Introduction

Although carbon dioxide is a thoroughly studied molecule, being the end product of most combustion processes and G. Herzberg's (1966) book devotes more space to it than to any other triatomic molecule, almost all accurate calculations to date pertain to properties of the linear form of the $^1\Sigma_g^+$ ground state, leaving the rest of the potential energy surface unexplored. These parts of the adiabatic surface may reveal the existence of additional metastable species which could serve as intermediates in chemical reactions and an examination of the surface may provide information regarding interconversions between them, pertaining to possible reaction mechanisms. A quantitative knowledge of the surface also provides the basis for dynamical calculations.

For the chemical reaction of carbon with molecular oxygen, experimental data by Husain and Young (1975) suggest that $C(^3P)$ reacts rapidly with O_2, whereas the reaction of $C(^1D)$ with O_2 is not so fast according to Braum et. al. (1969) and Husain and Kirsh (1971). As regards the mechanism of this reaction, it is readily understood that an "end-on" attack of carbon on molecular oxygen gives an intermediate linear structure of the type C-O-O which then decomposes to CO + O, whereas an alternative attack of carbon on the π bond of the molecular oxygen leads to an intermediate cyclic carbene-type CO_2 isomer which rapidly opens up to the linear ground state according to Shevlin (1980). For the aforementioned processes the allowed electronic states of reactants and products are subject to the Wigner-Whitmer (1928) rules and depend upon the relative energies of the various atomic and molecular electronic states (cf. Moore, 1958). These constraints led Husain and Donovan (1970) in the construction of correlation diagrams connecting the states of C + O_2 and CO + O. They also suggest that possible intersections of the potential energy surfaces may exist. The latter can however be verified and determined only by exploring sufficiently large parts of the adiabatic potential surfaces of more than one electronic state.

B. Method of calculation

The reliable determination of global energy surfaces requires unbiased flexibility in the configuration mixing and orbital optimization. To this end, an MCSCF calculation in the full optimized valence space with an adequate basis set (sufficiently extended plus polarization functions) represents a very accurate approach. In the case of CO_2 this requires a configuration space generated by allowing the 16 valence electrons to be rearranged among 12 reactive orbitals. Such a wavefunction possesses the flexibility needed to account for any configurational changes which may occur at various points of the surface. The remaining 6 electrons can be safely assumed to reside in the three closed 1s core orbitals. The lowest spatial symmetry of the molecular system consisting of a carbon and two oxygen atoms is C_s and the number of configurations generated in the full valence space for the $^1A'$ representation is 35793. However, since both the cyclic isomer to be discussed below as well as the linear structure of the ground state have C_{2v} symmetry, it is of interest to examine first the part of the energy surface describing the ring opening to the linear geometry under preservation of C_{2v} symmetry. Within this higher symmetry the ground state belongs to the $^1A_1$ representation and the number of configurations is reduced to 18009. It is only in recent times that it has become possible to calculate large regions of energy surfaces in a configuration space of such magnitude with an extended basis set and very few have been reported.

We use the Dunning and Hay (1977) basis set plus polarization functions consisting of the segmented contractions (9s5p1d/3s2p1d) on both carbon and oxygen. For the d-type polarization functions the exponents ζ_c=0.75 and ζ_o=0.85 are used for carbon and oxygen respectively. This choice of the basis set encompasses a total of 45 functions. All geometry optimizing calculations are performed using the GAMESS program by Dupuis et. al. (1980) while all other single point energy calculations are performed with the MOLPRO program of Knowles and Werner (1984).

C. Mapping of the complete ground state $^1A'$ PES

The purpose of this study is to establish reliable information on the global ground state $^1A'$ potential energy surface of CO_2. On this surface the energy depends on three variables, e.g. the O-C-O angle ϕ and the two C-O bond lengths R_1 and R_2. Two-dimensional contour maps on which any of the above internal coordinates has a constant value depict cross sections through it. On these cross sections the energy is a function of the remaining two internal coordinates. The investigation proceeds in the following stages. First the optimal isosceles-triangle geometries having C_{2v} symmetry are calculated for the $^1A_1$, $^1A_2$, $^1B_1$ and $^1B_2$ states as functions of the single variable ϕ by setting $R_1 = R_2 = R$ and determining the value of R which minimizes the energy for each ϕ. The energy as a function of ϕ in these curves depicts the C_{2v} constrained dissociation $OCO \rightarrow C + O_2$. Then the entire C_{2v} ground state $^1A_1$ surface is computed within the full valence space FORS MCSCF approximation as a function of the coordinates ϕ and $R_1 = R_2 = R$. This PES unveils the existence of a cyclic carbene-type metastable species and governs its C_{2v} constrained conversion to the linear ground state. Finally, energies are determined for various cross sections of the complete ground state PES which have $R_1 \neq R_2$ and therefore lower symmetry (C_s). The electronic wavefunctions in this case are also obtained by MCSCF calculations in the full valence space and have 35793 configurations. Various cross sections corrsponding to $\phi = 0^\circ$, 94° and 180° are also calculated. The first two correspond to the exchange of O atoms with CO according to

$$O_\alpha C(^1\Sigma^+) + O_\beta(^1D) \rightarrow O{=}C{=}O(^1A_1;\phi) \rightarrow O_\alpha(^1D) + CO_\beta(^1\Sigma^+)$$

at the various angles ϕ respectively whereas the last one to the colinear reaction

$$C(^3P) + O_2(^3\Sigma_g^-) \rightarrow CO(^1\Sigma^+) + O(^1D)$$

Study of these cross sections provide useful insight in the understanding of the CO_2 dissociation mechanism to various products while at the same time investigate the possibility that other metastable species corresponding to different permutations of the nuclei among each other may exist on the ground state potential energy surface.

D. The lowest singlet states in C_{2v}

The potential energy curves for the ${}^1A_1$, ${}^1A_2$, ${}^1B_1$ and ${}^1B_2$ states of CO_2 are shown in Figure 3.1. The energy is plotted against the O-C-O angle ϕ while at the same time the C-O bond lengths are kept equal and relaxed by minimizing the energy for each value of ϕ. All energies are computed in the full valence space FORS MCSCF level using wavefunctions with as many as 18009, 17496, 17784 and 17496 configurations for the ${}^1A_1$, ${}^1A_2$, ${}^1B_1$ and ${}^1B_2$ states respectively. As it can be seen from Figure 3.1 there exist double minima on the C_{2v} potential energy curves for all states. Their internal coordinates and their relative energies with respect to the ground state ${}^1\Sigma_g^+$ minimum are shown in Table 3.1. These potential energy curves also describe the dissociation of the various states along a C_{2v} preserving path during which the central carbon is pulled away on the bisector of the O-O bond while the two end oxygens come together to form O_2 in its ground state. The ${}^1A_1$, ${}^1A_2$ and ${}^1B_1$ states correlate with C and O_2 in their ground states respectively while the ${}^1B_2$ state correlates with the ground state of $O_2({}^3\Sigma_g^-)$ and carbon in its ${}^1D$ first excited state as it is shown schematically in Figure 3.1 for small angles of ϕ. For $\phi = 180°$ the correlation of the above states with the ground and excited states of linear CO_2 is also indicated. It is worth noticing that the 3 singlet excited states of linear CO_2 do not correspond to minima on the analogous potential energy surfaces. As Figure 3.1 indicates the 3 singlet excited

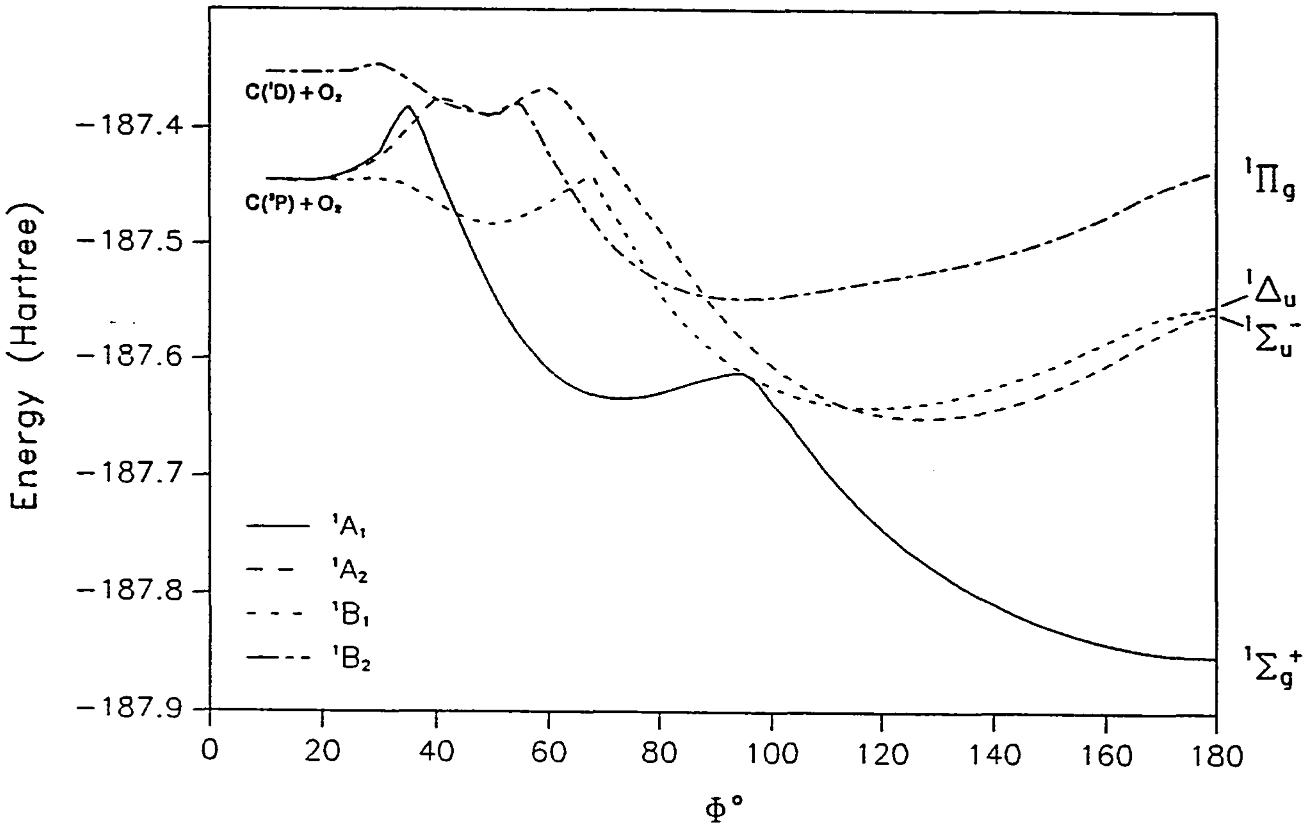

Figure 3.1. Dependence of the energies of the lowest $^1A_1$, $^1A_2$, $^1B_1$ and $^1B_2$ states of CO_2 upon the O-C-O angle ϕ when the two C-O distances are kept equal (C_{2v} symmetry) and are optimized for each ϕ

Table 3.1. Minima for the various C_{2v} states of CO_2

State	ϕ°	R (Å)	E (hartree)	ΔE^a (kcal/mol)
$^1A_1$	180.00	1.176	-187.8526012	0.0
	73.10	1.339	-187.6333377	137.6
$^1A_2$	127.01	1.272	-187.6497734	127.3
	48.35	1.711	-187.3913420	289.4
$^1B_1$	118.18	1.269	-187.6405622	133.1
	49.61	1.604	-187.4818999	232.6
$^1B_2$	94.67	1.363	-187.5463073	192.2

[a]: with respect to the ground state $^1\Sigma_g^+$ minimum.

states of CO_2 have C_{2v} rather than $D_{\infty h}$ symmetry.

The variation of the C-O and O-O optimized bond lengths as a function of ϕ is shown in Figures 3.2 and 3.3 for all singlet states in C_{2v}. These plots monitor the fashion in which the internal coordinates change along the C_{2v} preserving dissociation paths for all singlet states. For small values of ϕ in Figure 3.3 they all end up in the same asymptotic limit (1.23 Å) which is the O-O distance in $O_2(^3\Sigma_u^-)$ in the full valence space FORS MCSCF level of theory since they all correlate with the ground state of O_2.

E. The C_{2v} potential energy surface for the $^1A_1$ state

1. The ring minimum

As it can be seen from Figure 3.1 on the ground state $^1A_1$ surface besides the linear ground state there exists another minimum corresponding to a C_{2v} structure with an O-C-O angle of ϕ=73.1° and a C-O bond length of $R_1 = R_2 = 1.339$ Å lying 137.6 kcal/mol above the linear ground state. In order to establish whether this is a true minimum on the complete $^1A'$ potential energy surface, the curvature of this surface away from the C_{2v} symmetry is investigated by computing the energy at a geometry having the same value of ϕ (73.1°) and unequal bond lengths one being the same and the other differing by -0.01 Å from the corresponding ones of the ring structure. The MCSCF energy of this point (ϕ = 73.10°, R_1 = 1.339 Å, R_2 = 1.349 Å) is -187.6332739 hartree which is higher than the energy of the C_{2v} structure, listed in Table 3.1, indicating that the latter is indeed a minimum on the ground state $^1A'$ potential energy surface.

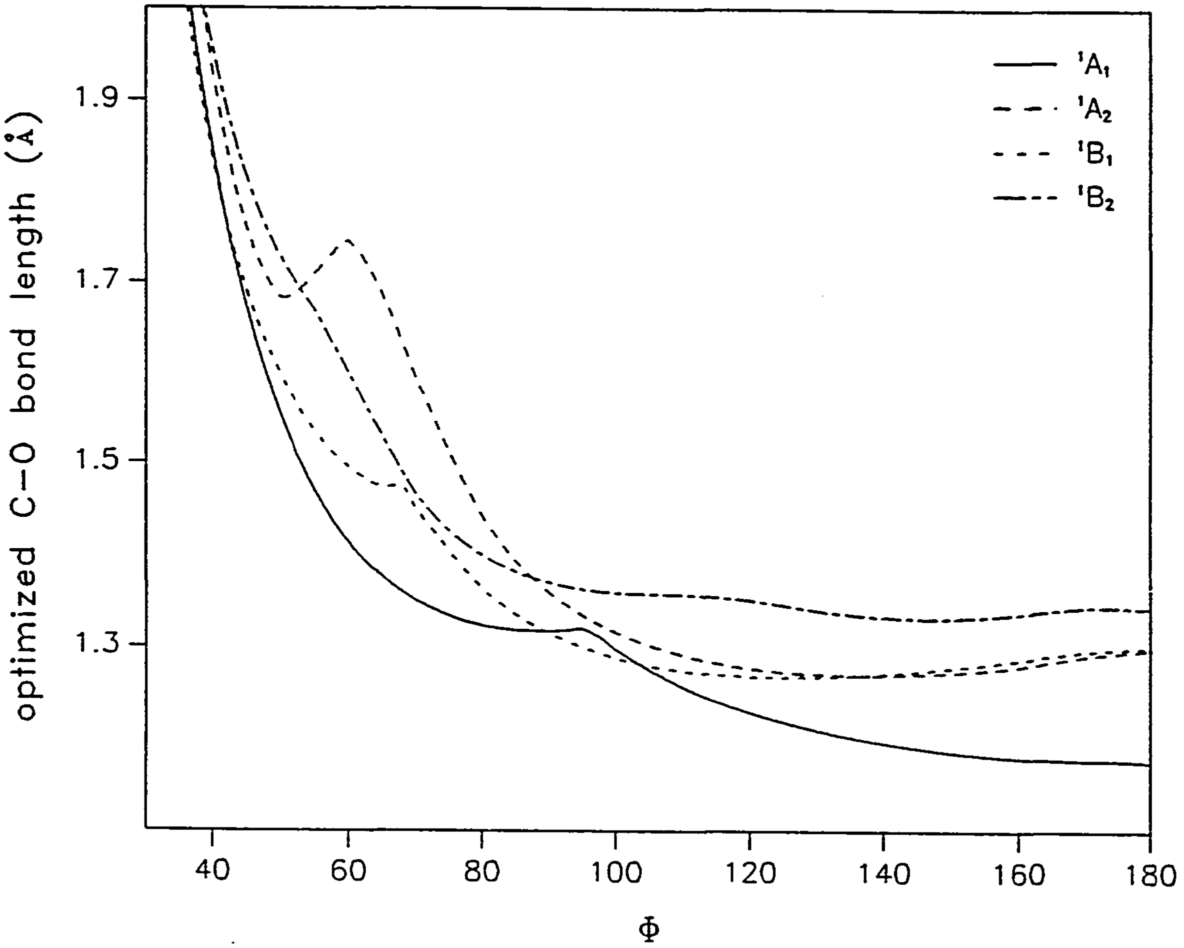

Figure 3.2. Variation of the optimized C-O bond lengths for the various C_{2v} states of CO_2 with angle ϕ

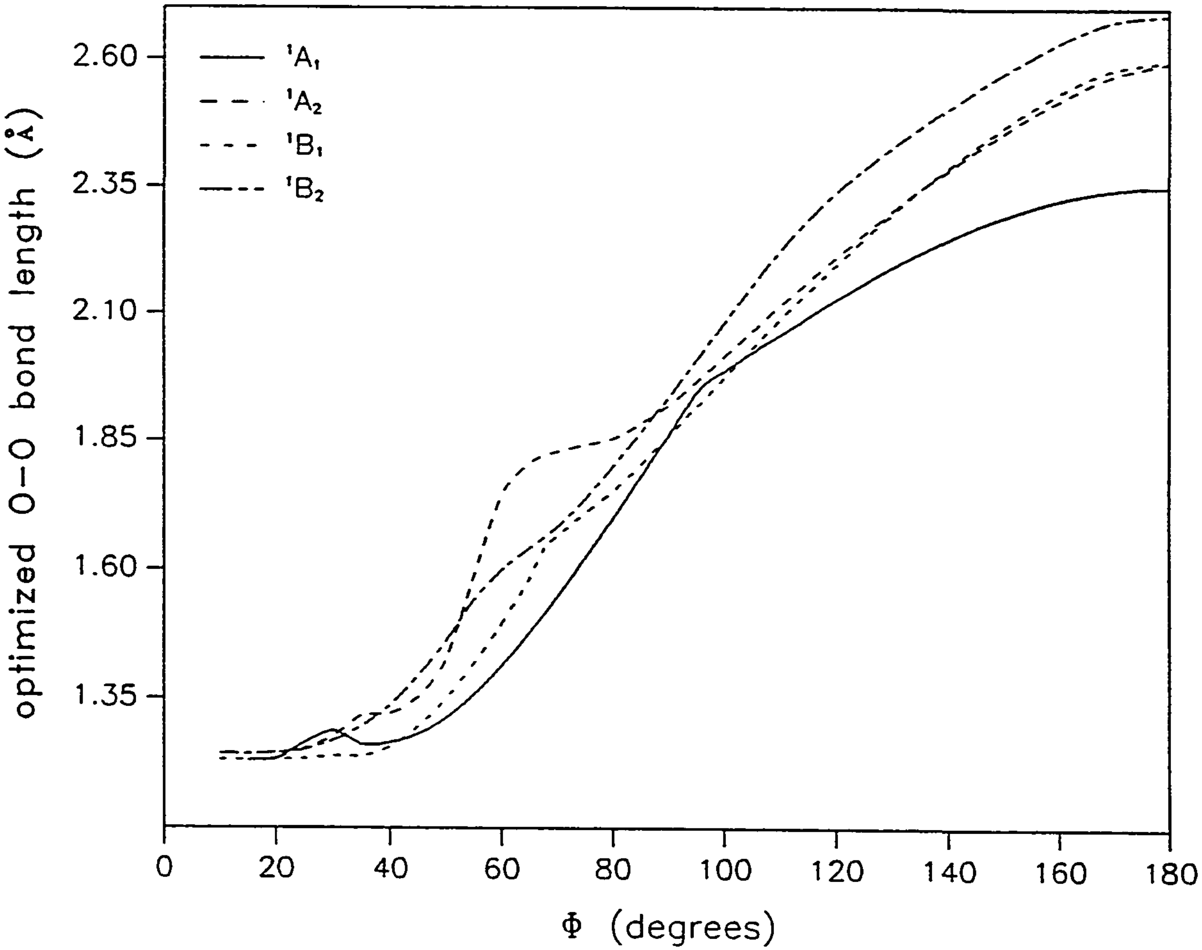

Figure 3.3. Variation of the optimized O-O bond lengths for the various C_{2v} states of CO_2 with angle ϕ

Table 3.2. Critical points on the C_{2v} energy surface of CO_2 ground state

ϕ°	R_{C-O} (Å)	Energy (a.u.)	Barrier[a]	ΔE[b]	Method	Reference
			(kcal/mol	)		
Linear $^1\Sigma_g^+$ ($D_{\infty h}$)						
180	1.162				exp. value	Herzberg (1966)
	1.153	-187.55972			SCF/[5s4p]	Pakansky et.al. (1975)
	1.176	-187.85260			MCSCF-18009 CSFs/DZP	Xantheas et. al. (1990)
	1.156	-188.10544			MP4/6-31G*	Illies et. al. (1987)
	1.160	-188.31141			MRCI[b]/[9s5p4d1f]	Knowles et. al. (1988)
Bent $^1A_1$ (C_{2v})						
63.7	1.374	-184.93281			SCF/STO-3G	Lathan et. al. (1973)
		-187.06714		161.3	SCF/4-31G	Lathan et. al. (1973)
68.7	1.298	-187.46202			SCF/Huzinaga [7s5p1d]	Xantheas et. al. (1990)
79.1	1.298	-187.46252			SCF/Huzinaga [7s6p1d]	Xantheas et. al. (1990)
79.1	1.304	-187.49760		111.3	MCSCF-2 config./DZP	Feller et. al. (1980)
		-187.88320		128.6	SD-CI/DZP	FEller et. al. (1980)
		-187.92860		136.8	SDQ-CI/DZP	Feller et. al. (1980)
73.1	1.339	-187.63334		137.6	MCSCF-18009 config./DZP	Xantheas et. al. (1990)
C_{2v} transition state						
97.8	1.298		0.5		MCSCF-2 config./DZP	Feller et. al. (1980)
			7.6		SD-CI/DZP	Feller et. al. (1980)
			9.0		SDQ-CI/DZP	Feller et. al. (1980)
94.2	1.320		14.0		MCSCF-18009 config./DZP	Xantheas et. al. (1990)

[a]: E(T.S) - E(bent minimum)

[b]: E(bent minimum) - E(linear minimum)

The point having asymmetric bond lengths has C_s symmetry and requires a wavefunction with as many as 35793 configurations in the full valence space FORS MCSCF (a′ irrep).

The geometries of the two minima as well as that of the C_{2v} transition state for ring opening all lying on the ground state $^1A_1$ potential energy surface, together with results from some previous calculations, are listed in Table 3.2. Most previous calculations by Krauss and Neumann (1972), England (1981) and England et. al. (1976) did not discover the bent minimum because they did not explore the range at sufficiently small values of ϕ. One three-configuration MCSCF calculation by Kombs and Lunell (1983) in which the O-C-O angle was varied from 60°-180°, failed to locate the bent minimum because the C-O distance was kept constant at the equilibrium value (1.162 Å) of the linear species. From the mentioned comparisons, the need for exploring large parts of the adiabatic potential energy surface using a level of theory which involves a large, unbiased configuration space and an extended basis set is apparent.

2. PES governing the ring opening process

Once the existence of the two minima on the ground state PES is established, it is desirable to investigate the mechanism of their interconversion. The ring opening process is governed by the ground state potential energy surface. Since the bent structure has C_{2v} symmetry and the linear ground state $D_{\infty h}$ symmetry respectively, the ring opening can, as a first guess, be thought as occurring along a C_{2v} preserving path. Along this path the O-C-O angle ϕ increases from 73.1° to 180° while at the same time the two C-O bond lengths change but remain equal. The C_{2v} symmetry

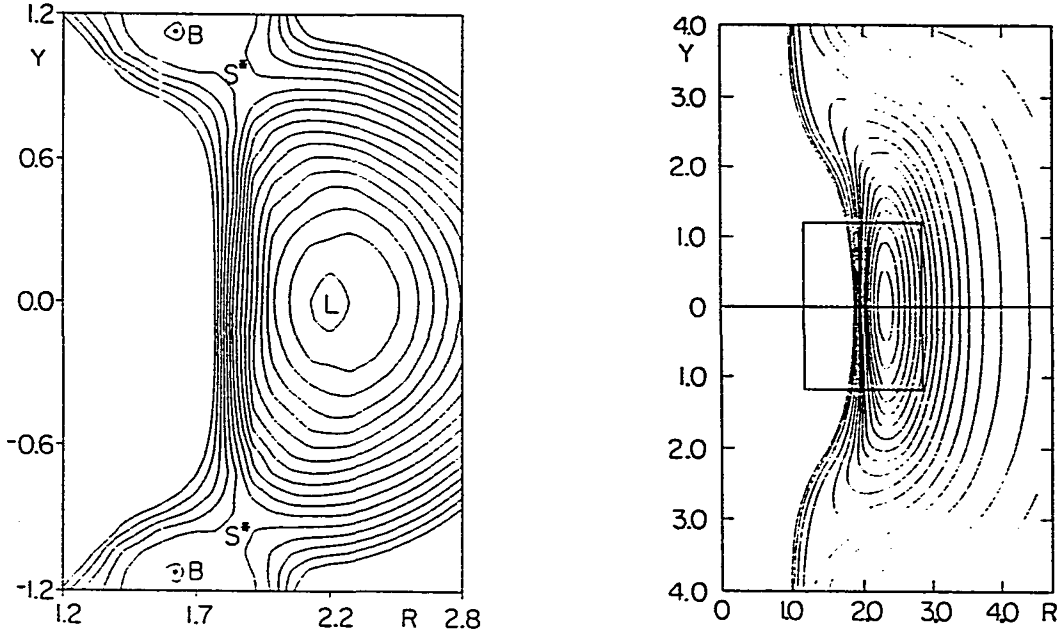

Figure 3.4. Left Surface: Ab initio energy contours for the C_{2v} constrained ring opening of triangular CO_2. Right surface: Spectroscopically estimated contours of Herzberg (1986, p.589). The coordinate area covered by the left figure corresponds to the area indicated by the frame on the right figure. Abscissa: O-O distance (Å). Ordinate: distance from C to O_2 midpoint (Å). Contour increment: 20 mhartree. L: linear minimum, B: bent minimum, S^*: saddle point.

restricted $^1A_1$ potential energy surface of CO_2 is depicted by the energy contours on the left hand side of Figure 3.4, where the coordinates are the O-O distance (abscissa x) and the perpendicular distance of the C nucleus from the O-O line (ordinate y). About 130 points of the $^1A_1$ surface are determined and the energy contours are plotted with an increment of 20 mhartree. For each of these points an MCSCF calculation is carried out in the 18009 dimensional configuration space, consuming approximately 5 hrs. of Cray-2 CPU time on the average. L corresponds to the linear ground state, B to the bent minimum and S^* to the C_{2v} restricted transition state. The same coordinate system was used by Herzberg (1966, p.436) in an analogous plot of the same surface which is shown on the right hand side of Figure 3.4. It was constructed by Pariseau et. at. (1965) from experimental data by assuming an anharmonic potential expanded in Taylor series up to fourth-order terms and it does not exhibit a minimum other than the linear structure.

3. Location of the ring opening transition state

The C_{2v} restricted saddle point, denoted as S^* in figure 3.4, has the internal coordinates $\phi^*(OCO) = 94.2°$, $R_1 = R_2 = R^*(CO) = 1.320$ Å and energy $E^* = -187.6109265$ hartree lying 14.0 kcal/mol above the ring minimum. The hessian matrix evaluated at this point has two negative eigenvalues, one corresponding to the ring opening under preservation of C_{2v} symmetry, shown in Figure 3.4, the other one corresponding to a distortion from C_{2v} to C_s. An MCSCF calculation in C_s symmetry (35793 configurations, a′ irrep) at the neighboring point:

$$(\phi = \phi^* = 94.2°, \quad R_1 = R^*+0.015 \text{ Å} = 1.335 \text{ Å}, \quad R_2 = R^*-0.015 \text{ Å} = 1.305 \text{ Å})$$

which represents an asymmetric stretch for fixed $\phi = \phi^*$, yields an energy of -187.6111919 hartree which is indeed lower than E^*. The possibility of an accidentally missed lower lying solution at the point (ϕ^*, R^*) is excluded by a full valence space MCSCF calculation at this point assuming only C_s symmetry and starting with the molecular orbitals from the aforementioned distorted geometry. The calculation yields the same orbitals and energy as the C_{2v} restricted calculation. This result indicates that the transition state of the ring opening has C_s rather than C_{2v} symmetry, corresponding to a structure with unequal C-O bond lengths. Accordingly, full valence space MCSCF calculations are made in C_s symmetry (involving a wavefunction with 35793 configurations) to determine $E(R_1, R_2; \phi)$ for various fixed angles. The energies in the following domain of the ground state PES:

$$90^\circ \le \phi \le 94^\circ, \qquad \Delta\phi = 1^\circ$$
$$1.35\ \text{Å} \le R_1 \le 1.50\ \text{Å}, \qquad \Delta R_1 = 0.05\ \text{Å}$$
$$1.20\ \text{Å} \le R_2 \le 1.30\ \text{Å}, \qquad \Delta R_2 = 0.05\ \text{Å}$$

are computed in the full valence space FORS MCSCF approximation with a wavefunction having 35793 terms. By fitting these energies to a regular quadratic polynomial with respect to the variables ϕ, R_1 and R_2 the transition state is located at $\phi^o = 91.706^\circ$, $R_1^o = 1.243$ Å, $R_2 = 1.406$ Å having an energy of $E^o = -187.61411841$ hartree which corresponds to a barrier of 12.1 kcal/mol with respect to the ring minimum. The C_s barrier is ≈15% (3 mhartree) less than the C_{2v} restricted barrier. The quality of the fit is measured by the magnitude of the mean square deviation which is 2.0%.

This result is at variance with conclusions reached by Feller, Katriel and Davidson (1980) on the basis of MCSCF calculations involving only 2 configurations, namely that the transition state for ring opening has C_{2v} symmetry. We believe that the distortion is related to an intersection between the $^1A_1$ and a $^1B_1$ surface in the vicinity of the transition state since both surfaces transform according to the a′ irreducible representation when the symmetry is lowered to C_s.

F. Exploration of the complete ground state PES $E(\phi, R_1, R_2)$

1. Introduction

As it is previously noted the energy on the complete ground state $^1A'$ surface of CO_2 within the Born-Oppenheimer approximation depends on 3 coordinates which can be chosen among any of the 3 angles, the 3 bond lengths or their combinations. By keeping any of the 3 internal coordinates fixed one obtains a 2-dimensional cut of the complete surface on which the energy depends on the remaining two internal coordinates for that fixed value of the third one. The choice of the internal coordinates on which the energy depends on is by no means unique in the sense that an arbitrary combination of any of the coordinates can be used. For example an alternative choice of the coordinates on which the energy of the complete ground state PES depends on is ϕ, $R_+ = (R_1 + R_2)/2$ and $R_- = (R_1 - R_2)/2$ where ϕ is the O-C-O angle and R_1, R_2 the two C-O bond lengths respectively. In such a case the $R_- = 0$ plane represents the situation where the two bond lengths are equal and the overall symmetry is therefore C_{2v}. The energy on the $R_- = 0$ plane depends on ϕ and R_+ (which is equal to $R_1 = R_2$) only and governs the motion of the nuclei upon preservation of C_{2v} symmetry whereas points having $R_- \neq 0$ represent asymmetric distortions away from C_{2v} symmetry. It is obvious that any combination of the 2 remaining coordinates (ϕ and R_+) can be used in order to depict the energy on the $R_- = 0$ plane. A typical example is already illustrated in Figure 3.4 where the energy is plotted as a function of $R = R_{O-O}$ and $Y = R_{C-O} \cdot \cos(\phi/2)$ on the $R_- = 0$ plane.

Different coordinate systems can be selected in order to show the variation of the energy on various 2-dimensional cuts of the complete potential energy surface while at the same time describing the various ways that the 3 nuclei can approach each other in order to form stable molecular systems as well as the various building blocks of these molecules in their appropriate electronic states. The advantage of choosing bond lengths as coordinates to describe the 2-dimensional cuts of the complete surface is that they can illustrate bond formations and breakings as well as the various dissociation channels leading to different fragments. The electronic states of the latter are derived by the extension of the Wigner-Whitmer (1928) rules in relating the states of a polyatomic molecule to the states of its fragments. For the system in hand the correlation diagram connecting the various electronic states of all possible fragments is shown in Figure 3.5. The ground state of $C(^3P)$ and $O_2(^3\Sigma_g^-)$ both being triplets correlate with the ground state of $CO(^1\Sigma^+)$ and $O(^3P)$ through a triplet PES in C_s which however does not include the ground state CO_2 which is a $^1\Sigma_g^+$ state. The latter correlates on one end to the ground states of C and O_2 but to $CO(^1\Sigma^+)$ and O in its first excited state ^3P on the other end through a $^1A'+^1A''$ PES as indicated in Figure 3.5. Since it is of interest to

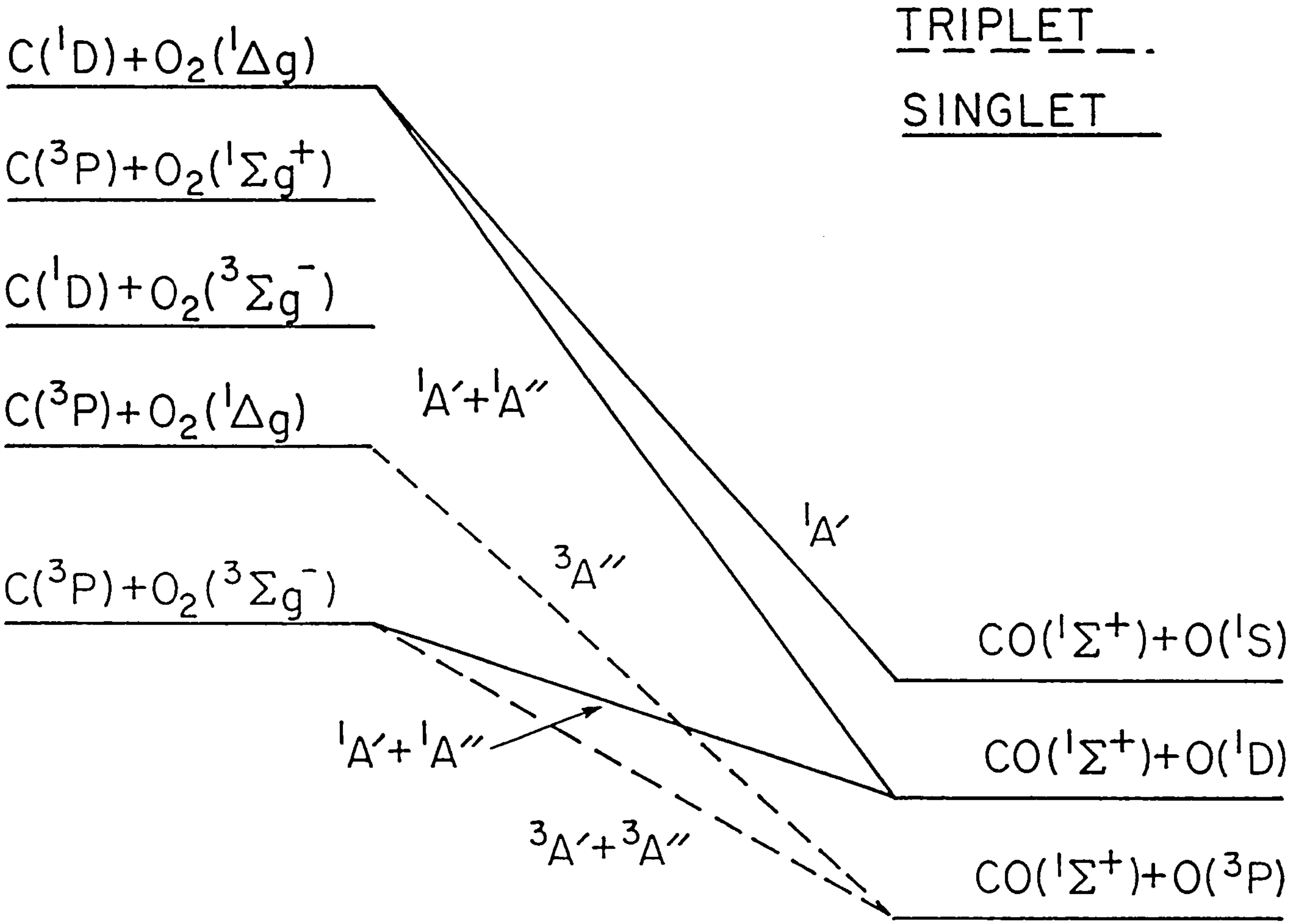

Figure 3.5. Diagram correlating the various electronic states of C and O_2 with these of CO and O

investigate the various dissociation channels of the ground state of CO_2, only parts of the complete singlet ground state are going to be calculated in C_s symmetry.

2. The panel for $\phi = 94°$

As a supplement to the discussion of section D.3 which described the location of the C_s ring opening transition state having asymmetric C-O bond lengths the panel depicting the variation of the energy with R_1 and R_2 for $\phi = 94.2°$ is calculated. The purpose of choosing this particular value of ϕ is becuase it corresponds to the C_{2v} restricted saddle point S^* shown in Figure 3.4. The variation of the energy, its contours drawn with an increment of 5 mhartree, with the two C-O bond lengths R_1 and R_2 is shown in Figure 3.6. The diagonal line represents all geometries having equal bond lengths and therefore C_{2v} symmetry. The C_{2v} symmetry restricted saddle point S^* of Figure 3.4 is also indicated on this line. It is obvious that although it is a minimum on the C_{2v} line this is not the case on the complete surface. The existence of the two minima, indicated as m on Figure 3.6 and lying 5 mhartree below S^*, at positions symmetric with respect to the C_{2v} line, suggest that S^* is not really a saddle point on the complete singlet ground state PES since the hessian of the energy evaluated at this point has two negative eigenvalues: one along the direction corresponding to the change of the O-C-O angle ϕ as shown in Figures 3.1 and 3.4 and a second along the C_{2v} symmetry breaking mode corresponding to asymmetric C-O bond lengths. The hessian of the energy at these two minima m has all positive eigenvalues on a ϕ = constant panel. However the energy of this minimum passes through a maximum value for

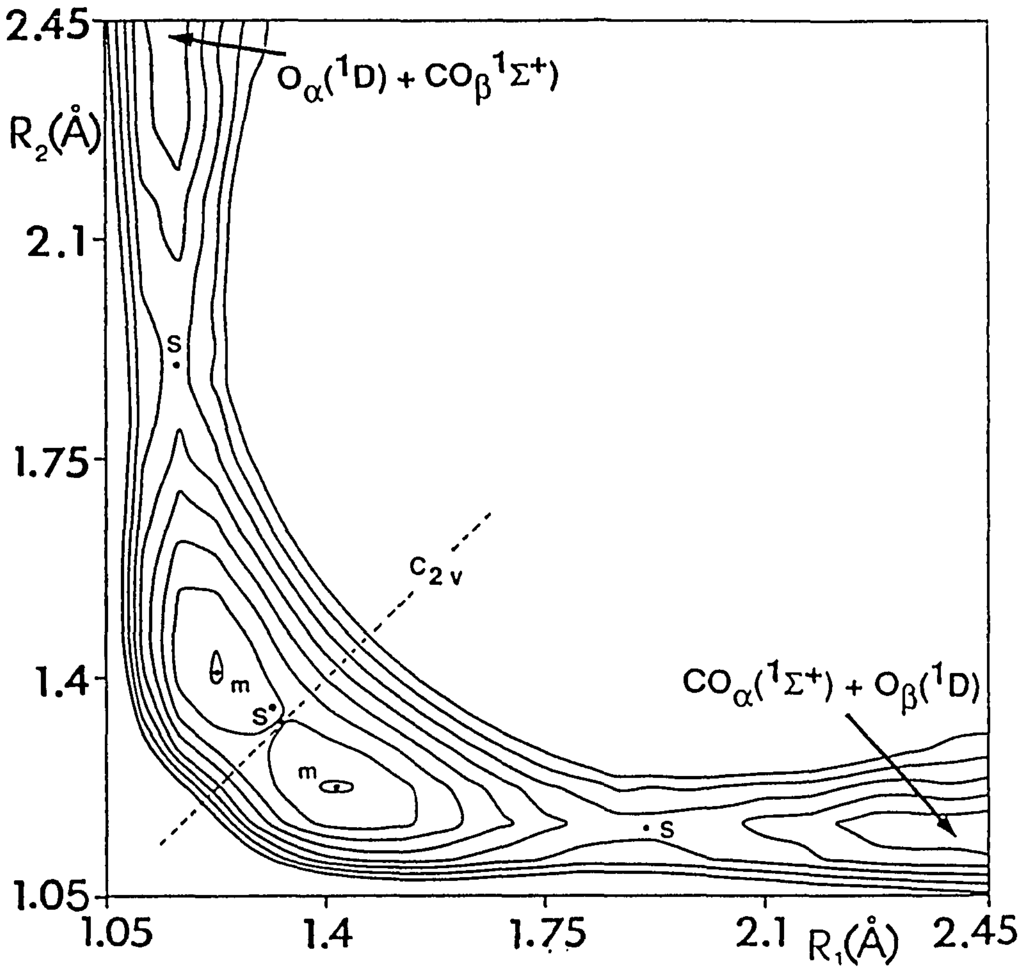

Figure 3.6. Variation of the energy with respect to the two C-O bond lengths for ϕ = 94.2°. Contour increment: 5 mhartree. S^*: C_{2v} restricted saddle point, m: minimum

$\phi = 91.706°$ and the location of the minimum for this value of ϕ on the (R_1, R_2) plane is $R_1 = 1.243$ Å and $R_2 = 1.406$ Å. This correponds to the computed in section D.3 transition state of the ring opening having asymmetric bond lengths since the hessian of the energy at this point has only one negative eigenvalue.

The fact that the computed ring structure of CO_2 is a real minimum on the C_s surface means that on an analogous panel depicting the energy variation with R_1 and R_2, on which $\phi = 73.10°$, there is only one minimum which lies on the line corresponding to C_{2v} symmetry. The ring opening process starts on a path along which the two C-O bond lengths are equal. As ϕ increases the eigenvalue of the hessian corresponding to asymmetric distortions of the C-O bond lengths gradually lessens until it becomes zero. This happens for $\phi = 90°$ as it is illustrated in Figure 3.7 with the presence of a minimum which is elongated along the perpendicular to the C_{2v} preserving direction. After this value of ϕ there appear two minima at symmetric with respect ot the C_{2v} line positions. The energies of these minima pass through a maximum value as ϕ increases. This is the transition state for the ring opening process. After the transition state there is a point where there exists an intersection of the surfaces corresponding to the $^1A_1$ and the $^1B_1$ states. Both states transform according to the same irreducible representation (a') as the symmetry is lowered to C_s. This intersection occurs in the domain $95.25° \leq \phi \leq 96.25°$. An enlargement of the intersection domain of the states $^1A_1$ and $^1B_1$ is shown in more detail in Figure 3.8 where the optimized values of R for both states are also indicated in parentheses. After the intersection area (i.e. for $\phi > 97°$) the ring opening proceeds with the increase of ϕ along a valley with

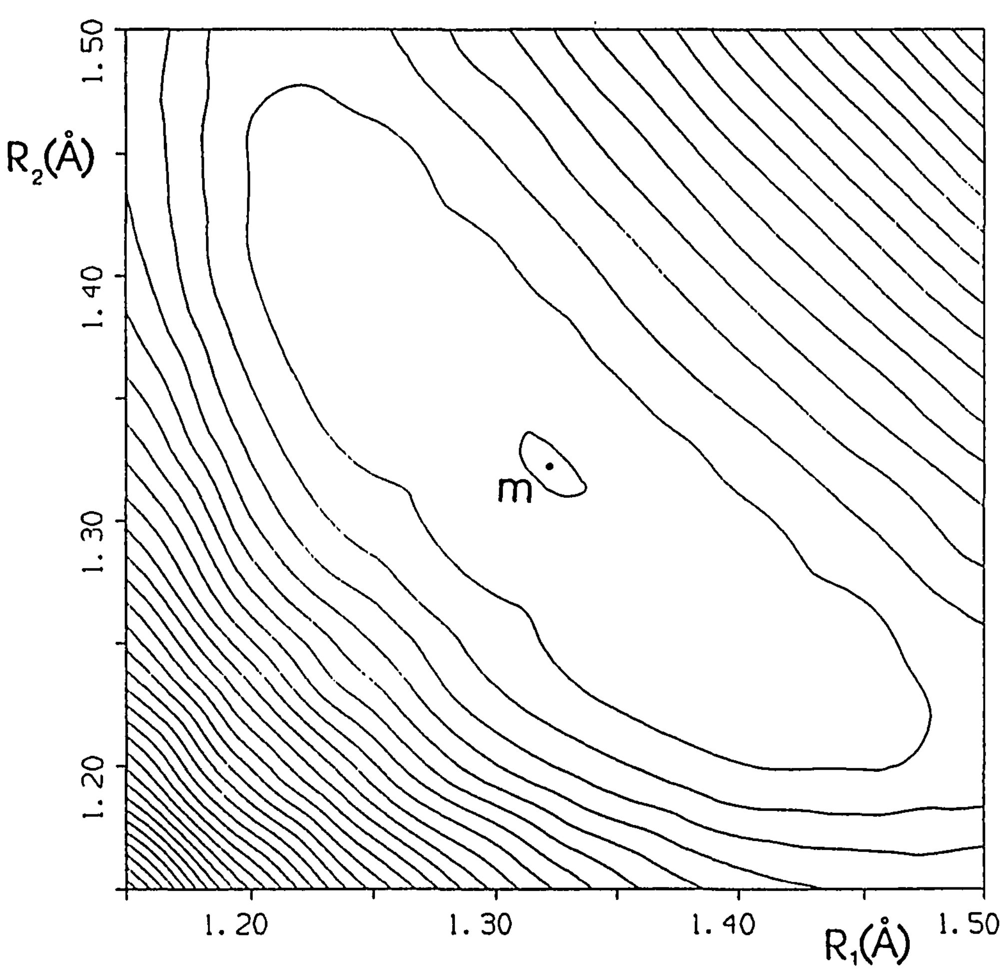

Figure 3.7. Variation of the energy with respect to the two C-O bond lengths for $\phi = 90^\circ$. m: minimum

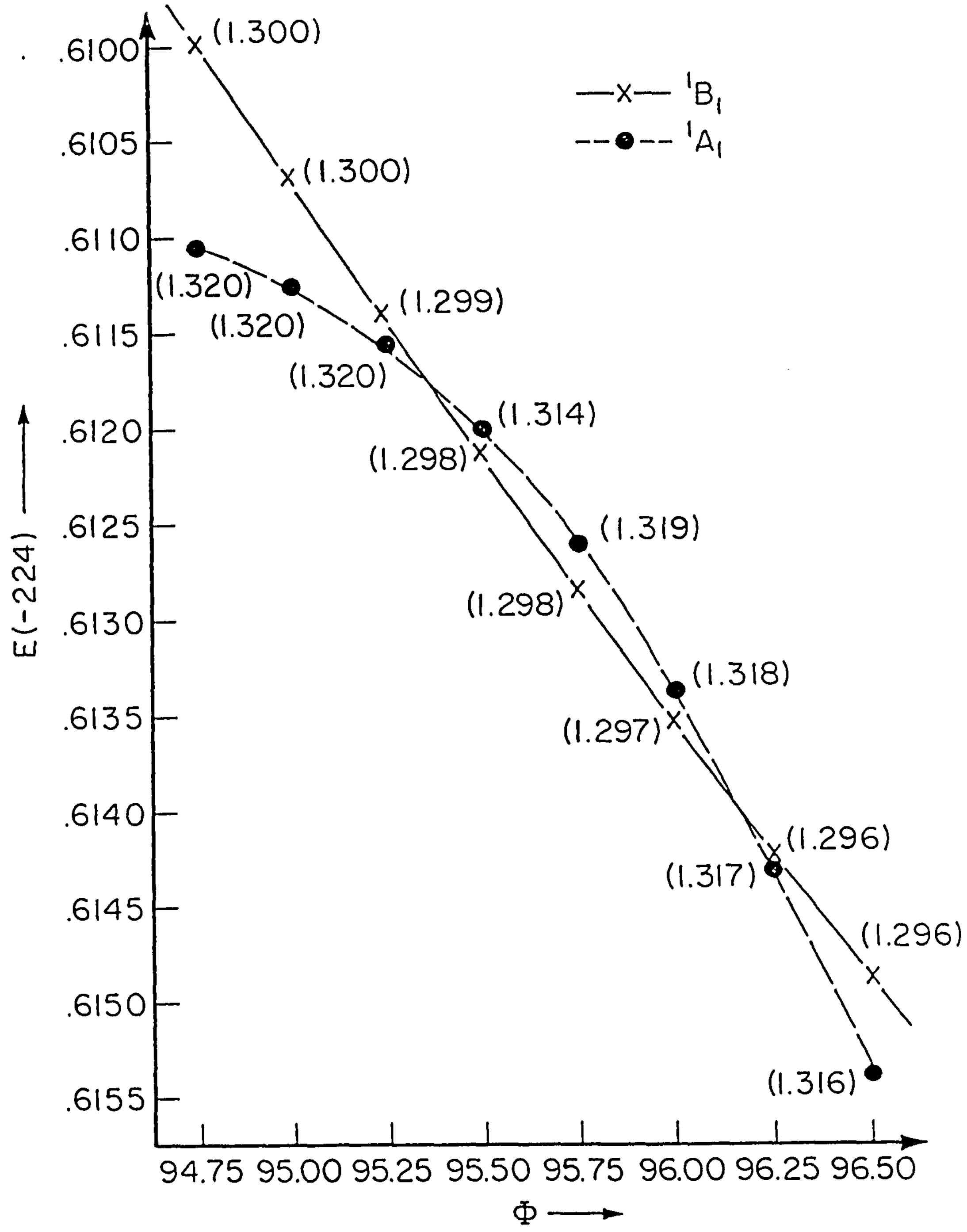

Figure 3.8. Intersection of the $^1A_1$ anf $^1B_1$ states of CO_2. The optimized values of the C-O bond lengths are shown in parentheses

respect to R_1 and R_2 down to the linear ground state. MCSCF calculations at points corresponding to asymmetric distortions by ±0.001 Å from the C_{2v} optimized values for the C-O bond lengths are preformed for $\phi = 100^\circ$, 110°, 120°, 130°, 140° and 160°. They all yield energies which are higher than the corresponding ones for the C_{2v} geometries shown in Figure 3.1 suggesting that the reaction path lies in the bottom of a valley in the 3-dimensional surface as ϕ increases to 180°.

Figure 3.6 also corresponds to the exchange of $O(^1D)$ atoms with $CO(^1\Sigma^+)$ the oxygen atom approaching and departing at an angle of 94.2° with respect to the CO molecule. The upper left part of the surface corresponds to the entrance channel while the lower right part to the exit channel. The barrier of the $O(^1D)$ absorption is ≈15 mhartree (9.5 kcal/mol) and there exist a minimum at $R_1 = 1.24$ Å and $R_2 = 1.41$ Å for this angle of approach of the oxygen atom.

3. The panel for $\phi = 180^\circ$: colinear approach of $O(^1D)$ to $CO(^1\Sigma^+)$.

The fact that the barrier of $O(^1D)$ absorption at $\phi = 94.2^\circ$ is of the order of 10 kcal/mol indicates that there might be another direction along which the $O(^1D)$ approaches the ground state of the CO molecule from the carbon side with a lower barrier. The preferred angle of approach of the oxygen atom - if any - should also result in the formation of a stable species on the ground state surface which is most probably the linear CO_2 species. It is therefore desired to compute the barrier of oxygen abstraction to CO upon colinear attack of the former to the latter from the carbon side and compare it with the previously computed barrier for $\phi = 94.2^\circ$.

Experimental data by Harding, Weston and Flynn (1988) and Zhu and Gordon (1990) suggest that the quenching of $O(^1D)$ by $CO(^1\Sigma^+)$ yields $O(^3P)$ and CO in its ground state in apparent violation of spin multiplicity rules. Isotopic labeling studies of Harding et. al. (1988) establish that the nonadiabatic reaction proceeds through a long-lived CO_2^* collision complex. Shortridge and Lin (1976) suggest that the dissociated $O(^1D)$ + $CO(^1\Sigma^+)$ state correlates adiabatically with $^1CO_2^*$ ($^1A_2$ or $^1B_2$) via a $^1A''$ surface. The quenching of $O(^1D)$ proceeds upon formation of a singlet CO_2 species in its $^1B_2$ state from which surface crossing to the $^3B_2$ state occurs in order to form $O(^3P) + CO(^1\Sigma^+)$. Zhu and Gordon (1990) have given the energy diagram depicting the energy levels of the various states of CO_2 indicated in Figure 3.9. The complex-formation mechanism given for $O(^1D)$ + $CO(^1\Sigma^+)$ is also demonstrated by the observation made by Shortridge and Lin (1976) that the absolute rate of $C^{16}O$ formation in the following ^{18}O-labelled experiment:

$$^{16}O(^1D) + C^{18}O \rightarrow C^{16}O + {}^{18}O(^3P)$$

is 50% of that measured in the $^{16}O(^1D) + C^{16}O$ reaction. It is therefore clear that the $^{16}OC^{18}O$ complex is involved in the reaction which produces $C^{16}O$ and $C^{18}O$ with equal probabilities. However the crossing of the singlet and triplet surfaces is not going to be investigated in this study.

The panel for the colinear approach of $O(^1D)$ to $CO(^1\Sigma^+)$ is shown in Figure 3.10. The contour increment is 25 mhartree and the minimum having $R_1 = R_2 = 1.176$ Å corresponds to the linear CO_2. The exothermicity of the oxygen absorption to form linear CO_2 is 152.8 kcal/mol (6.63 eV) as

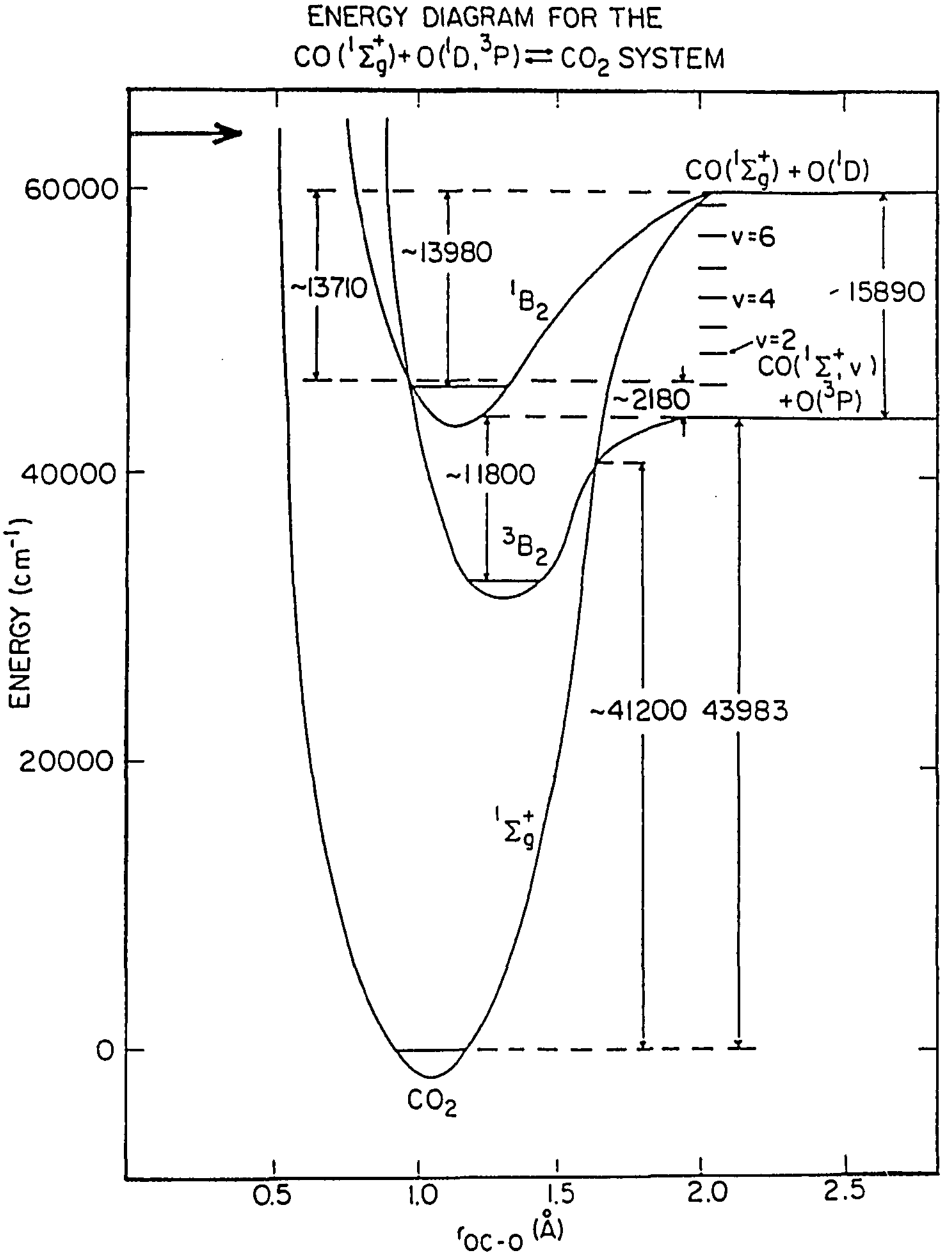

Figure 3.9. Energy diagram for the system $O + CO = CO_2$

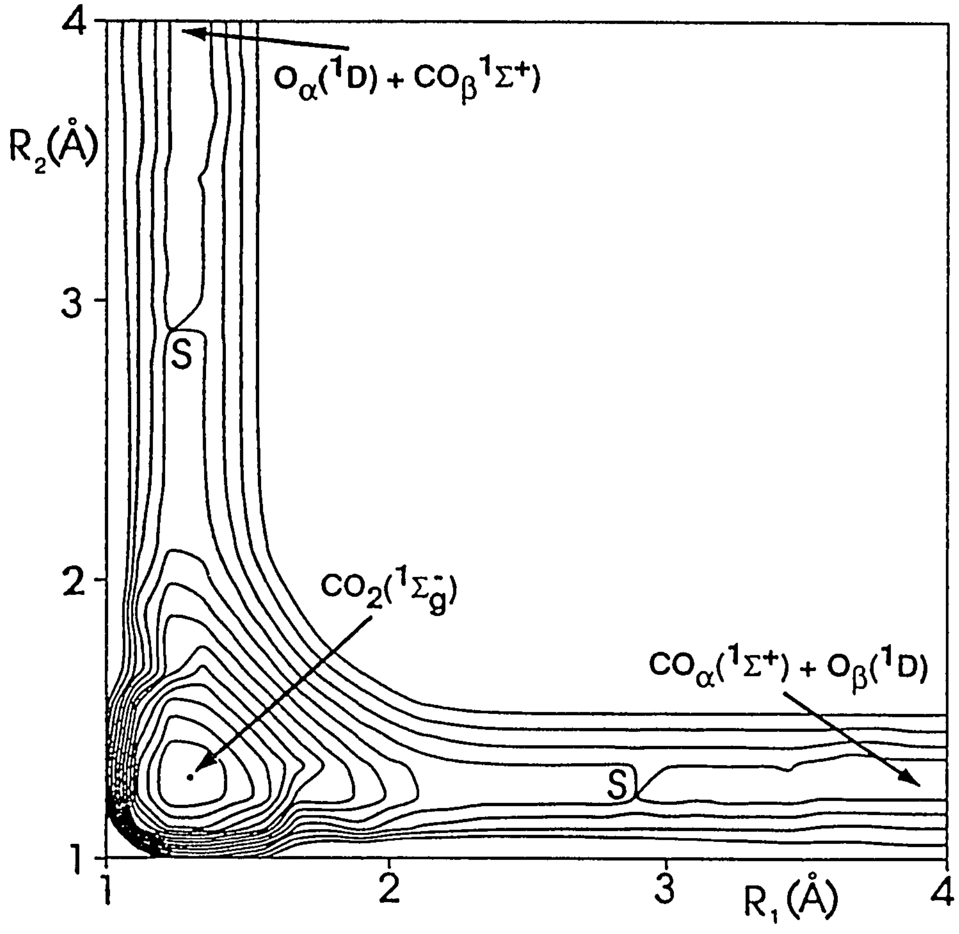

Figure 3.10. Variation of the energy with respect to the two C-O bond lengths for ϕ=180°. Increment: 25 mhartree. S: saddle point

compared to the experimantal value of 7.41 eV reported by Okabe (1978). Figure 3.10 suggests that there exists a very small barrier for the colinear oxygen abstraction of oxygen which is of the order of 1 kcal/mol. The computed saddle point on the surface has internal coordinates $R_1 = 1.13$ Å and $R_2 = 2.90$ Å. Taking into account that the full valence space FORS MCSCF calculations are within chemical accuracy (< 2 kcal/mol) with experimental results, the oxygen abstraction might be considered as proceeding without a barrier along a colinear direction to the CO molecule from the carbon side. The fact that the $O(^1D)$ deactivation by CO should not exhibit a significant activation energy was also suggested by Davidson et. al. (1978) by analogy with the isoelectronic $O(^1D) + N_2$ system. Finally, Tully (1975) has calculated the $O(^1D)$ deactivation rate constant to be 3×10^{-11} cm^3/molecule·s at 300 K using a statistical model.

4. The panel for $\phi = 0°$: colinear $C(^3P) + O_2(^3\Sigma_g^-) \rightarrow CO(^1\Sigma^+) + O(^1D)$

By fixing the O-C-O angle ϕ at 0° the 2-dimensional cut of the complete ground state surface depicts the colinear reaction of carbon and O_2. The diagrams in Figure 3.5 indicate that the ground states of both carbon and O_2 correlate with the ground state of CO and $O(^1D)$ through a singlet surface. A subspace of this surface on which all nuclei lie always on a line is shown in Figure 3.11. The minimum at $R_1 = 1.696$ Å and $R_2 = 1.149$ Å corresponds to a stable linear intermediate of the type C-O-O which is a *minimum* on the complete ground state singlet surface since it is stable upon variation of the C-O-O angle. The increment of the energy contours in Figure 3.11 is 20 mhartree. The stable C-O-O intermediate dissociates through a barrier of 4.1 kcal/mol to the CO + $O(^1D)$ asymptote

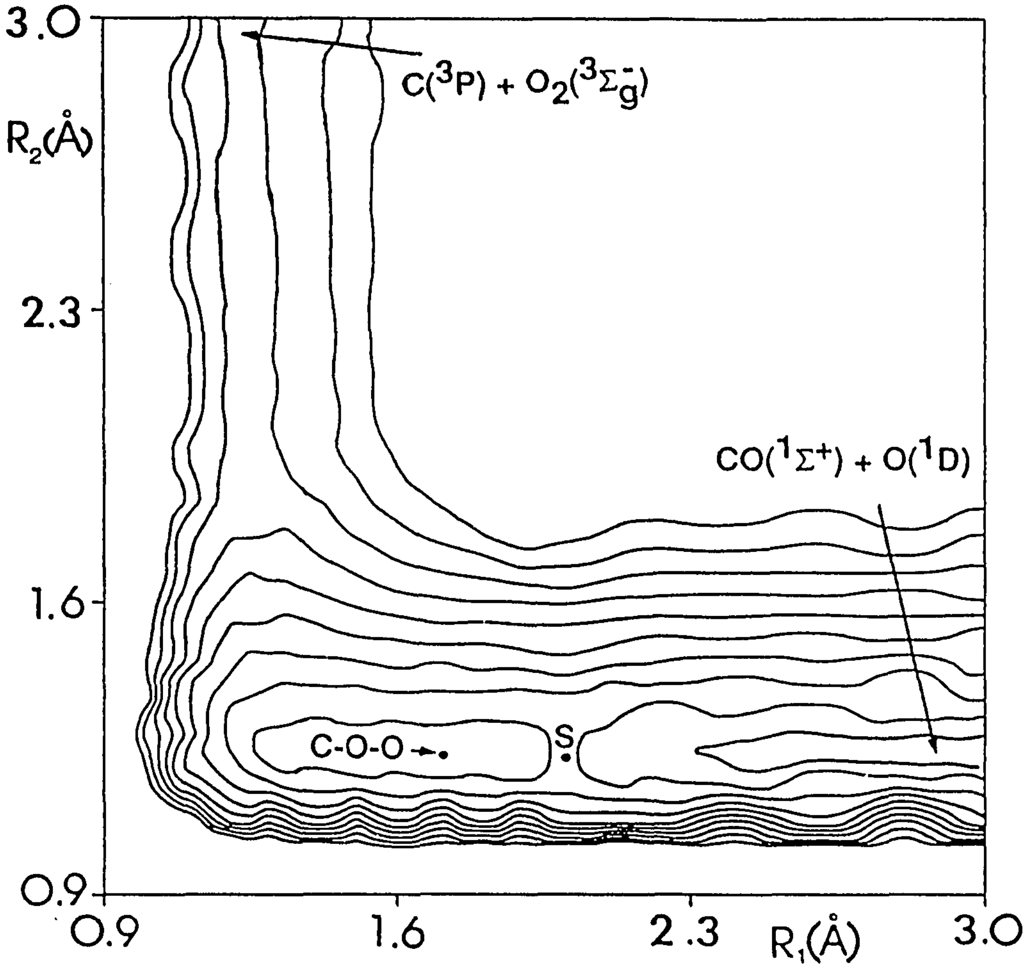

Figure 3.11. Variation of the energy with respect to the two C-O bond lengths for $\phi = 0°$. Increment: 20 mhartree. S: saddle point

which lies 5.3 kcal/mol below it. The saddle point of this dissociation (denoted as S in Figure 3.11) has bond lengths $R_1 = 1.14$ Å and $R_2 = 1.47$ Å. The existence of the C-O-O species has been speculated by Dubrin et. al. (1964) as an intermediate in the reaction of C with O_2. They have also estimated the exothermicity towards CO + O(^{1}D) formation to be 138 kcal/mol. Our value for this quantity is 105 kcal/mol in the full valence space FORS MCSCF approximation. Upon reaction of C with O_2, CO rather than CO_2 seems to be the dominant product (> 97%) even in the liquid phase as suggested by Brown and coworkers (1969). They estimated that the rate for the reaction producing CO is 3.3×10^{-11} cm^3/molecules•s.

G. Conclusions

The existence of a carbene-type ring structure of CO_2 on the ground state potential energy surface is established by means of ab-initio full valence space FORS MCSCF calculations with an extended basis set. The C_{2v} restricted potential energy surface govering the ring opening process to the linear minimum is also computed in the same level of theory. The transition state for the ring opening path is however found to lie off the C_{2v} surface having asymmetric C-O bond lengths. Parts of the complete ground state $^1A'$ potential energy surface corresponding to various ways that the 3 nuclei can interact with each other are also computed. It is found that the preferred approach of the O(^{1}D) to CO is colinear having a negligible barrier (≈1 kcal/mol). The 2-dimensional cut of the complete ground state PES corresponding to the colinear attack of C(^{3}P) to the ground state of O_2 is also computed. It reveals the existence of a metastable species having a linear C-O-O structure which dissociates to ground state CO and O(^1D).

IV. THE RING OPENING OF CYCLOPROPYLIDENE TO ALLENE

A. Key Regions of the Reaction Surface

1. Introduction

The mechanism of the ring opening of cyclopropylidene to allene represents a prototype reaction for bond fission of a cyclic carbene due to ring strain. Because of the consequential roles played by carbenes as well as by strained rings as reaction intermediates, this isomerization has fundamental implications for many organic reactions, including combustion phenomena.

Due to the reactant's very short life, the experimental study is extremely difficult. Previous theoretical results have suffered from various methodological shortcomings. This is due to the fact that the potential energy function depends on 15 internal coordinates and the various reaction paths are difficult to visualize in this multidimensional space. Valtazanos, Elbert, Xantheas and Ruedenberg (1990) have furnished a global overview over the potential energy surface governing the ring opening of cyclopropylidene to allene in terms of three internal coordinates, namely the ring opening angle Φ and two dihedral angles δ_1 and δ_2 which describe the rotations of the two CH_2 groups with respect to the CCC plane. The remaining 12 internal coordinates were relaxed by energy minimization for every $(\phi, \delta_1, \delta_2)$ triple. Their choice as regards the set of the 15 internal coordinates is shown in Figure 4.A.1. Limitations in

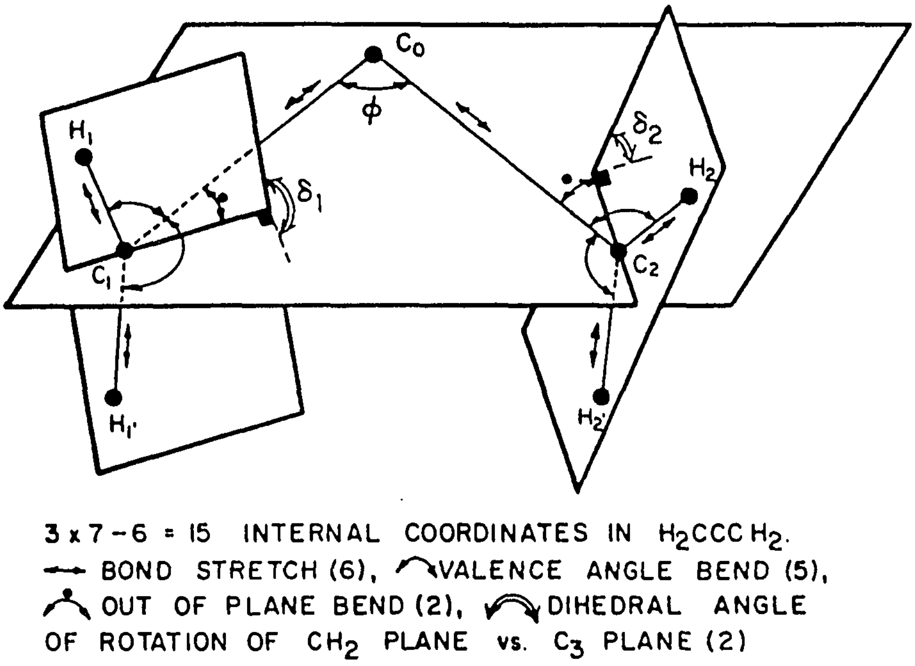

Figure 4.A.1. Definition of the 15 internal coordinates of C_3H_4

computational power dictated the use of a minimal basis set and a small full configuration space to accomplish this overview.

While STO-3G bases are known to yield reasonable geometries in general, and in particular in the case of hydrocarbons as suggested by Dykstra and Schaefer (1980), it is also known that extended basis sets better describe strong π-bonds, such as occur in allene, and that polarization functions will lead to stronger bent bonds in rings, such as occur in cyclopropylidene. Moreover, as it was pointed out by Ruedenberg and Sundberg (1976), the lack of flexibility in the minimal basis set tends to overestimate activation energies. Less serious is presumably the other limitation, namely the choice of the full space of 20 configurations generated by four electrons distributed over four "reactive" orbitals (two on the central carbon and one on each end carbon) between which electrons are rearranged to break bonds and form different bonds. The reaction orbitals as well as the numbering of the atoms are depicted schematically in Figure 4.A.2 for the reactant and the product respectively.

The purpose of this study is to determine how closely the results reported by Valtazanos, Elbert, Xantheas and Ruedenberg (1990) approximate the actual potential energy surface. In order to answer this question and to obtain reliable quantitative values regarding the ring opening mechanism, the investigation of Valtazanos et. al. (1990) is complemented by recalculating key regions on the energy surface using extended basis sets and enlarged configuration spaces. In particular, we examine the reactant cyclopropylidene, the product allene, the region around the ring-opening transition state, the ring opening reaction path, the allene isomerization reaction path, and also the isoenergetic shelf corresponding

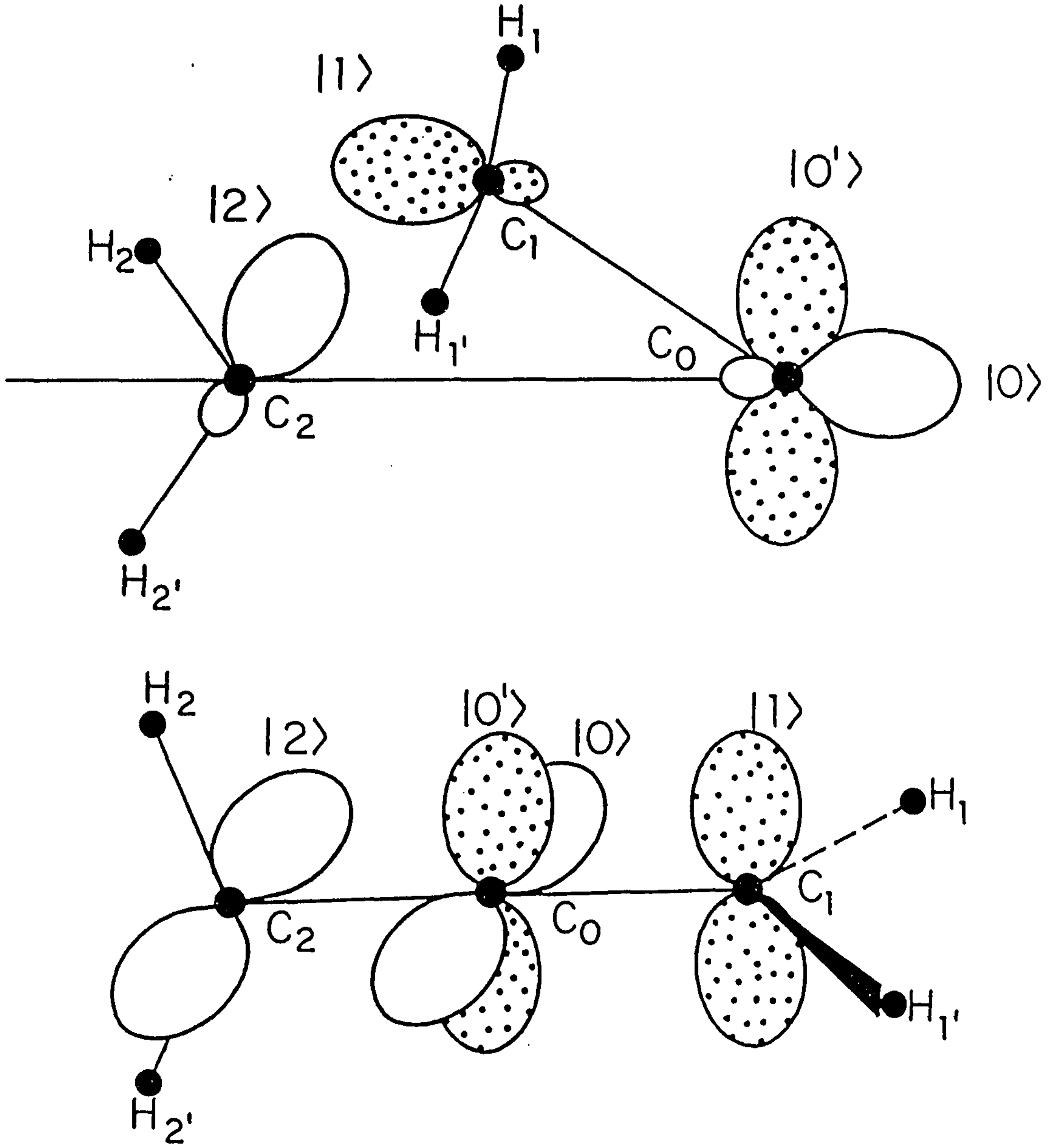

Figure 4.A.2. Qualitative sketch of the reactive orbitals |0>, |0'>, |1>, |2> in cyclopropylidene and allene

to the cogwheel-like synchronized rotation found for the two CH_2 groups. The results indicate that the previous calculations of Valtazanos et. al. (1990) provide a correct picture of the global potential energy surface. The topography around the transition state requires however a significant qualitative correction and that the quantitative value of the ring-opening barrier is considerably lowered. A new feature found is that the bifurcation occurs after the transition state, close to a conical intersection on the steepest descent path.

2. Method of calculation

2.1. Scope of calculations.

In the reduced reaction surface the energy is a function of the 3 internal coordinates Φ, δ_1 and δ_2. The number of energy calculations required for the reproduction of the entire reduced energy surface is of the order of 25 panels x 50 points/panel x 10 searches/point x 10 iterations/search = 125,000 MCSCF iterations, where we have used average values of 10 searches/point on the reduced energy surface to optimize the remaining 12 internal coordinates, and 10 iterations to converge each MCSCF energy calculation. A panel is a 2-dimensional cut through the 3-dimensional reduced energy surface where the energy is expressed as a function of the two dihedral angles δ_1 and δ_2 for a constant value of Φ. Additional CPU time is required for the evaluation of the gradient of the energy with respect to the nuclear coordinates in order to optimize the 12 remaining internal coordinates for each (ϕ,δ_1,δ_2) triple. The number of gradient evaluations is (25 panels) x (50 pts/panel) x (10 searches/pt.) x

(1 grad./search) = 12,500 gradient evaluations. Table 4.A.1 lists the estimated CPU times needed to carry out these calculations for the STO-3G basis and for an extended basis within the original FORS space (20 configurations) using the GAMESS program on various computers. Since the calculation of the entire surface for the extended basis is unrealistic due to the extensive CPU time which is required for this purpose, only the aforementioned key regions are investigated by the more accurate procedures.

2.2. Basis Sets.

The following basis sets were used to improve the quality of the calculations beyond that of the STO-3G basis (Basis i):

Basis (ii): A Dunning-Hay (1971) basis set plus polarization functions on Carbon consisting of the segmented contractions (9s5p1d/3s2p1d) for Carbon and (4s/2s) for Hydrogen. For the polarization function on Carbon the exponent $\varsigma_C=0.75$ was chosen.

Basis (iii): The basis set of (ii) plus p-type polarization functions on Hydrogen with exponent $\varsigma_H=1.0$.

Basis (iv): An even-tempered Gaussian basis of double-zeta quality contracted by the scheme (14s7p1d/3s2d1p) for Carbon and (6s/2s) for Hydrogen, with the Hydrogen exponents scaled by 1.2. The d polarization function exponents were the same as those for basis (ii).

These basis sets contain 106, 118 and 147 primitive atomic orbitals, contracted to 53, 65 and 53 quantitative basis orbitals respectively.

Table 4.A.1. CPU time needed to compute the entire reduced energy surface[a]

Machine	STO-3G	Dunning-Hay[b]
VAX-11/780	0.60	40.00
FPS-164	0.12	6.13
SCS-40		1.25
CRAY-1/XMP		0.43

[a]: in CPU years using the GAMESS program.

[b]: projected time.

The geometry optimizations of the reactant, transition state, product and the allene isomerization transition state were performed with basis sets (ii) and (iii) using the GAMESS program by Dupuis, Spangler and Wendoloski (1980). The calculations with the large even-tempered Gaussian basis (iv) set were performed using the ALIS program by Elbert, Cheung and Ruedeneberg (1980).

2.3. Configuration Spaces.

The original full configuration space of 4 electrons in 4 reactive orbitals (two on the central carbon and one on each end carbon), hereafter referred to as FORS1, consists of the following 20 configurations:

$$
\begin{array}{ll}
A\ (\ \mathrm{Core}|0^2 1^2>\ \Theta_0\ )/2 & A\ (\ \mathrm{Core}|0^2 2^2>\ \Theta_0\ )/2 \\
A\ (\ \mathrm{Core}|0'^2 1^2>\ \Theta_0\ )/2 & A\ (\ \mathrm{Core}|0'^2 2^2>\ \Theta_0\ )/2 \\
A\ (\ \mathrm{Core}|0^2 0'^2>\ \Theta_0\ )/2 & A\ (\ \mathrm{Core}|1^2 2^2>\ \Theta_0\ )/2 \\
A\ (\ \mathrm{Core}|0^2 0'1>\ \Theta_0\ )/\sqrt{2} & A\ (\ \mathrm{Core}|0^2 0'2>\ \Theta_0\ )/\sqrt{2} \\
A\ (\ \mathrm{Core}|0'^2 01>\ \Theta_0\ )/\sqrt{2} & A\ (\ \mathrm{Core}|0'^2 02>\ \Theta_0\ )/\sqrt{2} \\
A\ (\ \mathrm{Core}|0^2 12>\ \Theta_0\ )/\sqrt{2} & A\ (\ \mathrm{Core}|0'^2 12>\ \Theta_0\ )/\sqrt{2} \\
A\ (\ \mathrm{Core}|1^2 00'>\ \Theta_0\ )/\sqrt{2} & A\ (\ \mathrm{Core}|1^2 02>\ \Theta_0\ )/\sqrt{2} \\
A\ (\ \mathrm{Core}|1^2 0'2>\ \Theta_0\ )/\sqrt{2} & A\ (\ \mathrm{Core}|2^2 00'>\ \Theta_0\ )/\sqrt{2} \\
A\ (\ \mathrm{Core}|2^2 01>\ \Theta_0\ )/\sqrt{2} & A\ (\ \mathrm{Core}|2^2 0'1>\ \Theta_0\ )/\sqrt{2} \\
A\ (\ \mathrm{Core}|00'12>\ \Theta_1\ ) & A\ (\ \mathrm{Core}|00'12>\ \Theta_1\ )
\end{array}
$$

where Core = $c_1^2 c_2^2 \ldots C_9^2\ (\alpha\beta-\beta\alpha)^9/2^{9/2}$, $c_1 \ldots c_9$ the core orbitals

$\Theta_0 = (\alpha\beta-\beta\alpha)(\alpha\beta-\beta\alpha)/2$ singlet coupling

$\Theta_1 = (\alpha\alpha\beta\beta+\beta\beta\alpha\alpha-(\alpha\beta+\beta\alpha)(\alpha\beta+\beta\alpha)/2)\sqrt{3}$ triplet coupling

A = antisymmetrizer

This space was used to optimize the geometries of the reactant, product and transition states using the extended basis sets (ii) and (iii). In order to get an indication for additional correlations among these four electrons, CI calculations were performed for these optimized geometries in the space of the 13700 configurations generated by taking all single and double excitations from the SCF wavefunction to the MCSCF reactive and virtual orbitals.

Next, the set of orbitals which generate the full active space was extended to include four additional molecular orbitals, namely a CC-σ-bonding MO and a CC-σ-antibonding MO in each of the two CC-bonds. The resulting FORS space (FORS2), arising from distributing eight electrons over eight orbitals in all possible ways is spanned by 1764 configurations. (In the previous 20-dimensional FORS space, the CC-σ-bonding MO's had been doubly occupied core orbitals whereas the CC-σ-antibonding MO's had remained unoccupied.) This enlargement of the full configuration space is intended to account for correlation changes in the CC-σ-bonds whose lengths do change during the ring opening, in contrast to the rather invariant CH bonds.

Starting orbitals for the two CC-σ bonding MO's were obtained by localizing the core orbitals of the previous 20-configuration FORS calculation, using the Edmiston-Ruedenberg (1963) procedure. This localization separates the core MO's into three carbon 1s shells, four CH bonds and two CC bonds. Starting orbitals for the CC-σ-antibonding MO's can be similarly obtained by localization of the virtual orbitals of the previous calculation which separates the CH antibonds from the CC antibonds. Since the regions investigated here have either C_s or C_{2v}

symmetry, localization within each symmetry species only is sufficient to achieve the desired separations in space between CC bonds and CH bonds, and this was done for the core orbitals. Moreover, an inspection of the virtual orbitals revealed that two of these MO's had already the desired CC-antibonding character approximately and they were chosen without further localization as MCSCF starting orbitals. After completion of the MCSCF optimizations in the enlarged FORS space, all optimized orbitals were examined and it was found that the new MO's had indeed the desired CC-σ bonding and antibonding character. Thus, the correlation improvement had not moved into the CH bonds.

For all choices of the coordinate triples $(\phi, \delta_1, \delta_2)$ for which the 1764 configuration wavefunction was determined, the geometries of the twelve secondary internal coordinates were reoptimized using the basis set (ii) as had been done for the 20 dimensional FORS space.

Table 4.A.2 gives a summary of the theoretical and computational methods used and how they will be referred to in the sequel. For example, (FORS1/ii) means a 20 configuration calculation with basis set (ii).

3. Critical Regions

3.1. The ring opening transition state

The region around the ring opening transition state is the main place among the key regions on the potential energy surface where the results of the more accurate calculations differ from those of Valtazanos et. al. (1990) comouted with the STO-3G minimal basis set in more than quantitative detail. We therefore begin by discussing this region.

Table 4.A.2. Theoretical and computational methods

	Internal Coordinates		Calculational Procedure		
Method	Φ, δ_1, δ_2	Other 12	AO basis	FORS space	Optimization
1[a]	Entire surface	Optimized	MBS(STO-3G)	20	MC-SCF
2	Critical points	Optimized	DH + d on C	20	MC-SCF
3	Critical points	Optimized	DH + d on C + p on H	20	MC-SCF
4	Critical points	From 2	Even tempered	20	MC-SCF
5	Critical points	From 2	DH + d on C	13700	CI
6	Critical points	From 2	DH + d on C	1764	MC-SCF

In the calculation with the STO-3G basis set (FORS1/i) the reaction path bifurcated, breaking C_s symmetry, before the transition state. There were thus two transition states, both of C_1 symmetry and being each other's mirror images with respect to the C_s mirror plane perpendicular to the CCC plane. However the deviation of these transition states from C_s symmetry was only small and, more importantly, the energy changed only little on a path leading from one of these transition states to the other, the maximum occurring at the midpoint which has C_s symmetry, i.e. at the C_s-average of the two transition states. The energy of this "average transition state" lies only 0.2 Kcal/Mole above that of the two transition states having C_1 symmetry. While the reliability of such a detailed prediction by a STO-3G based calculation was clearly open to question, it seemed likely that the actual energy surface would indeed be quite flat in this entire region.

In view of this feature, it was furthermore likely that the transition state would shift in a more accurate calculation and the first question of interest was therefore to establish the location of the transition state obtained by such a calculation. Thus, using the extended basis (ii) and the original 20-dimensional FORS1 space, a transition state search was initiated at one of the transition states computed with the STO-3G basis set. This search led to a moderate displacement of this transition state. While the ring opening angle Φ was virtually unchanged, the two CH_2 rotation angles δ_1 and δ_2 were changed by about 6°. All internal coordinates are listed in row 6 of Table 4.A.3. These relatively minor changes in δ_1, δ_2 were however sufficient to yield a transition state which has C_s symmetry.

In order to confirm this result, we determined, at this level of theory, a part of the potential energy surface in the transition state region. Figure 4.A.3 displays the results of this calculation. Energy contours are depicted in terms of the coordinates $\delta_+ = [(\delta_1 + \delta_2)/2 - 90°]$, $\delta_- = (\delta_1 - \delta_2)/2$, for a constant value of Φ. Three panels are given corresponding to $\Phi = 82°$, 84.45°, 87°. The contours are drawn in increments of 0.5 mh. Each panel is based on 21 calculated energy values. For each of these, the remaining 12 internal coordinates are optimized as mentioned before. It is seen that, for each panel, the minimum lies on the axis $\delta_+ = 0$ which corresponds to geometries which have C_s symmetry. Furthermore, the value of this minimum energy for constant Φ, considered as a function of Φ, has a maximum for $\Phi = 84.45°$. This point is therefore indeed a transition state. Diagonalization of the Hessian matrix at this point confirms this conclusion by yielding 14 positive eigenvalues and one negative eigenvalue describing a C_s preserving displacement corresponding to the reaction coordinate.

The simplest interpretation of these results is that, for the potential energy surface obtained by this type of calculation, the reaction path does not bifurcate before the transition state. Rather a C_s preserving channel leads from the reactant up to and across the transition state and the reaction path bifurcates thereafter. These conclusions were confirmed by calculating the steepest descent paths from the transition state to the reactant and towards the products. They will be displayed and discussed in Section 4.A.4.

In order to be sure that these conclusions remain valid for wavefunctions of higher accuracy, two further transition state searches

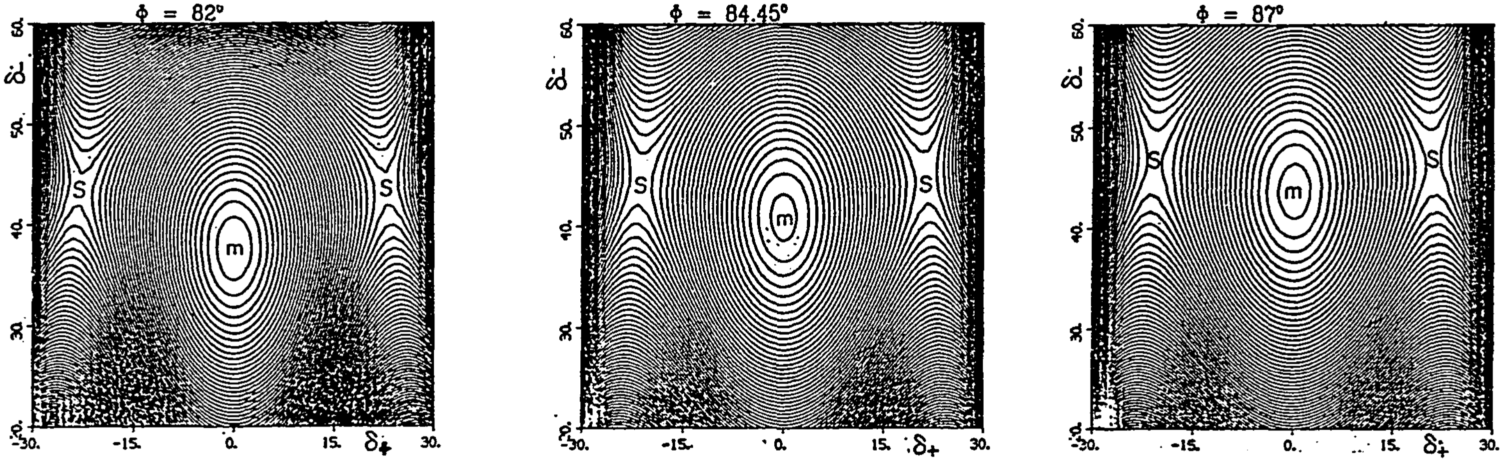

E_m = -115.80341
E_S = -115.78766

E_m = -115.80219
E_S = -115.79029
(Transition State)

E_m = -115.80376
E_S = -115.79293

Figure 4.A.3. MCSCF energy contours for Φ=82°, 84.45°, 87° as a function of δ_+ and δ_- (FORS2/ii).

Increment: 0.5 mhartree. m: minimum; S: saddle point;

E_m, E_S: energies of m, S respectively were made, both starting with the transition state geometry just found. One search using the same FORS1 space but the basis set (iii), including hydrogen polarization functions, and another search using the basis set (ii) but the enlarged 1764 dimensional FORS2 space including CC-σ bond correlations. These calculations yielded only slightly displaced transition states, both with C_s symmetry. For the latter calculation the eigenvalue spectrum of the Hessian was redetermined and it turned out to be very similar to the one mentioned in the preceding paragraph.

The coordinates of all transition states are listed in rows 5 to 8 of Table 4.A.3. The two sets of normal mode frequencies are listed in Tables 4.A.4A and 4.A.4B.

Finally, the influence of higher order correlations was examined through CI calculations in the configuration space spanned by all single and double excitations out of the four active orbitals of the dominant configuration of the 20 dimensional FORS1 space, using the orbital basis (ii). These calculations were performed for all points of the panel for $\Phi = 84.45°$ on Figure 4.A.3, using the geometric parameters of the former calculations. The new calculations lead to the contour plot exhibited in Figure 4.A.4 which is almost quantitatively identical with the corresponding plot of Figure 4.A.3 (except, of course, for the absolute value of the energy at the minimum): For both plots, the minimum occurs at the same position, the energy difference between the saddlepoints and the minimum is about 10 Kcal/mole and the increment is 0.5 mhartree.

Thus, all calculations involving the larger basis sets (ii) and (iii) lead to a transition state with C_s symmetry and we conclude that the transition state region of the actual energy surface is adequately depicted

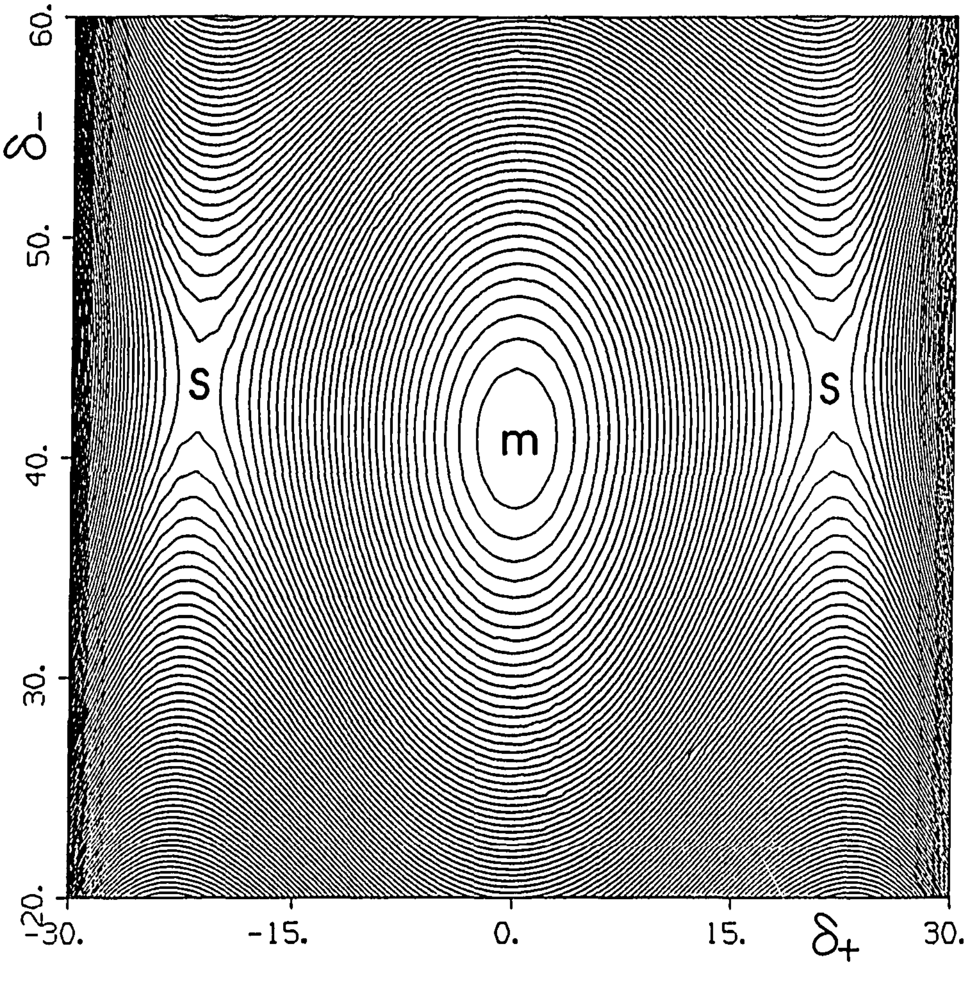

Figure 4.A.4. CI (1764 configurations) energy contours for Φ=84.45°.

Increment: 0.5 mhartree. m:minimum; S: saddle point by the displayed contour plots. Consequently, the channel leading up to the ring-opening transition state as well as the channel leaving the transition state preserve C_s symmetry and the bifurcation of the reaction path into two branches, which are each other's mirror images and lead to the two isomeric products, must occur after the transition state. The basis set improvement from the STO-3G basis to the extended bases leads therefore to a shift of the bifurcation from before to after the transition state.

Because of the flatness of the energy surface in this region, this qualitative change is, however, the result of relatively small quantitative changes on the energy surface.

3.2. The other critical points.

In the preceding section we saw that the more accurate calculations lead to a somewhat different topography around the ring opening transition state than was obtained in the first paper. For the other critical points, viz. the reactant cyclopropylidene, the product allene and the allene isomerization transition state the changes are less dramatic. As was done for the ring-opening transition state, the geometries of all these critical points were reoptimized with respect to all fifteen coordinates for the following levels of approximation:

the 20 configuration FORS1 space with basis set (ii),
the 20 configuration FORS1 space with basis set (iii),
the 1764 configuration FORS2 space with basis set (ii).

Table 4.A.3 also lists the results for all critical points including the ring-opening transition state. It can be seen that, for all

Table 4.A.3. Optimized geometries of the critical points of the ground state recation surface

Φ	δ_1	δ_2	r_{01}	r_{02}	r_{11}	$r_{11'}$	r_{22}	$r_{22'}$	α_{011}	$\alpha_{011'}$	α_{022}	$\alpha_{022'}$	β_1	β_2
C 59.45	90.0	90.0	1.532	1.532	1.081	1.081	1.081	1.081	117.1	117.1	117.1	117.1	33.1	33.1
60.33	90.0	90.0	1.504	1.504	1.078	1.078	1.078	1.078	116.1	116.1	116.1	116.1	35.8	35.8
60.41	90.0	90.0	1.503	1.503	1.077	1.077	1.077	1.077	116.1	116.1	116.1	116.1	35.6	35.6
58.62	90.0	90.0	1.549	1.549	1.077	1.077	1.077	1.077	115.7	115.7	115.7	115.7	36.4	36.4
T 84.24	57.1	134.8	1.448	1.448	1.086	1.081	1.086	1.081	118.3	125.9	118.3	125.9	5.9	4.0
84.45	51.0	129.0	1.422	1.422	1.079	1.077	1.079	1.077	117.8	127.2	117.8	127.2	1.3	1.3
86.52	48.4	131.6	1.429	1.429	1.080	1.078	1.080	1.078	118.1	126.6	118.1	126.6	0.4	0.4
82.37	51.3	128.7	1.449	1.119	1.079	1.078	1.079	1.078	116.7	128.1	116.7	128.1	0.3	0.3
A 180.0	0.0	90.0	1.320	1.320	1.083	1.083	1.083	1.083	121.5	121.5	121.5	121.5	0.0	0.0
180.0	0.0	90.0	1.324	1.324	1.076	1.076	1.076	1.076	120.9	120.9	120.9	120.9	0.0	0.0
180.0	0.0	90.0	1.323	1.323	1.076	1.076	1.076	1.076	120.9	120.9	120.9	120.9	0.0	0.0
180.0	0.0	90.0	1.342	1.342	1.075	1.075	1.075	1.075	120.7	120.7	120.7	120.7	0.0	0.0
I 134.3	0.0	0.0	1.392	1.392	1.081	1.082	1.081	1.082	121.1	121.7	121.1	121.7	0.0	0.0
135.0	0.0	0.0	1.385	1.385	1.076	1.076	1.076	1.076	121.0	121.0	121.0	121.0	0.0	0.0
135.0	0.0	0.0	1.385	1.385	1.074	1.077	1.074	1.077	121.0	120.8	121.0	120.8	0.0	0.0
136.7	0.0	0.0	1.403	1.403	1.074	1.077	1.074	1.077	121.1	120.6	121.1	120.6	0.0	0.0

C: Cyclopropylidene, T: Transition State, A: Allene, I: Allene Isomerization Transition State

First entry: FORS1/i, Second Entry: FORS1/ii, Third Entry: FORS1/iii, Fourth Entry: FORS2/ii

Column labels: r_{01} = C_0-C_1 stretch r_{11} = C_1-H_1 stretch r_{22} = C_2-H_2 stretch
r_{02} = C_0-C_2 stretch $r_{11'}$ = C_1-$H_{1'}$ stretch $r_{22'}$ = C_2-$H_{2'}$ stretch
α_{011} = C_0-C_1-H_1 bend α_{022} = C_0-C_2-H_2 bend β_1 = C_0-($C_1H_1H_{1'}$) out of plane bend
$\alpha_{011'}$ = C_0-C_1-$H_{1'}$ bend $\alpha_{022'}$ = C_0-C_2-$H_{2'}$ bend β_2 = C_0-($C_2H_2H_{2'}$) out of plane bend

r in Å; α, β, δ, Φ in degrees

Table 4.A.4A. Comparison between experimental and calculated frequencies of the normal modes of allene

Frequency (cm^{-1})	Assignment	Experimental[a] Raman	IR	Calculated[b] FORS1	FORS2
ν_{11} (e)	C=C=C bending	353		189.4	313.4
ν_4 (b_1)	C=C=C twisting	820		890.6	883.9
ν_{10} (e)	C=C=C bending	838	852	790.7	870.2
ν_9 (e)	CH_2 rocking		1031	1055.5	1057.9
ν_3 (a_1)	C=C	1071		1125.5	1076.6
ν_7 (b_2)	CH_2		1389	1563.9	1597.3
ν_2 (a_1)	CH_2	1432		1618.0	1551.4
ν_6 (b_2)	C=C	1956	1980	2065.0	1954.3
ν_5 (b_2)	CH		2960	3339.5	3337.5
ν_1 (a_1)	CH	2993		3347.0	3341.6
ν_8 (e)	CH	3061		3432.4	3442.4
Zero-point E (Kcal/mol)				35.6	35.9

[a]: Herzberg (1966, p.640)

[b]: With basis set (ii)

Table 4.A.4B. Calculated normal mode frequencies (in cm^{-1})

	Cyclopropylidene	Transition State	Allene Isomerization Transition State
1	652.5 655.4	-253.0 -98.2	-1376.9 -1458.2
2	883.4 757.7	702.3 575.6	357.6 320.8
3	914.2 865.5	925.0 971.6	490.7 473.0
4	920.9 867.6	982.0 1027.9	664.9 725.3
5	1062.1 906.4	1038.2 1043.0	669.0 734.4
6	1124.7 1072.6	1053.8 1068.0	987.1 968.0
7	1136.4 1100.9	1173.5 1113.9	1054.4 1005.0
8	1289.2 1179.1	1312.5 1170.3	1252.4 1195.0
9	1368.8 1375.2	1348.0 1264.5	1419.5 1373.3
10	1548.0 1546.3	1606.0 1601.7	1599.0 1586.2
11	1585.4 1572.9	1678.5 1659.9	1616.7 1601.0
12	3302.6 3305.5	3306.5 3299.1	3321.1 3311.7
13	3306.2 3310,7	3320.6 3311.1	3333.4 3319.1
14	3387.7 3395.6	3395.9 3392.8	3429.5 3428.9
15	3403.6 3409.5	3411.8 3405.5	3445.8 3444.1
ZPE	37.0 36.2	36.1 35.6	33.8 33.6

First entry: FORS1/ii ; Second entry: FORS2/ii calculations, the CC bond lengths change by more than 10% during the ring opening whereas the CH bond length change by less than 0.2%. It can also be seen that inclusion of the hydrogen p-orbitals [basis set (iii)] produces only negligible changes in geometries and energetics. It seems therefore justified to consider correlations in the CC-σ-bonds, but not in the CH bonds. Overall, the geometries furnished by the calculations of the first paper are not changed greatly by the more accurate calculations. In fact, for allene, the only species for which experimental data are available, the STO-3G results are somewhat closer to the experimental values (CC = 1.308 Å, CH = 1.087 Å, HCH = 118.2° cf. Herzberg p.640, 1966). These results support the confidence in the STO-3G calculations as furnishing a good overall picture of the global energy surface.

The energies of the four critical points at the various levels of theory are listed in Table 4.A.5. The table also contains the results of calculations with a very large even-tempered Gaussian basis set [Basis (iv) of section (4.A.2.2)]. The first row contains the energies resulting from calculations with the STO-3G basis set. However, also for these (FORS1/i) calculations, the ring opening transition state energy listed is that at the averaged C_s geometry between the two actual (FORS1/i) transition states (which have C_1 symmetry). As mentioned in Section 4.A.3.1, the energy difference between the two geometries is only 0.2 Kcal/Mole. The reason for choosing the C_s average is that this geometry was also used for the calculations in the second row with basis set (iv) because, from the results discussed in the preceding section, it is clear that the geometry optimization with this basis set would yield a ring opening transition state with C_s symmetry.

Table 4.A.5. Energies (in hartree) of critical points on the ground state reaction surface

AO Basis, Configuration Space	Cyclopropylidene C_{2v}	Transition State C_s	Allene D_{2d}	Allene isomerization T.S., C_{2v}
Geometries Optimized with Minimal Basis Set				
1. FORS1/i	-114.39557	-114.33331	-114.49936	-114.43350
2. FORS1/iv	-115.82693	-115.80462	-115.93060	-115.86369
Geometries Optimized with Extended Basis Sets				
3. FORS1/ii	-115.82073	-115.80016	-115.92827	-115.85970
4. FORS1/iv	-115.82775	-115.80505	-115.93094	-115.86376
5. FORS1/iii	-115.82900	-115.80821	-115.93663	-115.86798
6. FORS2/ii	-115.87169	-115.85885	-115.98780	-115.91222
7. CISD from SCF/ii	-115.84768	-115.83590	-115.95347	-115.88093
Number of Configurations(a)				
FORS1	8/20	12/20	12/20	4/20
FORS2	508/1764	900/1764	492/1764	432/1764
CISD from SCF	3603/13700	6912/13700	3580/13700	3163/13700

(a): First entry: configurations in the corresponding symmetry group
Second entry: number of configurations in C_1

Table 4.A.6. Critical energy differences (in Kcal/mol) for the ground state reaction surface

AO Basis, Configuration Space	Ring opening exothermicity	Ring opening barrier	Allene isomerization barrier
Geometries Optimized with Minimal Basis Set			
1. FORS1/i	-65.1	39.1	41.3
2. FORS1/iv	-65.1	14.0	42.0
Geometries Optimized with Extended Basis Sets			
3. FORS1/ii	-67.5	12.9	43.0
including ZPE	-68.9	12.0	41.2
4. FORS1/iv	-64.8	14.2	42.2
5. FORS1/iii	-67.5	13.0	43.1
6. FORS2/ii	-72.9	8.1	47.4
including ZPE	-73.2	7.5	45.1
7. CISD from SCF	-66.4	7.4	45.5

At the bottom of Table 4.A.5, the number of configurations for the various FORS spaces are listed. In each case, the first number denotes the number of configurations that are left in the relevant irreducible representation of the applicable symmetry group indicated in the heading. This is the number of configurations pertinent for the energy calculation at the critical point. The second number is the number of configurations in C_1 symmetry which are required for calculations at slightly displaced geometries which are needed for determining the Hessian matrix.

The vibrational frequencies in cm^{-1} obtained by diagonalizing the hessians for two types of calculations (FORS1 and FORS2 with basis set (ii); rows 3 and 6 of Table 4.A.5) are listed in Table 4.A.4A. Also listed are the total zero-point energies (in Kcal/Mole), viz. $(\Sigma_k h\upsilon_k/2)$ where the sum goes over all 15 frequencies for cyclopropylidene and allene, but only over the 14 real frequencies ($k = 2$ to 15) for the two transition states. Experimental values are available for allene and they are also listed in Table 4.A.4B.

Of interest to chemists are the energy differences between the various critical points. They are listed in Table 4.A.6 for the various levels of theory reported in Table 4.A.5. For the two types of calculations for which the vibrational analysis was performed, the energy differences including the zero-point energy corrections are also given. It is apparent that the ring-opening exothermicity and the allene isomerization barrier are remarkably independent of the level of theory used. However, as expected, the ring opening barrier is significantly reduced by going to the more accurate wavefunctions. This is essentially due to the extension of the basis set as is evident from the second row which differs from the first only in the increase in the size of the basis set (the configuration space and the geometry being the same). It reduces the barrier from 39 Kcal/Mole to 14 Kcal/Mole. Enlargement of the configuration space to include CC-σ bond correlations (Row 6) lowers the barrier to about 8 Kcal/Mole and inclusion of higher order correlations to 7.4 Kcal/Mole. From row 3 and 6 it is seen that the zeropoint energy corrections to the barrier is about 0.5 to 1 Kcal/Mole. Combining this result with the barrier given in row 7, one can estimate a value around 7 Kcal/Mole. This inference is in agreement with the estimate of 5-6 Kcal/Mole which has been estimated from experimental results of related reactions (Warner, 1988).

4. Reaction paths

4.1. The steepest descent: Qualitatively.

The possible relationships between transition states, bifurcations and reaction paths, modeled as steepest descent curves on an energy surface, have been discussed in detail by Valtazanos and Ruedenberg (1986). One of the observations made by these authors was that steepest descent curves descending from a transition state with C_s symmetry either start out perpendicular to the C_s plane or lie in the C_s plane, in which case they maintain C_s symmetry until they meet another point where the gradient vanishes or is multivalued.

The steepest descent curves which are relevant for the energy surface obtained by the more accurate (FORS1/ii) calculations are shown in Figure 4.A.5. Reaction paths are shown as curves in the δ_1,δ_2 plane with the appropriate values of Φ indicated in parenthesis at various points. The alternative coordinate $\delta_+ = (\delta_1+\delta_2)/2 - 90°$ breaks C_s symmetry, whereas $\delta_- = (\delta_1-\delta_2)/2$ preserves C_s symmetry when $\delta_+ = 0$. The heavy lines depict the steepest descent paths passing through the transition states. On them, the point R ($\Phi = 60.4°$) indicates the reactant cyclopropylidene and the point P on the line $\delta_+ = 45°$ ($\Phi = 180°$) denotes the product allene. Actually, the entire line $\delta_+ = 45°$ ($\Phi = 180°$), represents allene, a displacement along this line corresponding to a rotation of allene around its molecular axis. The line $\delta_+ = -45°$ ($\Phi = 180°$) corresponds to the isomeric mirror image of allene indicated by P′. The point TS ($\Phi = 84.5°$) is the ring opening transition state and the point TS* ($\Phi = 135°$) is the transition state for the isomerization between the two allene isomers. The steepest descent lines emanating from TS preserve C_s symmetry, one ending at the reactant R, the other at the transition state TS*. The downhill steepest descent lines starting at TS* and ending at the two isomeric allene products do not preserve C_s symmetry.

Since TS* is a normal second order saddle point and the downhill directions are towards the allenes, the steepest descent line arriving at TS* from TS must do so on a ridge and this is confirmed by the normal mode frequencies listed in Table 4.A.4B. However, at TS this steepest descent line starts out as a downhill valley, as can also be seen from the normal modes in table 4.A.4B as well as from the discussion in Section (4.A.3.1), in connection with Figure 4.A.3. Consequently, the steepest path from TS to TS* must turn from a valley into a ridge someplace in between: i.e. it has a valley ridge inflection point.

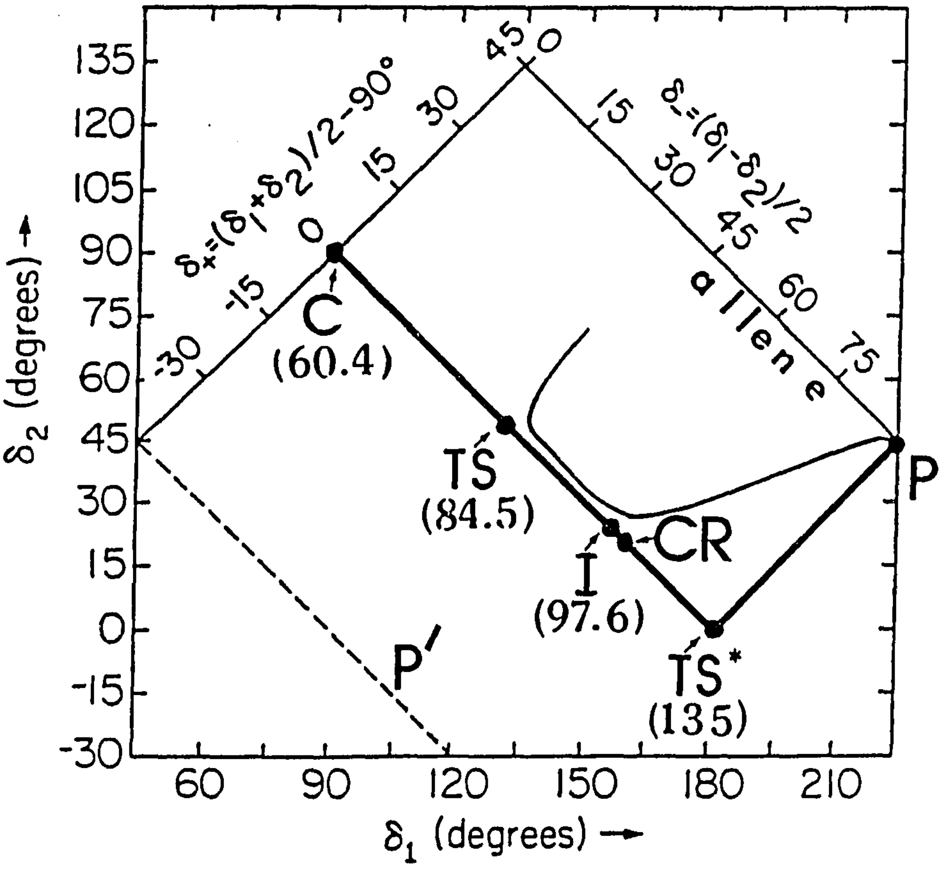

Figure 4.A.5. Intrinsic Reaction Coordinate in the (Φ,δ_1,δ_2) space (FORS2/ii). Heavy line: IRC; Thin line: another steepest descent line. C: cyclopropylidene; TS: transition state I: valley-ridge infelction point; CR: intersection point; TS*: allene isomerization transition state; P,P′: allene Φ values are given in parentheses

There exists however a further complication due to the fact, discussed in Section 4.B.4.3. that the ground state wavefunction at the transition state TS belongs to a different irreducible representation with respect to the C_s mirror plane than the groundstate wavefunction at the transition state TS*. At TS, the irreducible representation is A′, at TS* it is A″. It follows that, in the C_s preserving internal coordinate subspace, there are two states, one of symmetry A′, the other of symmetry A″ such that E(A″) > E(A′) at TS and E(A′) > E(A″) at TS*. These two states cross between TS and TS* at a point which is denoted by CR on Figure 4.A.5. Outside the C_s subspace, the two states belong to the same irreducible representation, namely A of C_1.

We shall see that near the intersection CR, the lower surface is a ridge on the A' side as well as on the A" side of CR. The steepest descent path starting out as a valley at TS must therefore turn into a ridge at a point before reaching CR. This point on the A' curve is denoted as I (for "inflection") on Figure 3.A.5. The steepest descent path along the A" curve from CR to TS*, on the other hand, remains a ridge all the way. The steepest descent paths from TS* to the two allene products P, P' are valleys.

Finally, it will be seen that, at the crossing point CR, the gradient continues to point in a C_s preserving direction. Hence, following the steepest descent on A' from TS to CR and on A" from CR to TS*, the path will run at first along the floor of a valley, then atop a ridge. It is evident that dynamic trajectories will not stay atop the ridge, but fall off it due to the slightest destabilization. Therefore, if one wishes to use steepest descent lines as rough models for reaction paths which end up at the allene products, then the only option is to start anew at a reasonable point nearby I or CR on a different, C_s symmetry breaking steepest descent paths. Whether the neighborhood of the valley-ridge inflection point I or that of the crossing point CR is most appropriate for this restart, is of no consequence in this case since the two points lie so close to each other.

We shall now substantiate and elaborate upon this qualitative description in quantitative detail. The following discussion are based on calculations made at the (FORS1/ii) level.

4.2. The steepest descent: Quantitatively

From R to TS

First, as mentioned in Section 4.A.3.1, the steepest descent curve from the ring opening transition state TS to the reactant R (cyclopropylidene) was determined. It preserves C_s symmetry and corresponds to the straight line between C and TS or Figure 4.A.5. The values of the ring opening angle Φ are given in parentheses. The energy along this path is displayed as a function of Φ in Figure 4.A.6 by the curve between R and TS. It is denoted by A', the irreducible representation of this state in C_s. The dependence upon the symmetry preserving coordinate δ_- and the secondary coordinates γ_j is suppressed.

Table 4.A.7 lists the energy and all 15 coordinates for a number of points on this steepest descent path.

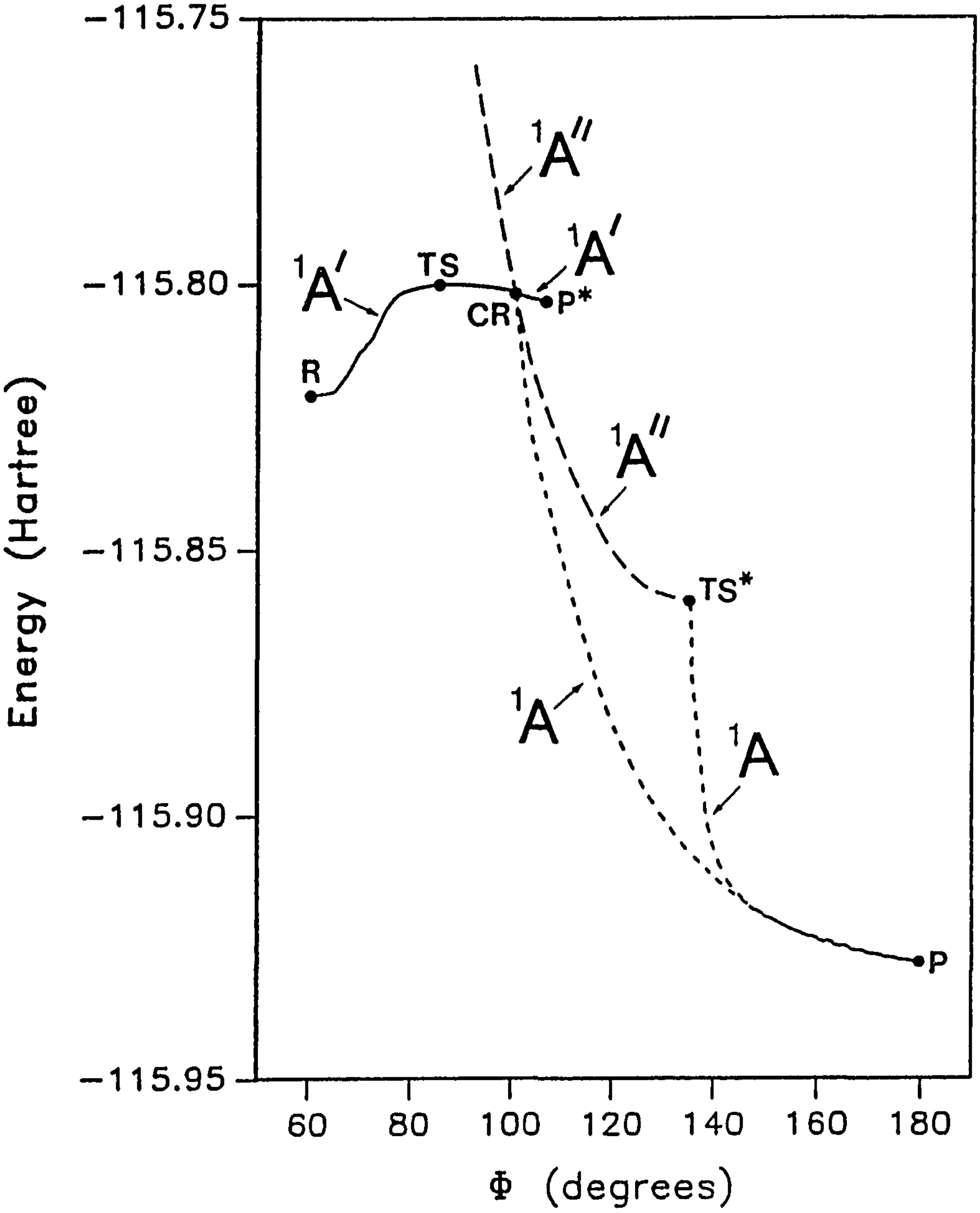

Figure 4.A.6. The various reaction paths

From TS to CR

Next the steepest descent path from the transition state TS towards increasing values of Φ was determined. In principle, this path preserves C_s symmetry. However, because numerical problems can be expected after $\Phi = \Phi(I)$, when the path runs atop a ridge, the steepest descent calculations were performed under restriction to C_s symmetry with the wavefunction restricted to the A′ irreducible representation. The energy is displayed as a function of Φ by the remainder of the curve denoted by A′ in Figure 4.A.6. It is seen to descend very slowly to a minimum at a ring opening angle of about $\Phi = 105°$ which lies only 2 kcal/mole lower than the transition state TS.

We then determined the energy of the lowest A" state along the same path in internal coordinate space, i.e. all internal coordinates were chosen to be identical to those of the steepest descent path of the A′ state listed in Table 7. This energy is displayed, as a function of Φ by the left part of the curve labelled A" in Figure 4.A.6. It starts out higher than the A′ energy, decreases very rapidly and crosses the A′ curve at $\Phi = 100°$, which is thus the point CR.

On Figure 4.A.5, the Φ values, given in parentheses along the straight line depicting the steepest descent path force TS to CR, are those of the A′ state.

Finally, we calculated energies at various points close to the steepest descent curve by choosing $\delta_+ = 0.5°$ and leaving the other 14 coordinates unchanged. We determined the valley-ridge inflection point I where the energy increase with δ_+ changes into an energy decrease with δ_+. It was found to occur for $\Phi = \Phi(I) = 97.6°$.

Table 4.A.7. Internal coordinates of points along the various reaction paths

	Φ	δ_1	δ_2	r_{01}	r_{02}	r_{11}	$r_{11'}$	r_{22}	$r_{22'}$	α_{011}	$\alpha_{011'}$	α_{022}	$\alpha_{022'}$	β_1	β_2	Energy
From R (Cyclopropylidene) to P* ($^1A'$ Planar Allene) via TS on the $^1A'$ surface																
R	60.33	90.0	90.0	1.532	1.532	1.081	1.081	1.081	1.081	117.1	117.1	117.1	117.1	33.1	33.1	-115.82073
	76.40	60.4	119.6	1.439	1.439	1.084	1.078	1.084	1.078	116.5	127.3	116.5	127.3	8.9	8.9	-115.80130
	78.00	60.0	120.0	1.422	1.422	1.079	1.077	1.079	1.077	116/3	128/5	116/3	128/5	4.2	4.2	-115.80045
TS	84.45	51.0	129.0	1.422	1.422	1.079	1.077	1.079	1.077	117.8	127.2	117.8	127.2	1.3	1.3	-115.80016
	92.41	41.4	138.6	1.415	1.415	1.091	1.078	1.091	1.078	118.9	126.2	118.9	126.2	3.2	3.2	-115.80042
	94.00	39.1	140.9	1.414	1.414	1.093	1.078	1.093	1.078	119.1	126.0	119.1	126.0	3.6	3.6	-115.80058
	95.52	36.7	143.3	1.414	1.414	1.094	1.077	1.094	1.077	119.4	125.7	119.4	125.7	3.9	3.9	-115.80077
	97.01	34.2	145.8	1.413	1.413	1.095	1.077	1.095	1.077	119.7	125.5	119.7	125.5	4.0	4.0	-115.80098
	98.53	31.4	148.7	1.413	1.413	1.096	1.076	1.096	1.076	119.9	125.3	119.9	125.3	4.0	4.0	-115.80124
CR	100.33	27.6	152.4	1.412	1.412	1.097	1.075	1.097	1.075	120.2	125.0	120.2	125.0	3.8	3.8	-115.80157
	101.00	21.8	158.2	1.416	1.416	1.084	1.080	1.084	1.080	120.4	125.0	120.4	125.0	2.9	2.9	-115.80211
	104.50	1.7	178.3	1.417	1.417	1.085	1.080	1.085	1.080	121.1	124.6	121.1	124.6	0.2	0.2	-115.80305
P*	106.48	0.0	180.0	1.414	1.414	1.086	1.080	1.086	1.080	120.9	124.5	120.9	124.5	0.0	0.0	-115.80328
To the TS* (Allene Isomerization Transition State) on the $^1A''$ Surface																
	92.41	41.4	138.6	1.415	1.415	1.091	1.078	1.091	1.078	118.9	126.2	118.9	126.2	3.2	3.2	-115.75900
	96.53	35.0	145.0	1.413	1.413	1.095	1.077	1.095	1.077	119.6	125.6	119.6	125.6	4.0	4.0	-115.78232
	98.53	31.4	148.7	1.413	1.413	1.096	1.076	1.096	1.076	119.9	125.3	119.9	125.3	4.0	4.0	-115.79273
CR	100.33	27.6	152.4	1.412	1.412	1.097	1.075	1.097	1.075	120.2	125.0	120.2	125.0	3.8	3.8	-115.80157
	101.94	27.1	152.9	1.407	1.407	1.082	1.074	1.082	1.074	121.2	123.3	121.2	123.3	3.9	3.9	-115.80867
	105.44	25.7	154.3	1.396	1.396	1.075	1.072	1.075	1.072	120.3	123.1	120.3	123.1	3.9	3.9	-115.81999
	110.46	22.8	157.2	1.388	1.388	1.075	1.071	1.075	1.071	117.5	125.1	117.5	125.1	3.8	3.8	-115.83259
	116.13	17.9	162.1	1.385	1.385	1.078	1.068	1.078	1.068	116.6	125.6	116.6	125.6	3.0	3.0	-115.84416
	122.08	11.1	168.9	1.384	1.384	1.079	1.073	1.079	1.073	117.4	124.7	117.4	124.7	1.8	1.8	-115.85323
	127.91	4.5	165.5	1.384	1.384	1.078	1.072	1.078	1.072	118.8	123.2	118.8	123.2	0.7	0.7	-115.85791
	133.42	1.0	179.0	1.385	1.385	1.077	1.075	1.077	1.075	120.6	121.8	120.6	121.8	0.1	0.1	-115.85946
TS*	135.00	0.0	180.0	1.385	1.385	1.076	1.076	1.076	1.076	121.0	121.0	121.0	121.0	0.0	0.0	-115.85970

Table 4.A.7. (continued)

	Φ	δ_1	δ_2	r_{01}	r_{02}	r_{11}	$r_{11'}$	r_{22}	$r_{22'}$	α_{011}	$\alpha_{011'}$	α_{022}	$\alpha_{022'}$	β_1	β_2	Energy
From TS* (Allene Isomerization Transition State) to P (D_{2d} Allene) via a C_1 route																
TS*	135.0	0.0	180.0	1.385	1.385	1.076	1.076	1.076	1.076	121.0	121.0	121.0	121.0	0.0	0.0	-115.85970
	135.1	-5.3	174.7	1.384	1.384	1.074	1.075	1.073	1.075	121.1	121.0	121.2	120.9	1.4	1.4	-115.86316
	135.4	-11.7	168.4	1.380	1.380	1.071	1.059	1.067	1.063	121.4	120.8	121.4	120.8	2.9	2.9	-115.87282
	138.5	-27.9	152.1	1.356	1.356	1.071	1.116	1.084	1.105	123.1	119.5	123.0	119.6	6.0	6.0	-115.90119
	141.8	-36.1	144.1	1.342	1.342	1.056	1.121	1.079	1.105	123.8	118.6	123.6	118.7	6.6	6.6	-115.91119
	145.0	-40.2	140.1	1.337	1.337	1.044	1.118	1.071	1.101	123.9	118.2	123.7	118.4	6.6	6.6	-115.91534
	151.3	-43.5	136.8	1.332	1.332	1.039	1.110	1.060	1.094	123.5	118.4	123.4	118.5	5.9	5.9	-115.91982
	157.3	-44.2	135.6	1.328	1.328	1.050	1.114	1.059	1.100	122.4	119.6	122.4	119.5	4.9	4.9	-115.92268
	161.6	-44.6	135.6	1.327	1.327	1.050	1.111	1.055	1.103	122.0	120.0	122.0	119.9	4.2	4.2	-115.92396
P	180.0	-45.0	135.0	1.324	1.324	1.076	1.076	1.076	1.076	120.9	120.9	120.9	120.9	0.0	0.0	-115.92827
From CR (Intersection point) to P (D_{2d} Allene) via a C_1 route																
CR	100.3	27.6	152.4	1.412	1.412	1.097	1.075	1.097	1.075	120.2	125.0	120.2	125.0	3.8	3.8	-115.80157
	103.6	33.0	164.6	1.406	1.391	1.080	1.078	1.080	1.077	121.3	123.3	121.8	122.9	3.8	3.8	-115.82687
	111.8	40.2	173.2	1.377	1.373	1.072	1.049	1.075	1.046	126.3	117.6	123.9	119.5	6.8	-1.6	-115.85849
	117.0	45.0	-168.4	1.359	1.366	1.074	1.121	1.091	1.079	126.3	117.5	124.2	119.1	6.9	-3.7	-115.87502
	120.8	47.9	-163.6	1.351	1.360	1.066	1.123	1.094	1.075	126.1	118.9	124.1	118.9	6.8	-5.0	-115.88461
	130.5	52.7	-155.1	1.342	1.349	1.088	1.104	1.058	1.039	126.1	116.6	124.1	118.4	6.5	-7.0	-115.90145
	139.2	54.7	-150.6	1.334	1.340	1.096	1.116	1.063	1.049	124.8	117.5	123.4	118.7	6.0	-7.6	-115.91093
P	180.0	55.0	-145.0	1.324	1.324	1.076	1.076	1.076	1.076	120.9	120.9	120.9	120.9	0.0	0.0	-115.92827

From CR to TS*

For Φ larger than Φ(CR) = 100°, the curve A" lies below the curve A′ on Figure 4.A.6 and, hence, the ground state belongs to the irreducible representation A" on this part of the C_s preserving coordinate subspace. We therefore determined the ground state steepest descent curve from CR to TS* under the restriction that the wavefunction belongs to A" symmetry. Its energy is displayed as a function of Φ by the right part of the curve labelled A" on Figure 4.A.6. On Figure 4.A.5, this steepest descent path is depicted by the straight line from CR to TS*, the Φ values in parentheses are those of the A" state.

It is apparent that the A" energies for Φ < 100° and the A′ energies for Φ > 100° are part of the lowest excited state. It was verified that it has in fact a minimum, i.e. an equilibrium geometry at Φ = 105°.

From TS* to A

The steepest descent paths shown in Figure 4.A.5 from TS* to the two allene products P, P′ are each other's mirror images. Again the appropriate Φ values are indicated in parentheses and the energy is displayed as a function of Φ in Figure 4.A.6. This path is a model for the isomerization of the allene ground state.

From I/CR to P/P′

As discussed in Section 4.A.4.1, the C_s preserving steepest descent path from I over CR to TS* is unsuited as a reaction path model because it runs atop a ridge. We therefore calculated a C_s-symmetry breaking steepest descent curve which lead directly to the product P. It was obtained by starting near the intersection point CR. All internal coordinates of this starting point were chosen as those of the point CR, except that $\delta_+ = 0°$ was replaced by $\delta_+ = 0.5°$. The resulting steepest descent curve is shown as a light line on Figure 4.A.5 and its energy is displayed as a function of Φ in Figure 4.A.6 by the curve denoted as A.

The internal coordinates and energies of the points on the various steepest descent paths are listed in Table 4.A.7.

5. The Intersecting Coordinate Subspace (ICS)

The point CR is not the only point where the two states corresponding to the symmetries A′ and A″ (in C_s) cross. In fact, there exists a multidimensional region in the coordinate space where E(A′) = E(A″). We call it the "intersecting coordinate subspace (ICS)". Since we are not aware of previous explicit examinations of high dimensional potential energy surface intersections, we shall discuss the present ICS in some detail. We shall be particularly concerned with the ICS in the neighborhood of the point CR since this has a bearing on the steepest descent curves near CR which, in turn, are relevant for the mentioned restarting of the steepest descent near I or CR toward the products.

5.1. Dimensionality.

Two potential energy surfaces do not have to intersect. However, if they do then it is to be expected (i.e. the opposite is highly unlikely) that there exist, embedded in the space spanned by all internal coordinates q_1, q_2 ... q_M regions having the character of multidimensional curvilinear

linear surfaces on which $E_1 = E_2$. The ensemble of these regions forms the intersecting coordinate subspace for the two states. This ICS is determined by having to satisfy two conditions, namely

$$\Delta H(q_1 \ldots q_M) = H_{11}(q_1 \ldots q_M) - H_{22}(q_1 \ldots q_M) = 0 , \quad (4.A.1)$$

$$H_{12}(q_1 \ldots q_M) = 0 , \quad (4.A.2)$$

where H_{11}, H_{22}, H_{12} are hamiltonian matrix elements with respect to a certain many-electron function basis F_1, F_2. As indicated, they are functions of the M internal coordinates $q_1 \ldots q_M$ of the molecule. In general, it is therefore to be expected that, if the Eqs. (4.A.1,2) have any real solutions at all, then the solutions space, i.e. the ICS is a hyperspace of dimension (M-2). This conclusion must however be modified in those cases where, for all values of the coordinates $q_1 \ldots q_M$ the molecule is invariant under a symmetry group and the two intersecting states belong to different irreducible representations. In this situation the functional bases F_1, F_2 can be chosen as belonging to these two irreducible representations without reference to the hamiltonian of the system and, hence, the matrix element H_{12} vanishes identically for all values of $(q_1 \ldots q_M)$. Consequently, F_1 and F_2 are in fact the two states and only Eq. (4.A.1) provides a true restriction. Thus, the ICS is of dimension (M-1) in this case. Similar reasoning applies if a coordinate subspace is invariant under some symmetry group, as will be seen below.

In the present case, the overall symmetry group is C_1 and the full internal coordinate species of dimension 15. Since C_1 has only one irreducible representation, the ICS is of dimension 15-2 = 13.

There exists however, as we have seen, a coordinate subspace in which the molecule has C_s symmetry. It is apparent that the ring opening coordinate Φ preserves C_s symmetry when it exists and that the remaining 14 internal coordinates (δ_1, δ_2, γ_1, γ_2 ... γ_{12}) come in pairs such that, for each pair, the sum and the difference are either symmetric or antisymmetric with respect to the C_s symmetry plane. Let δ_+, γ_1', γ_2,' ... γ_6' denote the antisymmetric combinations and δ_-, γ_1'', γ_2'' ... γ_6'' the symmetric ones. It follows then that the preservation of C_s symmetry is equivalent to the seven "C_s symmetry-breaking" coordinates δ_+, γ_1', γ_2' ... γ_6' remaining zero and, when this is the case, that the C_s preserving coordinate subspace is spanned by the eight "C_s symmetry preserving" coordinates Φ, δ_-, γ_1'', γ_2'' ... γ_6''.

Since, within this subspace, the two states under consideration belong to different irreducible representation of C_s (viz. A' and A"), it follows from what has been said before that, within the C_s preserving subspace, the ICS is of dimension $8 - 1 = 7$. Thus, of the 13 degrees of freedom the intersecting coordinate subspace has in C_1, seven maintain C_s symmetry and $13-7=6$ break C_s symmetry.

5.2. Linear approximation near CR

From Eqs. (4.A.1) and (4.A.2) it is apparent that, in the immediate neighborhood of CR, the ICS hypersurface coincides to first order with the tangential hyperplane which is perpendicular to the gradient of ΔH and that of H_{12}. These two gradients have simple forms. First, since, as we have seen earlier, the energies vary quite slowly with the twelve secondary coordinate γ_1, γ_2 ... γ_{12}, we can neglect the partial derivatives with respect to these coordinates. It is furthermore evident that H_{11} and H_{22}, and hence also ΔH, are symmetric with respect to deviations from C_s symmetry whereas H_{12} is antisymmetric with respect to such displacements. Hence the partial derivative of ΔH with respect to the antisymmetric coordinate δ_+ vanishes as do the partial derivatives of H_{12} with respect to the symmetric coordinates Φ and δ_-. Expansion of the two conditions (4.A.1) and (4.A.2) to first order yields therefore

$$\Delta H = a_1 \hat{\Phi} + a_2 \hat{\delta}_- = a \xi = 0 , \qquad (4.A.3)$$

$$H_{12} = b \delta_+ = 0 , \qquad (4.A.4)$$

where

$$\begin{aligned} \hat{\Phi} &= \Phi - \Phi(CR) = \text{displacement of } \Phi \text{ from CR} \\ \hat{\delta}_- &= \delta_- - \delta_-(CR) = \text{displacement of } \delta_- \text{ from CR} \qquad (4.A.5) \\ \delta_+ &= \delta_+ - \delta_+(CR) = \text{displacement of } \delta_+ \text{ from CR} \end{aligned}$$

$$a_1 = [\partial(\Delta H)/\partial\Phi]_{CR}, \quad a_2 = [\partial(\Delta H)/\partial\delta_-]_{CR}, \quad b = [\partial H_{12}/\partial\delta_+]_{CR} \qquad (4.A.6)$$

and

$$\xi = (a_1 \hat{\Phi} + a_2 \hat{\delta}_-)/a, \quad \text{with} \quad a = [a_1^2 + a_2^2]^{1/2} . \qquad (4.A.7)$$

It is now apparent that, near CR, the ICS is approximated by the 13-dimensional hyperplane defined by

$$\delta_+ = 0 \,, \qquad \xi = 0 \,. \qquad (4.A.8)$$

Conversely, the coordinates spanning the ICS hyperplane near CR are the six C_s symmetry breaking coordinates γ_1', γ_2' ... γ_6' and the seven C_s symmetry preserving coordinates γ_1'', γ_2'' ... γ_6'' and

$$\eta = (a_2 \hat{\Phi} - a_1 \hat{\delta}_-)/a \,. \qquad (4.A.9)$$

The coordinates ξ, η are obtained from Φ, δ_- by an orthogonal transformation.

In fact, we shall see in the next section that $a_2 << a_1$, so that, approximately, $\xi \approx \Phi$ and $\eta \approx \delta_-$. The reason for this is as follows. The orbital analysis to be discussed in Sections 4.B.4.2 and 4.B.4.3 will show that the crossing of the A′ and the A″ energies is due to the shift of approximately one electron from the lone orbital on the central carbon, with A′ symmetry, to the nonbonding molecular orbital between the two end carbons, with A″ symmetry. This shift is a consequence of the fact that, as the ring opens, the orbital energy of the A′ orbital increases (due to increasing p character) whereas that of the A″ orbital decreases (due to the increasing distance between the end atoms). Since these energy changes are essentially determined by the ring-opening angle Φ, one would indeed expect that, to first order, one has approximately

$$\Delta H \approx a_1 \hat{\Phi} \,. \qquad (4.A.10)$$

Near CR, the ICS is then approximately the hyperplane satisfying

$$\hat{\Phi} = \Phi(CR), \qquad \delta_+ = \delta_+(CR) = 0. \qquad (4.A.11)$$

5.3. Determination of the linear approximation

Near the point CR on the ICS, the lower energy surface is given by the expression

$$E = E(CR) + \bar{H} - [(\Delta H)^2 + (H_{12})^2]^{1/2} \qquad (4.A.12)$$

where, in agreement with (4.A.3) - (4.A.7), the terms ΔH and H_{12} are given by

$$\Delta H = a_1 \hat{\Phi} + a_2 \hat{\delta}_- , \qquad (4.A.13)$$

$$H_{12} = b\ \delta_+ , \qquad (4.A.14)$$

and the term $\bar{H}$ is given by

$$\bar{H} = (H_{11} + H_{22})/2 = c_1 \hat{\Phi} + c_2 \hat{\delta}_- \qquad (4.A.15)$$

The partial derivative of $\bar{H}$ with respect to δ_+ vanishes for the same reason as it does for ΔH.

The coefficients a_1, a_2, b, c_1, c_2 were determined as follows. After having found the crossing coordinates $\Phi(CR)$, $\delta_-(CR)$ and all γ_j (CR), as described in Section (4.A.4.2), the energy of the molecule was calculated for the following geometries

(i) $\hat{\phi} = 0$, $\hat{\delta}_- = 0$, $\delta_+ = 1°$

(iia) $\hat{\phi} = 0$, $\hat{\delta}_+ = 0$, $\hat{\delta}_- = 1°$

(iib) $\hat{\phi} = 0$, $\hat{\delta}_+ = 0$, $\hat{\delta}_- = -1°$

(iiia) $\delta_+ = 0$, $\hat{\delta}_- = 0$, $\hat{\phi} = 1°$

(iiib) $\delta_+ = 0$, $\hat{\delta}_- = 0$, $\hat{\phi} = -1°$

(iva) $\delta_+ = 0$, $\hat{\delta}_- = \hat{\phi}$, $\hat{\phi} = 1°$

(ivb) $\delta_+ = 0$, $\hat{\delta}_- = \hat{\phi}$, $\hat{\phi} = -1°$

Reference to Eqs. (4.A.11) - (4.A.15) shows that calculation (i) yields b, calculations (iia) and (iib) yield $|a_2|$ and c_2, calculations (iiia) and (iiib) yield $|a_1|$ and c_1, calculations (iva) and (ivb) yield $|a_1 + a_2|$ and $(c_1 + c_2)$. From calculation (ii), (iii) and (iv) one obtains a_1 and a_2 and one can check $(c_1 + c_2)$ against c_1 and c_2 to verify the validity of the linear approximation. The following values were found:

$$\begin{aligned} a_1 &= 1729 \text{ microhartree} & a_2 &= 260 \text{ microhartree} \\ c_1 &= -1891 \text{ microhartree} & c_2 &= -325 \text{ microhartree} \qquad (4.A.16) \\ b &= 93 \text{ microhartree.} \end{aligned}$$

5.4. Steepest descent lines near CR.

Insertion of the values of Eq. (4.A.16) into the definition (4.A.7), (4.A.9) for ξ, η and into the energy expression (4.A.12) to (4.A.15) yields

$$E - E(CR) = -1918\,\xi - 40\eta - [(1748\xi)^2 + (93\delta_+)^2]^{1/2}\,, \qquad (4.A.17)$$

where E given in microhartrees and

$$\xi = 0.9889\hat{\phi} + 0.1487\hat{\delta}_- \qquad (4.A.18)$$
$$\eta = -\ 0.1487\hat{\phi} + 0.9889\hat{\delta}_-.$$

The line $\xi = 0$ is part of the ICS. On it the energy varies according to $E\text{-}E(CR) = -\ 40\eta$. (The other six coordinates of the ICS in C_s are γ_1'', γ_2'' ... γ_6''). The slow descent for $\xi < 0$ belongs to the A′ state, the steep descent for $\xi > 0$ belongs to the A″ state. In agreement with an earlier statement, the steepest descent lines are nearly parallel to the ξ axis which, in turn, is very close to the $\hat{\Phi}$ axis.

The following conclusions can be drawn: (i) Only one steepest descent line arrives at CR from $\xi < 0$ and only one steepest descent line leaves CR towards $\xi > 0$; (ii) Both, the steepest descent line arriving at CR from $\xi < 0$ and the one leaving CR towards $\xi > 0$, maintain C_s symmetry (i.e. δ_+ remains zero); (iii) Within the C_s preserving coordinate subspace, there occurs a relatively small change in the direction and a very large change in the magnitude of the steepest descent lines when they cross the ICS near CR. It follows that one has to restart on a steepest descent line that does not pass through CR, if one wishes to follow a C_s symmetry-breaking steepest descent to the allene product.

5.5. Intersecting Coordinate Subspace and reduced energy surfaces

In the discussion of the global features of the potential energy surface by Valtazanos et. al. (1990) as well as in the discussion of the ring opening transition state in Section 4.A.3.1 we relied heavily on the reduced potential energy surface which is easier to visualize. It is obtained by optimizing the energy for each choice of (Φ,δ_1,δ_2) and hence a function $E(\Phi,\delta_1,\delta_2)$. This function is the collection of all these points on the full surface $E(\phi,\delta_1,\delta_2,\gamma_1,\gamma_2\ldots\gamma_{12})$ which satisfy the twelve conditions

$$(\partial E/\partial\gamma_j)_{\phi\delta_1\delta_2} = 0, \qquad j = 1,\ 2,\ \ldots\ 12\ . \qquad (4.A.19)$$

In the present section we examine the relation between the reduced surface, and the intersecting coordinate space. We must now deal with two reduced surfaces, namely

$$E_1(\phi,\delta_1,\delta_2) \text{ defined by } (\partial E_1/\partial j_j)_{\phi\delta_1\delta_2} = 0\ ,\ j=1,2\ldots12, \qquad (4.A.20)$$

$$E_2(\phi,\delta_1,\delta_2) \text{ defined by } (\partial E_2/\partial j_j)_{\phi\delta_1\delta_2} = 0\ ,\ j=1,2\ldots12. \qquad (4.A.21)$$

Complications arise from the fact that, for a given choice of (ϕ,δ_1,δ_2), the values of the optimized secondary coordinates $(\gamma_1,\gamma_2\ldots\gamma_{12})$ of $E_1(\phi,\delta_1,\delta_2)$ are in general different from those of $E_2(\phi,\delta_1,\delta_2)$.

Consider the 13 dimensional ICS in C_1. The twelve additional derivative conditions (4.A.20) define a line on the ICS which is also a line on the reduced surface $E_1(\phi,\delta_1,\delta_2)$. Similarly, addition of the twelve derivative conditions (4.A.21) will define another line on the ICS which, at the same time, lies on the reduced surface $E_2(\phi,\delta_1,\delta_2)$. In general, these two lines on the ICS are not identical, they will not even intersect.

Similar reasoning holds in the C_s preserving subspace defined by $\delta_+ = \gamma_1' = \gamma_2' = \ldots = \gamma_6' = 0$. Since the derivatives with respect to these antisymmetric coordinates vanish as well when C_s is present, the twelve Eqs. (4.A.19) can be replaced by the six conditions

$$(\partial E/\partial \gamma_j'')_{\phi,\delta_-,\delta_+=0} = 0, \qquad j = 1,2, \ldots 6. \qquad (4.A.22)$$

These six additional conditions define a line in the 7-dimensional ICS in C_s which also lies on the reduced surface $E(\phi,\delta_+=0,\delta_-)$. Again, the lines corresponding to E_1 and E_2 are different and cannot be expected to intersect.

For both reduced surfaces $E_1(\phi,\delta_1,\delta_2)$, $E_2(\phi,\delta_1,\delta_2)$ the ICS line found in C_1 symmetry can be identical with that found for C_s symmetry, i.e., it can lie entirely in the C_s preserving subspace. This does not have to be so, but we believe it to be the case here.

To illustrate these observations, we made calculations involving a further reduction of the potential energy surface by minimizing also with respect to δ_-. The resulting surfaces $E_1(\phi,\delta_+)$ and $E_2(\phi,\delta_+)$ were considered in the C_s preserving subspace. I.e., we examined the reduced energy curves $E_1(\phi)$, $E_2(\phi)$ which we obtained by setting $\delta_+ = 0$ and adding the respective condition

$$(\partial E_j/\partial \delta_-)_{\phi,\delta_+=0} = 0, \qquad j = 1,2 \qquad (4.A.23)$$

to Eq. (4.A.22). The apparent intersection of the reduced energy curves for Φ ranging from 84° to 105°, shown in Figure 4.A.7, is not a true intersection since the two curves differ in the values of the optimized coordinates, in particular δ_-.

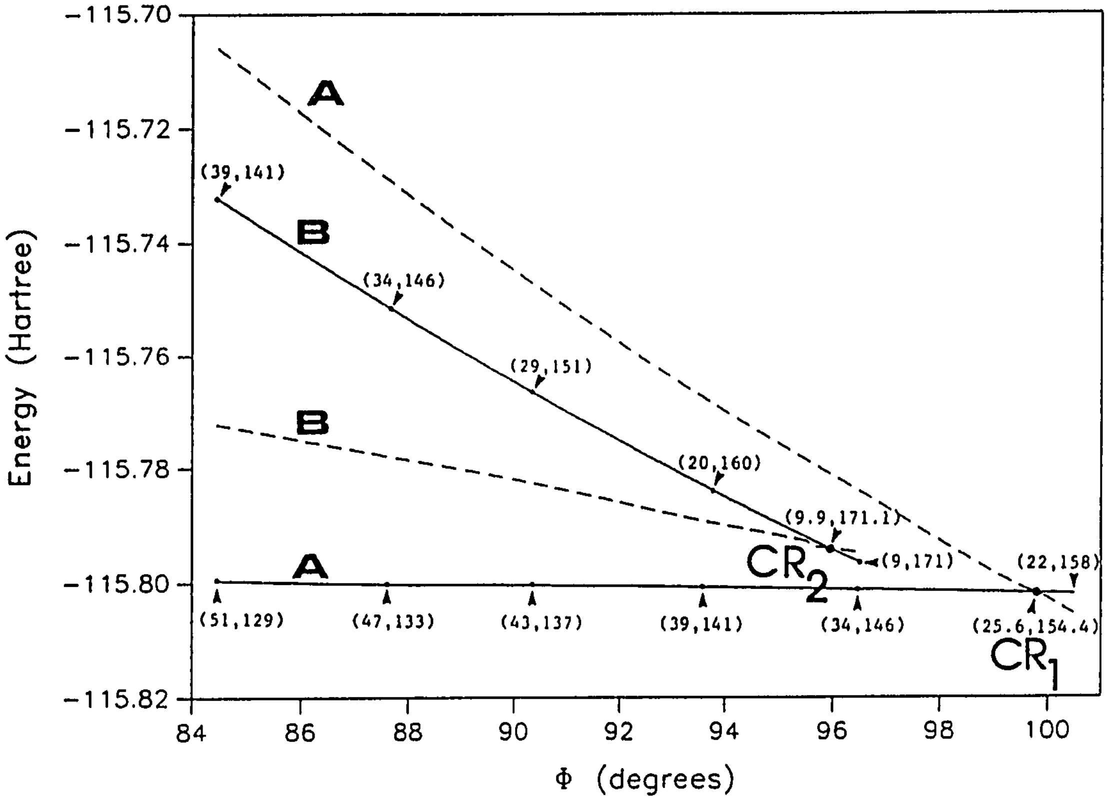

Figure 4.A.7. Location of the CR_1 and CR_2 points.

Type-(A) curves: geometries optimized in the $^1A'$ state.

Type-(B) curves: geometries optimized in the $^1A''$ state.

Solid curves: minimum in C_s; dashed curves: geometries optimized in the other state. Optimized (δ_1, δ_2) values are shown in parentheses

The intersection points CR_1 and CR_2 of the two curves with the ICS were determined as follows. For the optimized coordinates (δ_-, γ_1'' ... γ_6'') of the A′ state (solid A′ line) we calculated the A″ energies at various ϕ values. The latter is plotted as the dashed line labelled A″ in Figure 4.A.7 (it lies of course above the solid A″ line). The crossing point CR_1 of the solid A′ line and the dashed A″ line, is the point which the reduced surface $E_1(\phi)$ has in common with the ICS. Similarly, the dashed line labelled A′ (which lies above the solid A′ line) is a plot of A′ energies calculated for the coordinates (δ_-, γ_1'' ... γ_6'') optimized for A″ (solid A″ line). The crossing point CR_2 of the dashed A′ and the solid A″ line is the point which the reduced surface $E_2(\phi)$ has in common with the ICS.

It is seen that the two points CR_1 and CR_2 are fairly close to the earlier found point CR which lies on the steepest descent curve. All three points have C_s symmetry and lie on the ICS. One would therefore expect that the coordinates of CR, CR_1, CR_2 would satisfy Eqs. (4.A.8) which defines the ICS to first order near CR. From Figure 4.A.7 and Eq. (4.A.16) one finds the ξ-values $\xi(CR_1) = -0.23°$, $\xi(CR_2) = -1.73°$ which are indeed small.

6. The free internal rotation of the CH_2 groups

A very distinctive feature found on the potential energy surface of Valtazanos et. al. (1990) for values of Φ larger than about 100° outside the C_s preserving subspace, i.e. for $\delta_1 + \delta_2 \neq n \cdot 180°$ (n = integer) was an almost free, cogwheel-like, synchronized internal rotation of the two CH_2

groups for fixed ring-opening angles. It was depicted by isoenergetic shelves in valleys which, approximately, followed the lines $\delta_1 + \delta_2 = 90° + n \cdot 180°$ (n = integer) on the contour panels Φ = constant > 100°. The panel for $\Phi = 100°$ computed with the STO-3G basis set and the FORS1 space is displayed in Figure 4.A.8a. The valley is seen to sway back and forth slightly from the line $\delta_1 + \delta_2 = 90°$ and it contains slight minima, the one denoted by m lying at $\delta_1 + \delta_2 = 37°$.

Since this is a very characteristic feature, it was considered important to confirm that it would be preserved by the more accurate calculations. To this end, we recalculated the entire panel for $\Phi = 100°$ at the (FORS1/ii) level and the resulting contours are displayed in Figure 4.A.8b. While the absolute energies are of course different from those computed with the STO-3G basis, the contour increment is the same as in Figure 4.A.8a (5 millihartree). It is seen that the overall topography is the same in both figures, namely valleys weaving around the average line $\delta_1 + \delta_2 = (90° + n \cdot 180°)$ and separated by ridges following the lines $\delta_1 + \delta_2 = n \cdot 180°$. For the more accurate calculations, the maxima are somewhat broader and force a more undulatory character on the valleys. The valley minimum denoted by m occurs for $\delta_1 = \delta_2 = 29°$. However, the very slight barrier along the valley floor is almost the same for both calculations (2.5 Kcal/mole for the STO-3G basis set, 3.1 Kcal/mole for the extended basis set (ii) of Section 4.A.2.2) and so is the energy difference between the minimum m and the maximum M (about 45 Kcal/Mole for both calculations).

There exists a slight possibility that the differences between the contours in Figures 4.A.8a and 4.A.8b are somewhat exaggerated due to the method of calculation. For the minimal basis set calculations the contours

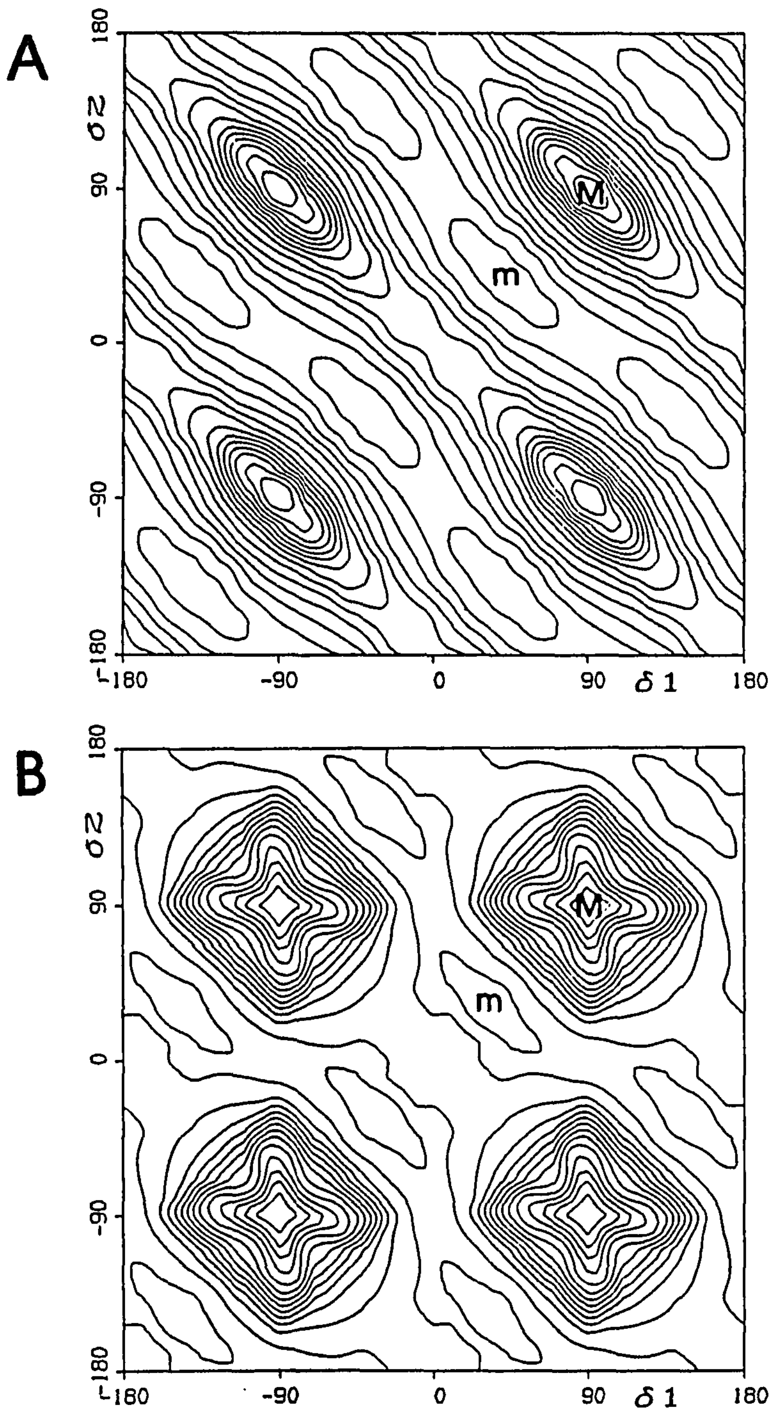

Figure 4.A.8. Panels for Φ=100°. A: FORS1/i, B:FORS1/ii.

Increment: 5 mhartree; m:minimum; M: maximum of each panel were based on 50 points. We found, however, that the contour map for $\Phi = 100°$ remained virtually unchanged when only the 25 points

$$\delta = 20n_1 + 10n_2, \qquad \delta_2 = 10n_2$$

$$n_1 = 0,2,4, \ldots (9-n_2), \qquad n_2 = 1,3,5,7,9.$$

were used. Therefore, the more accurate calculations were only performed at these points and the contours of both, Figure 4.A.8a and 4.A.8b, are based on this set of points. It is possible, although not very likely, that the two contour maps might look more similar to each other, had both been based on 50 points.

Incidentally, the savings in computing time hoped for by calculating only 25 points was not realized because the reduction in the number of points was offset by the increase in computation needed for each point (Φ,δ_1,δ_2). This was so since, due to the larger distance between the individual 25 points, the initial approximations to the geometries of the 12 secondary coordinates were poorer as were the starting orbitals for the MCSCF calculations. Consequently, convergence was considerably slower for both these iterative procedures.

B. Ab-initio Interpretation of the Electronic Rearrangements in Terms of Quasiatomic Orbitals

1. Introduction

Upon examining the energy changes that are exhibited by a potential energy surface with the complexity of that found for the cyclopropylidene ground state ring opening chemists can be expected to ask whether ab-initio theory can also produce insightful explanations for the computed energy changes. In view of the advances made over the past decade in quantum chemical calculations it stands to reason that one would hope for equally rigorous quantifications regarding the interpretation of such calculations in terms of chemical and physical concepts.

A fundamental tenet of intuitive chemical thinking is the interpretation of molecules in terms of interactions between atoms. Such an interpretation does not emerge trivially from ab-initio quantum chemistry because, in principle, all electrons in a molecule must be treated on an equal footing and molecular wavefunctions must be antisymmetrized with respect to all electronic coordinates. Moreover, decompositions in terms of atomic contributions present particular difficulties in the simplest and most widely used ab-initio method, namely the conventional Hartree-Fock self-consisted-field model. This is because, even in their most localized forms, self-consistent-field bonding orbitals necessarily cover several atoms. Any decomposition of such orbitals in terms of atomic contributions requires a split of individual bonding MO's into parts which are assigned to different atoms. Such segmentations (as for example formalized by Mulliken's population analysis) are fundamentally arbitary, they tend to be basis-set dependent and, for calculations with extended basis sets, they often loose their meaning. Since multiconfigurational calculations are inherently more complex than the SCF approach, there may exists a perception that the problem of interpreting molecules in terms of atoms becomes even more difficult when proceeding from the SCF approximation to more sophisticated descriptions. In any event,there do not yet exist well established quantitative ab-initio procedures for the interpretation of bonding interactions between atoms in a molecular system, in particular when the latter is far from its equilibrium positions.

Through the present investigation we hope to show that the situation is much more favorable when one considers molecular wavefunctions obtained within the FORS framework even though the latter is considerably more sophisticated than the self-consistent-field (SCF) model. It is a multi-configuration-self-consistent-field (MCSCF) approach that includes the major fraction of that part of the electron correlation energy which changes in the course of a reaction. Nonetheless the FORS model provides, without arbitary additional assumptions, an effective vehicle for the analysis of molecular systems in terms of atomic subsystems. It leads in a natural manner to definitions of deformed atoms in molecules and of interactions between them.

We shall use this approach here to gain insight into the electronic rearrangements that occur during the cyclopropylidene ring opening. In particular, we shall examine the ring-opening barrier, the allene isomerization barrier and the cogwheel-type free synchronized rotations of the CH_2 groups. The understanding obtained in this manner for this reaction is found to fit in with the spirit of physical organic chemistry. This result suggests that the developed analysis, based on FORS wavefunctions, can yield ab-initio interpretations which may furnish the foundation for a closer integration of ab-initio calculations and chemical intuition.

2. Method of analysis

2.1. Localized FORS MO's as Molecule-Adapted Deformed Minimal-Basis-Set Atomic Orbitals: Quasi-Atomic Orbitals.

The nature of FORS wavefunctions is described in Section 4.A.2.3. Two facts are essential in the present context:

(i) FORS wavefunctions are obtained by an MCSCF procedure in a full configuration space, i.e. they are expanded in terms of all configurations that can be generated from a given set of "reactive" or "active" orbitals;

(ii) The number of these configuration-generating orbitals is equal to the number of conceptual minimal-basis atomic orbitals that are involved in the reaction under study.

The interpretative procedure to be described here takes advantage of the circumstance that a full configuration space remains invariant when the molecular orbitals which generate the configurational basis are subjected to orthogonal transformations. Such orbital transformations do yield new configurational bases, but these span the same configuration space. The same (optimal) wavefunction can therefore be expressed as a superposition of many different types of configurations.

Several sets of FORS molecular orbitals prove useful for the case at hand. They will be called:

(i) Quasi-atomic FORS MO's,

(ii) Natural FORS MO's,

(iii) Chemically localized FORS MO's.

The various orbital bases, and the associated configurational bases generate different (but equivalent) descriptions of the arrangements of the electrons in a molecule and, thereby, illustrate different aspects of one and the same electronic distribution. They furnish complementary insights which can be combined to yield a balanced interpretation of the electronic structure.

It is expedient to begin with the quasi-atomic FORS orbitals. This molecular orbital set results from localizing the configuration generating FORS MOs as much as possible. It has been demonstrated in detail in a series of previous publications, and it will be seen again here, that such maximally localized FORS MOs have the character of molecule-adapted deformed minimal-basis-set atomic orbitals. They effect an intrinsic partitioning of the electron population according to atoms and we therefore call them quasi-atomic MO's.

In the case at hand we have a wavefunction with a nine orbital SCF-type core and a full reactive space generated by four electrons in four reactive orbitals. In such a case the core orbitals and the reactive orbitals must be localized separately. The localization of the core orbitals yields three inner shell orbitals on the three carbons; two carbon-carbon sigma bonds (for C_0C_1 and C_0C_2) and four carbon-hydrogen sigma bonds. The localization of the four reactive FORS MOs on the other hand yields quasi-atomic molecular orbitals |0>, |0'>, |1>, |2> which, as we shall see, look very much like the reactive atomic valence orbitals that are qualitatively sketched in Figure 4.B.1 for the reactant (cyclopropylidene), the product (linear staggered allene) and the allene isomerization transition state (bent planar allene).

2.2. Density and Population Analysis of a FORS Wavefunction.

Meaningful insights into the electronic structure are obtained by examining the electron density kernel ρ of the FORS wavefunction. The expansion of ρ in terms of the aforementioned quasiatomic localized FORS MO's has the form

$$\rho = 2 \sum_{\nu} |\nu\rangle\langle\nu| + \sum_{i,j} p_{ij} |i\rangle\langle j| \quad , \qquad (4.B.1)$$

where the index ν runs over the nine localized core MO's and the indices i,j run over the four localized reactive MO's, i.e. the quasi-atomic orbitals |0>, |0'>, |1>, |2>.

Because of the orbital orthogonality the diagonal elements of the density matrix p lie between 1 and 2 and they are the rigorous occupation numbers of the localized FORS MOs. Since the latter are quasi-atomic orbitals, the p_{ii} yield therefore directly an unambiguous population analysis in terms of the orthogonalized deformed atoms in the molecule.

Furthermore, since the bonding and antibonding contributions to the molecular energy can be shown to arise predominantly from interference

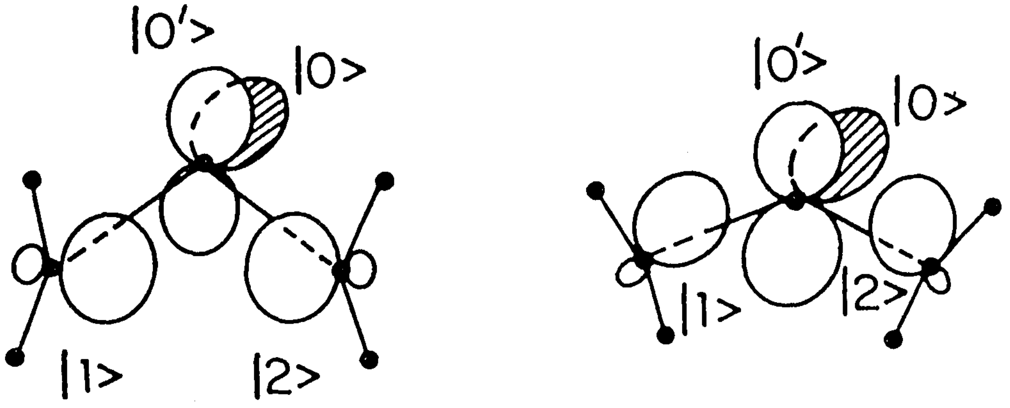

CYCLOPROPYLIDENE TRANSITION STATE

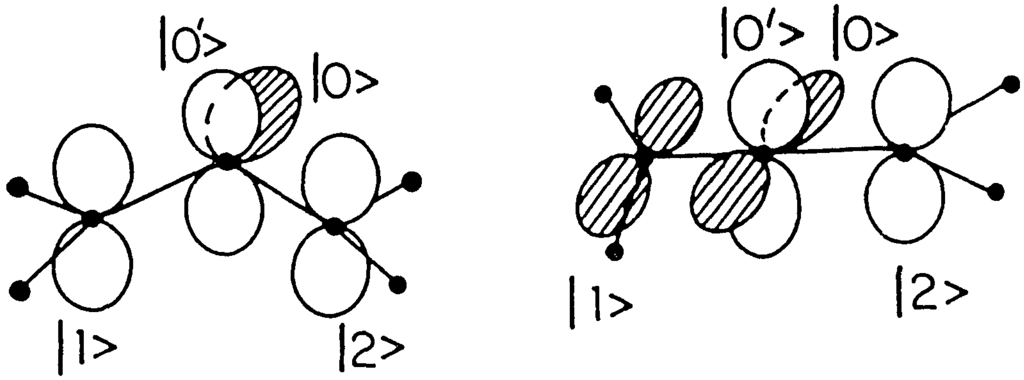

ALLENE ISOMERIZATION T.S. ALLENE

Figure 4.B.1. Qualitative sketch of quasiatomic FORS MO's

energy terms of the type $p_{ij}<i|h|j>$, the off- diagonal density matrix elements p_{ij} have the significance of bond orders which locate bonding, nonbonding and antibonding effects between the different quasi-atomic orbitals, depending upon appropriate values of the resonance integrals $<i|h|j>$. From the example of a doubly occupied diatomic homonuclear molecular orbital, which is expressed in terms of two orthogonalized atomic orbitals as $\phi = (A+B)/\sqrt{2}$, it can be seen that the maximum absolute value which this type of bond order can assume is unity.

Further insight into the nature of the density matrix p_{ij} is obtained by bringing it into diagonal form. This transformation yields the natural MO's. If the orthogonal matrix T diagonalizes the matrix p, then we have

$$(T^{+}pT)_{nm} = N_n \delta_{nm} \tag{4.B.2}$$

whence

$$p_{ij} = \sum_{n} N_n \, T_{in} \, T_{jn} \tag{4.B.3}$$

With the help of Eq. (4.B.3) the density is easily expressed as

$$\rho = 2 \sum_{\nu} |\nu><\nu| + \sum_{n} N_n |\psi_n><\psi_n| \quad , \tag{4.B.4}$$

where the

$$\psi_n = \sum_i \chi_i T_{in} \qquad (4.B.5)$$

are the natural FORS MO's expressed in terms of the quasiatomic FORS MO's χ_i. The eigenvalues N_n are the occupation numbers of the natural FORS MO's ψ_n.

The quasiatomic and the natural representations of the density can be combined into a decomposition scheme which is conceptually close in spirit to Mulliken's population analysis. It is obtained by defining the intermediate population contributions

$$p_{ii}^n = N_n T_{in} T_{in} \qquad (4.B.6)$$

which can be summed in two ways, namely

$$\sum_n p_{ii}^n = p_{ii} \qquad \textit{and} \qquad \sum_i p_{ii}^n = N_n \qquad (4.B.7)$$

Similarly the bond orders can be decomposed into natural orbital contributions

$$p_{ij} = \sum_{n} p^{n}_{ij} \qquad (i \neq j) \qquad (4.B.8)$$

where

$$p^{n}_{ij} = N_n T_{in} T_{jn} \qquad (4.B.9)$$

The quantities p^{n}_{ij} (i = and ≠ j) contain all the information that is contained in the quantities p_{ij}, N_n and T_{in}. This FORS population-bond-order analysis implements the conceptual objectives of Mulliken's (1955) analysis in terms of a basis-set independent formalism with a non-arbitary intrinsic population definition that, moreover, does not suffer from the kind of problems illustrated, e.g., by Mulliken (1977, page 37, Figure 4).

The interpretative significance of the natural orbitals derives from the fact that they furnish a division of the molecular orbitals into strongly occupied ones, which reveal "where the action is", and into weakly occupied ones which are required to provide the wavefunction with the flexibility to describe what are generally considered the effects of electron correlation. It is the FORS population analysis of the strongly occupied molecular orbitals that would correspond to Mulliken's population analysis of self-consistent-field wavefunctions where all MO's are natural orbitals with occupation number 2. The FORS population analysis provides in addition a complementary analysis of the correlating orbitals.

In section B.4 we shall find that, in some cases, a third set of FORS molecular orbitals is useful to facilitate chemical insight. They are the

FORS analogues to the traditional localized SCF orbitals and are obtained by localizing the strongly occupied FORS MO's and the weakly occupied FORS MO's separately as proposed by Edmiston and Ruedenberg (1963). The resulting molecular orbitals still yield quite small off-diagonal density matrix elements and, hence, are still near-natural orbitals. They combine the separation into strong and weakly occupied orbitals with the localization into regions of chemical interest. For this reason we shall call them chemically localized FORS MO's (as contrasted to the atom-localized quasiatomic FORS MO's). They were called chemically adapted FORS MO's by Ruedenberg et al. (1982a). Sometimes it is illuminating to formulate the population and bond order analysis in terms of these orbitals.

2.3. Configurational Analysis of a FORS Wavefunction.

The configurations which are generated by the localized FORS MO's are also instructive. Since the localized MO's have the character of molecule-adapted minimal-basis atomic orbitals, the configurations generated by them have the formal appearance of valence-bond structures between quasi-atomic orbitals. In the case at hand, they are spin-adapted antisymmetrized products (SAAP's) which look like valence bond structures between the localized reactive FORS MO's $|0\rangle$, $|0'\rangle$, $|1\rangle$, $|2\rangle$ of Figure 4.B.1. They form three groups: Four neutral configurations which have the formal appearance of covalent VB structures:

$$C_0{}^0C_1{}^0C_2{}^0\text{:}\ \ |0^2 12\rangle,\ |0'^2 12\rangle,\ |00'12S\rangle,\ |00'12T\rangle$$

where S and T imply the four-electron singlet and triplet spin couplings; fourteen "singly-ionic" configurations:

$C_1^-C_2^+$: $|0^21^2>$, $|0'^21^2>$, $|00'1^2>$
$C_1^+C_2^-$: $|0^22^2>$, $|0'^22^2>$, $|00'2^2>$
$C_0^+C_1^-$: $|021^2>$, $|0'21^2>$
$C_0^-C_1-$: $|0^20'2>$, $|0'^202>$
$C_0^+C_2^-$: $|012^2>$, $|0'12^2>$
$C_0^-C_2^+$: $|0^20'1>$, $|0'^201>$;

and two "doubly-ionic" configurations:

$C_0^{2-}C_1^+C_2^+$: $|0^20'^2>$, $C_0^{2+}C_1^-C_2^-$: $|1^22^2>$.

The explicit forms of the listed wavefunctions (SAAPs) are defined in Section 4.A.2.3. The orbital symbols and the numbering of atoms is apparent from Figure 4.A.1.

The physical meaning and chemical interpretation of these SAAP's differs however significantly from that of traditional VB structures because, their quasi-atomic character notwithstanding, the localized FORS MO's are mutually orthogonal and so are therefore the SAAPs constructed from them.

While it is still true that, in the case of nonpolar bonding, such as encountered here, the dominant configuration Ψ_0 is a SAAP which looks like a covalent VB structure, it is readily seen that this configuration embodies no interference (resonance) interactions between the quasi-atomic localized FORS orbitals when the latter are orthogonal. Its energy contains only intra- atomic deformation energies and those interatomic effects which arise from non-bonded repulsions and coulombic interactions. We therefore call it "neutral" (i.e. without charge tranfer) or "unshared" rather than "covalent".

Electron sharing between atoms results from the admixture of additional configurations Ψ_{+-} which have the formal appearance of ionic VB structures. They describe electrons moving back and forth between the orthogonal molecule-adapted quasi-atomic orbitals on different atoms. It is these "electron jumps" which lead to chemical bonding because it is found that the essential, energy lowering interference (resonance) terms $p_{ij}\langle i|h|j\rangle$ are embedded in the interaction matrix elements $\langle\Psi_0|H|\Psi_{+-}\rangle$. The magnitudes of the coefficients of these electron hopping configurations provide therefore an indication of where bonds are established so that inferences can be drawn from the FORS-CI expansion. These matters will become clearer by an examination of the specific cases.

On the other hand, the configurations in terms of the natural MO's have the well known property of compacting the configurational expansion. In general they can be grouped into "principal" configurations of the SCF type and "secondary" configurations providing electron correlation for the former.

2.4. The Localization Process.

Since the localization of FORS MO's into quasi-atomic form is a fundamental prerequisite of the present analysis, it requires further comment.

An analysis such as the one developed here is useless unless the entire procedure is basis-set-independent. In order to establish this independence we have performed the analysis for the minimal-basis-set as well as for the extended basis sets optimized geometries of the important species of the reaction surface. The results of the former analysis are discussed in Sections B.3, 4, 5; the results of the latter analysis are discussed in Section B.6. The comparison of the two analyses establishes (i) that it is in fact possible to localize FORS MO's into quasiatomic form, in agreement with conclusions of earlier investigations by Ruedenberg et. al. (1982a, b, c) and (ii) that these quasi-atomic MO's are indeed basis-set-independent orbitals which are intrinsic to the wavefunction.

In the present investigation, all localizations were accomplished with the Edmiston-Ruedenberg (1963) procedure. However, since it is now established that the localized FORS MO's have quasi-atomic character, it would seem desirable in future applications to maximize this atomic character. One way to do this is to maximize the projection of these MO's on the orbital space apanned by the relevant (core and/or valence) SCF or MCSCF orbitals of the free atoms.

The results of Section B.6.1 (Table 4.B.17) indicate that the two localization procedures give very similar results in the present case.

3. The ring opening barrier

3.1. Quasi-atomic FORS MO's.

In order to gain insight into the origin of the barrier, we consider the wavefunctions for the geometry of the reactant and for that of the transition state.

Reactant

For cyclopropylidene, one of the reactive natural MOs has B_2 symmetry and it is already localized on the central carbon. It corresponds to the π-orbital $|0'\rangle$ of Figure 4.B.1. We therefore applied the localization only to the three natural MOs of A_1 symmetry and this procedure yields orbitals corresponding to $|0\rangle$, $|1\rangle$, $|2\rangle$ of Figure 4.B.1. Contours of these four localized reaction orbitals as well as of the localized core orbitals mentioned in Section 4.B.2.1, corresponding to the six sigma bonds, are depicted in panels A to F of Figure 4.B.2. The contours for the CC bonds (shown on panel A) and for the reactive orbitals $|1\rangle$, $|2\rangle$ (shown on panel D) are drawn in the CCC plane. The contours of the orbitals $|0\rangle$ (panel E) and $|0'\rangle$ (panel F) are drawn in the symmetry plane perpendicular to the CCC plane. The contours for any two CH bonds on the same side of the CCC plane are also shown on one panel (panels B or C) and drawn in the plane containing the carbon atoms C_1, C_2 and the two hydrogen atoms. The bonding character of the sigma bonding MOs and the non-interactive character of the orbitals $|0\rangle$ and $|0'\rangle$ are apparent. It is moreover seen that the orbitals $|1\rangle$ and $|2\rangle$ have the character of two strongly overlapping atomic orbitals which can establish a bond between them. We reiterate that the four localized reactive orbitals $|0\rangle$, $|0'\rangle$, $|1\rangle$, $|2\rangle$, their manifestly atomic nature notwithstanding are in fact mutually orthogonal optimized molecular orbitals of the FORS wavefunction. They are molecular orbitals which have the character of molecule-adapted deformed atomic orbitals, i.e. they are quasi-atomic MO's.

The drawings also contain the projections of the molecular skeleton

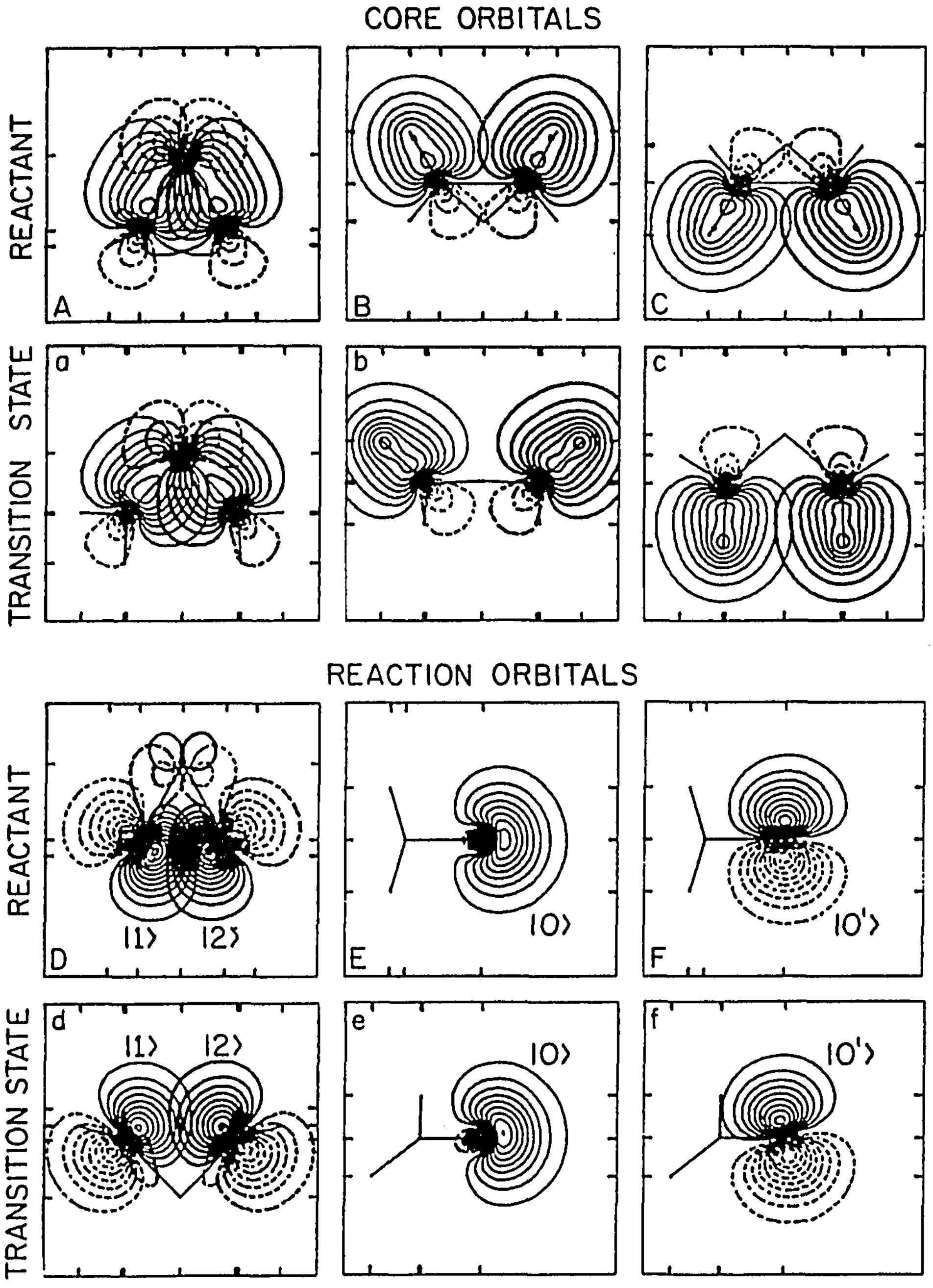

Figure 4.B.2. Quasiatomic FORS MO's for cyclopropylidene (panels A to F) and for the averaged transition state (panels a to f). Solid lines - positive; dashed lines - negative

on the plane in which the orbital is drawn. Therefore, in panels E and F one can see the inclinations of the CH bonds with respect to the CCC ring which appears as a line. These inclinations are just the inclinations of the planes in which the contours of panels B and C are drawn. The CCC ring therefore appears as a triangle on these panels. It is also apparent that the orbital |1> on atom C_1 points in the direction of one member of a roughly tetrahedral hybrid AO quadruple whose other three members point in the bent-bond directions towards the neighboring atoms H_1, H_2, C_0 (see Figure 4.A.1 for the numbering of atoms). The analogous statement is true for the orbital |2> on C_2.

Transition state

In choosing the transition state geometry, we have to keep in mind that, in order to establish the basis-set independence of the analysis, the results for the minimal basis set calculations must be compared with those for the extended basis. For the latter the transition state has however C_s symmetry while the former yielded two transition states of C_1 symmetry with a very flat surface between them. Since the point halfway between these two transitions states lies only 0.2 kcal/mole higher and, moreover, has C_s symmetry, we choose to carry out the analysis for the minimal basis set calculation at this "average transition state" with the coordinates $\phi = 84.25°$, $\delta_1 = 51.15°$, $\delta_2 = 128.85°$.

Although the CCC plane is no longer a plane of symmetry for this geometry, there still exists an orbital on the central carbon which has essentially π character. We dealt with this problem as follows. First we determined the localized orbitals in the space of all four reaction orbitals and this gave the orbitals |1> and |2> as well as two orbitals on the central carbon which were of the familiar "rabbit-ear" type, as found e.g. on oxygen in H_2O. We then simply formed the normalized sum and difference of the two rabbit-ear orbitals to yield |0> and |0'>. Contours for these orthogonal localized FORS MOs are shown in Figure 4.B.2 on panels a to f opposite the corresponding orbitals of the reactant.

From panels e and f we see that the non-interacting orbitals on the central carbon are now somewhat tilted. By combining the projective views of the CH bonds given on panels b and e one can visualize the direction of the CH bonds above the CCC plane in three dimensions. By doing the same for panel c and e we can visualize the directions of the CH bonds below the CCC plane. As before, the contours in panels b and c are drawn in the respective planes containing all four bonded atoms. The direction of orbital |1> can again be estimated by imagining it to be the fourth orbital of an approximately tetrahedral hybrid AO quadruple on the carbon C_1, with the other three hybrid AOs pointing towards the three bonded neighbor atoms H_1, $H_{1'}$, C_0 (see Figure 4.A.1 for the numbering of atoms). The analogous statement holds for orbital |2>. The projection of the central carbon atom on panel d indicates that |1> and |2> both point somewhat above the CCC plane. The actual angle of elevation is 21.4°.

3.2. Population and Bond Order Analysis.

Reactant

The density matrices between the four localized reaction orbitals just discussed are listed in Table 4.B.1A for the reactant cyclopropylidene. From it, we can draw the following inferences.

Table 4.B.1. Occupation numbers and bond orders for the reactive quasiatomic FORS MO's of the reactant and of the averaged transition state

A. Density matrix elements p_{ij} of reactant (cyclopropylidene)

	|0>	|0'>	|1>	|2>
|0>	1.93086	0	-0.00383	-0.00383
|0'>	0	0.06899	0	0
|1>	-0.00383	0	1.00008	0.97114
|2>	-0.00383	0	0.97114	1.00008

B. Density matrix elements pij of averaged transition state

	|0>	|0'>	|1>	|2>
|0>	1.95653	0.07416	-0.02901	-0.02901
|0'>	0.07416	0.33098	0.46349	0.46349
|1>	-0.02901	0.46349	0.85625	0.71324
|2>	-0.02901	0.46349	0.71324	0.85625

Since the diagonal elements, which represent the occupation numbers of the quasi-atomic orbitals, are exactly unity for the orbitals |1> and |2>, and sum to exactly 2 for the orbitals |0> and |0'>, there is no interatomic charge transfer between the atoms. From the off-diagonal elements, which are the bond orders, a strong bonding interaction is inferred to exist between orbitals |1> and |2>, which closes the ring in cyclopropylidene. The orbital |0> is a lone pair, it has only a very slight non-bonded repulsions with respect to orbitals |1> and |2>. The fact that the bond order between |0> and |0'> is zero implies that the slight occupation of orbital |0'> is entirely due to two-electron interactions, i.e. it serves to correlate the motions of the electrons in orbital |0>. These inferences are confirmed and illustrated in a different way through the natural FORS MO's which diagonalize the density matrix. Each column in Table 4.B.2 lists the expansion coefficients of one natural FORS MO in terms of the quasi-atomic localized FORS MO's |0>, |0'>, |1>, |2>. From these expansion coefficients and from the occupation numbers listed in the last two rows, the character of each natural FORS MO is apparent.

In the reactant (Table 4.B.2A) nearly two electrons occupy the natural orbital in the first column. Since it consists to 98% of the quasi-atomic s orbital |0>, it essentially describes a s lone pair on the central carbon and is denoted by |lp>. Similarly, nearly two electrons occupy the natural orbital in the third column. Since it consists to 98% of the in-phase linear combination of the quasi-atomic orbitals |1> and |2> it essentially describes a bonding electron pair between the end carbons and is denoted by |12b>. The weakly occupied natural orbital in the second column consists entirely of the quasi- atomic p-orbital |0'> which has a

Table 4.B.2. Natural FORS MO's for Reactant and Averaged Transition State

A. Cyclopropylidene

	$\vert 1p\rangle$	$\vert 1pc\rangle$	$\vert 12b\rangle$	$\vert 12c\rangle$
$\vert 0\rangle$	0.991418	0	-0.130730	0
$\vert 0'\rangle$	0	1	0	0
$\vert 1\rangle$	0.092440	0	0.701038	0.707107
$\vert 2\rangle$	0.092440	0	0.701038	-0.707107
N_n	1.930145	0.068991	1.971927	0.028937
Sum	1.999136		2.000864	

B. Averaged Transition State

	$\vert 1p\rangle$	$\vert 1pc\rangle$	$\vert 10'2b\rangle$	$\vert 10'2c\rangle$
$\vert 0\rangle$	0.996130	-0.044076	0.076035	0
$\vert 0'\rangle$	0.010221	0.917379	0.397883	0
$\vert 1\rangle$	-0.061723	-0.279708	0.646493	0.707107
$\vert 2\rangle$	-0.061723	-0.279708	0.646493	-0.707107
N_n	1.960883	0.044782	1.851327	0.143008
Sum	2.005665		1.994335	

node in the region of the lobe of |lp>. It thus provides out-of-plane correlation for the lone electron pair in the natural orbital |lp> and it is therefore denoted by |lpc>. Similarly, the weakly occupied natural orbital in the fourth column consists of the antibonding linear combination of the quasi-atomic orbitals |1> and |2> which have a node in the region of the lobe of |12b>. It thus provides left-right correlation for the bonding electron pair in the natural orbital |12b> and it is therefore called |12c>. With the inclusion of the correlation orbitals there are exactly two electrons on C_0 and another two electrons in the C_1C_2 bond.

It should be noted that, since the transformations listed in Table 4.B.2 are orthogonal, they can also be read in the inverse directions, i.e. they also represent the expansion of the quasi-atomic orbitals in terms of the natural orbitals. Thus, e.g., the orbital |1> results from linearly superposing the natural orbitals |lp>, |12b>, and |12c> with the coefficients listed in the row headed by the label |1>.

The conclusions inferred for the populations from the localized and the natural representation can be intelligibly combined by means of the quantities $p^n{}_{ii} = N_n T^2{}_{in}$ which were defined by Eq. (4.B.6) of Section 4.B.2.2. This approach leads to the summary population analysis given in Table 4.B.3A. The quantities $p^n{}_{ii}$ form the center bloc. Each column adds up to the value in the row labelled N_n, i.e. the populations of the natural orbitals. Each row adds up to the value in the column labelled p_{ii}, i.e. the populations of the quasi-atomic orbitals. Thus, the $p^n{}_{ii}$ yield an atomic breakdown of the natural orbital population as well as a natural-orbital breakdown of the atomic populations - as expressed by the Eqs. (4.B.7) of Section 4.B.2.2. The table shows that the population in the s quasi-atomic orbital |0> essentially comes from the lone pair natural orbital |lp> and that the populations of |1> and |2> come essentially from the bonding orbital |12b>. It furthermore shows how the smaller population contributions due to correlation as well as orbital delocalization round out the total population picture. Thus the naive qualitative reasoning, while correct in principle, must be tempered in two respects in order to fit in with the quantitative ab-initio analysis: First, the concept of a pure atomic orbital must be replaced by that of a deformed quasi-atomic orbital. Secondly, even these deformed atomic orbitals get slightly mixed when the natural orbitals are formed which describe the lone pair, bonding and correlation roles of electrons.

The corresponding bond order decomposition in terms of natural orbital contributions, corresponding to Eqs. (4.B.8) and (4.B.9) of Section 4.B.2.2 is given in Table 4.B.4A. It shows that the bond order between |1> and |2> arises essentially from the bonding orbital |12b>.

Transition state

The density matrix of the transition state in Table 4.B.1B shows that there has occured a substantial charge transfer from the end carbons to the central carbon atom. Each of the orbitals |1> and |2> has given up 0.1438 electrons. Almost all of the total amount of 0.2877 electrons, namely 0.2620 electrons, has been donated to the orbital |0'> on the central carbon; only 0.0257 has gone to |0>. The substantial positive bond orders between the orbitals |0'>, |1>, |2> imply that we have an in-phase three-center delocalization of the two electrons which, in the reactant, formed the |1>-|2> bond. The reason must be that, due to the increase in

Table 4.B.3. FORS population Analysis for Reactant and Averaged Transition State

A. Cyclopropylidene

		Natural FORS MO's					
		|1p>	|1pc>	|12b>	|12c>	p_{ii}	Atoms
Quasi-atomic FORS MO's	|0>	1.89716	0	0.03370	0	1.93086	1.99985
	|0'>	0	0.06899	0	0	0.06899	
	|1>	0.01649	0	0.96911	0.01447	1.00007	1.00007
	|2>	0.01649	0	0.96911	0.01447	1.00007	1.00007
N_n		1.93015	0.06899	1.97193	0.02894		
Sum		1.99914		2.00086		4	4

B. Averaged Transition State

		Natural FORS MO's					
		|1p>	|1pc>	|10'2b>	|10'2c>	p_{ii}	Atoms
Quasi-atomic FORS MO's	|0>	1.94574	0.00009	0.01070	0	1.95653	2.26750
	|0'>	0.00020	0.03769	0.29309	0	0.33098	
	|1>	0.00747	0.00350	0.77377	0.07150	0.85624	0.85624
	|2>	0.00747	0.00350	0.77377	0.07150	0.85624	0.85624
N_n		1.96088	0.04478	1.85133	0.14301		
Sum		2.00566		1.99434		4	4

distance between the end carbons (from 1.53 to 1.94 Å), the interaction between |1> and |2> has considerably weakened and, as a consequence, the orbitals |1> and |2> have rotated in order to strengthen their interactions with the closer orbital |0'>. This accounts for the rotations of the hydrogen atoms as well as for the tilting of the |0'> orbital evident in Figure 4.B.2f. The relatively large bond order between orbitals |1> and |2> is the consequence of the in- phase |1>-|0'>-|2> delocalization and does not imply a strong direct |1>-|2> bond since the resonance integral <1|h|2> is presumably small. The energetic gain obtained from the establishment of the delocalized three-center bond |1>-|0'>-|2> is of course partly offset by the need for substantial electron donation to the central carbon which clearly does not come free. Thus we conclude that the energy barrier results from the breakage of the |1>-|2> bond and that its smallness results from the establishment of the three-center bond through electron donation into the previously empty orbital |0'>.

The natural orbital |1p> of the first column of Table 4.B.2B still describes a lone electron pair essentially lodged in the quasi-atomic σ orbital |0> on the center atom. The major change compared to cyclopropylidene is the in-phase delocalization of the bonding natural orbital of the third column of Table 4.B.2B over the quasi-atomic π-orbital |0'> of the central atom. We have therefore labelled it |10'2b>. The natural orbital |1pc> of the second column is still essentially the quasi-atomic π-orbital |0'>, but it is somewhat delocalized over the orbitals |1> and |2> in an out-of-phase (antibonding) fashion. This orbital therefore still essentially provides out-of-phase correlation for the lone pair natural orbital |1p>, but it also provides some bond-parallel

Table 4.B.4. FORS Bond Order Analysis for Reactant an Averaged Transition State

A. Cyclopropylidene

		Natural FORS MO's				
		$\vert 1p\rangle$	$\vert 1pc\rangle$	$\vert 12b\rangle$	$\vert 12c\rangle$	p_{ij}
Quasi-	(00')	0	0	0	0	0
atomic	(01)	0.17689	0	-0.18072	0	-0.00383
FORS	(02)	0.17689	0	-0.18072	0	-0.00383
MO	(0'1)	0	0	0	0	0
pairs	(0'2)	0	0	0	0	0
	(12)	0.01649	0	0.96911	-0.01447	0.97113

B. Averaged Transition State

		Natural FORS MO's				
		$\vert 1p\rangle$	$\vert 1pc\rangle$	$\vert 10'2b\rangle$	$\vert 10'2c\rangle$	p_{ij}
Quasi-	(00')	0.01996	-0.00181	0.05601	0	0.07416
atomic	(01)	-0.12056	0.00055	0.09100	0	-0.02901
FORS	(02)	-0.12056	0.00055	0.09100	0	-0.02901
MO	(0'1)	-0.00124	-0.01149	0.47621	0	0.46348
pairs	(0'2)	-0.00124	-0.01149	0.47621	0	0.46348
	(12)	0.00747	0.00350	0.77377	-0.07150	0.71324

correlation for the three-center bond orbital |10'2b>. The major bond-parallel correlation for this three- center bond still comes from the natural orbital |10'2c> which, in fact, has a higher occupancy than it had in cyclopropylidene.

The information from the localized and natural density decompositions are again integrated in the form of a population analysis and a bond order analysis in Tables 4.B.3B and 4.B.4B. The comparison of these tables with the Tables 4.B.3A and 4.B.4A reconfirms that the bonding orbital |10'2b> has now delocalized its population over the π-orbital |0'> on the central carbon. Its correlating orbital |10'2c> has increased its population sevenfold presumably because, due to the longer C_1-C_2 distance, it is now much less antibonding and therefore more effective for correlation. The usage of the atomic orbital |0'> for delocalized bonding in the natural orbital |10'2b> has conversely induced an antibonding delocalization of the correlating orbital |1pc> over the atomic orbitals |1> and |2>. Thereby it has become less effective for correlating the lone pair orbital |1p> which has concentrated more on the quasi-atomic σ orbital |0>. The fact that this orbital on the central carbon is still essentially doubly occupied indicates that its energy is still sufficiently below that of the quasi-atomic π orbital |0'>.

3.3 FORS Configuration Analysis.

We now examine the configurations (SAAPs - Spin Adapted Antisymmetrized Products) which are generated by the discussed localized FORS MOs. They are listed, in the order discussed in Section 4.B.2.3, in the first column of Table 4.B.5. The second column contains the corresponding expansion coefficients for the wavefunction of the reactant; the third column contains the wavefunction expansion coefficients for the molecule at the considered approximate transition state. Although the qualitative meaning of the configurations is the same, the orbitals are of course quantitatively different in the two cases as shown in Figure 4.B.2.

Reactant

For the reactant the dominant configuration is the SAAP $|0^2 12\rangle$ corresponding to a sigma lone pair on C_0 and one reaction electron each on C_1 and C_2. The SAAP $|0'^2 12\rangle$ clearly provides electron correlation for the sigma lone pair. We therefore consider

$$\Psi_B = 0.9827|0^2 12\rangle - 0.1855|0'^2 12\rangle$$

as the normalized neutral base function without electron sharing (See Section 4.B.2.3). It has a weight of 62% in the wavefunction. The double occupation of the sigma orbital $|0\rangle$ is due to the fact that, for such small CCC opening angle, the π-atomic orbital $|0'\rangle$ has a significantly higher orbital energy.

As explained above in Section 4.B.2.3, the base function Ψ_B by itself does not establish a bond between the orbitals $|1\rangle$ and $|2\rangle$. In the present case, covalent bonding arises from the admixture of the SAAPs $|0^2 1^2\rangle$ and $|0^2 2^2\rangle$ which, together with the SAAPs $|0'^2 1^2\rangle$ and $|0'^2 2^2\rangle$ practically account for the remaining 38% of the wavefunction. It is readily verified that these terms can be generated in just the right proportion from the base function Ψ_B by the substitution operations

Table 4.B.5. Expansion coefficients of wavefunctions for cyclopropylidene and the averaged transition state in terms of configurations generated from quasiatomic FORS MOs

SAAPS		Cyclopropylidene	Transition State
$C^0_0C^0_1C^0_2$:	$\|0^{2}12>$	0.772606	0.746158
	$\|0'^{2}12>$	-0.145750	-0.124982
	$\|00'12S>$	0.0	0.046221
	$\|00'12T>$	0.0	0.0
$C^-_1C^+_2$:	$\|0^{2}1^{2}>$	0.429145	0.265866
	$\|0'^{2}1^{2}>$	-0.081054	-0.041151
	$\|00'1^{2}>$	0.0	0.029490
$C^+_1C^-_2$:	$\|0^{2}2^{2}>$	0.429145	0.265866
	$\|0'^{2}2^{2}>$	-0.081054	-0.041151
	$\|00'2^{2}>$	0.0	0.029490
$C^-_0C^+_1$:	$\|0^{2}0'^{2}>$	0.0	0.365665
	$\|0'^{2}02>$	0.007386	-0.020085
$C^+_0C^-_1$:	$\|021^{2}>$	0.011068	0.019080
	$\|0'21^{2}>$	0.0	0.003320
$C^-_0C^+_2$:	$\|0^{2}0'1>$	0.0	0.365665
	$\|0'^{2}01>$	0.007386	-0.020085
$C^+_0C^-_2$:	$\|012^{2}>$	0.011068	0.019080
	$\|0'12^{2}>$	0.0	0.003320
$C_0^{2-}C_1^{+}C_2^{+}$:	$\|0^{2}0'^{2}>$	-0.001957	0.100078
$C_0^{2+}C_1^{-}C_2^{-}$:	$\|1^{2}2^{2}>$	-0.003294	-0.001356

$$R_{1\to2}\Psi_B = 0.982|0^2 2^2> - 0.185|0'^2 2^2>,$$

$$R_{2\to1}\Psi_B = 0.982|0^2 1^2> - 0.185|0'^2 1^2>,$$

where the orbital replacement operator $R_{i\to j} = \{|i>\to|j>\}$ can be interpreted as allowing an electron to jump from orbital |i> to orbital |j>. As discussed in Section 4.B.2.3, the admixture of these configurations introduces into the wavefunction electron sharing between the orthogonal orbitals |1> and |2> and, as a consequence, there occurs an energy lowering due to the interference terms in the hamiltonian matrix elements between Ψ_B and $R_{1\to2}\Psi_B$, $R_{2\to1}\Psi_B$. It is this energy lowering which establishes the bond between orbitals |1> and |2>.

Transition State

For the transition state we find from the third column of Table 4.B.5 the very similar normalized base function without electron sharing

$$\Psi_B = 0.986|0^2 12> - 0.165|0'^2 12>$$

which here has a weight of 57%. In this case the substituted configurations $R_{1\to2}\Psi_B$ and $R_{2\to1}\Psi_B$ account however for only 15% of the wavefunction, which indicates that electron sharing between |1> and |2> is energetically much less profitable, undoubtedly because of the greater distance between the carbon atoms 1 and 2. The remaining 28% are mainly due to configurations that describe electron sharing between C_1, C_2 and the central atom C_0, notably

$$|0^2 0'^2\rangle = R_{1\to 0'}|0^2 12\rangle,$$
$$|0^2 0' 1\rangle = R_{2\to 0'}|0^2 12\rangle.$$

These SAAPs describe electron donation from |1> and |2> to the previously empty quasi-atomic π-orbital |0'> on the central atom and therefore a delocalization of electrons from orbital |1> over orbital |0'> to orbital |2>.

The comparison of the wavefunction expansion of the reactant with that of the transition state thus shows again that the existence of the barrier is due to the loss of the covalent binding between the orbitals |1> and |2>, and that its small value is related to a compensating energy lowering which arises from delocalization of the same two electrons over the orbitals |1>, |0'>, |2>.

4. The Allene Isomerization barrier

In order to gain insight into the energy barrier to the isomerization of singlet allene, we examine the wavefunctions for the staggered linear equilibrium conformation and for the planar, bent (ϕ = 133°) transition state. No orbital plots are displayed since, from what has been seen before, the shapes and directions of the localized FORS MO's are manifestly as drawn in Fig. 4.B.1. For the linear conformation, |1> and |0> are parallel quasiatomic p-orbitals whereas |0'> and |2> are parallel quasiatomic p-orbitals at right angles to |1> and |0>. For the bent planar geometry, the orbitals |1>, |2> and |0'> are quasiatomic p-orbitals perpendicular to the molecular plane whereas |0> is a quasiatomic s-p hybrid-type orbital in the molecular plane pointing "backwards", i.e. away from the end carbons.

4.1. Staggered Linear Allene

The density matrix for the quasiatomic FORS MO's is listed in Table 4.B.6A. It is apparent that bonding exists between orbitals |0> and |1> as well as between orbitals |0'> and |2>. Concomitantly charge in the amount of 0.05 electrons is transferred from |0> to |1> and similarly from |0'> to |2>. Table 4.B.7A lists the natural orbitals. For each of the two bonds (01) and (0'2) we have one bonding and one correlating orbital. The population and bond order analyses, given in Tables 4.B.8A and 4.B.9A, quantify the preceding remarks further in a self-explanatory way.

The configurational expansion coefficients of the wavefunction in terms of the corresponding SAAPs are given in Table 10. The neutral base function without electron sharing is

$$\Psi_B = 0.997|010'2S\rangle + 0.069|010'2T\rangle.$$

The predominant term is the singlet coupled SAAP coupling |0> with |1> and |0'> with |2>, embodying the bond between |0> and |1> as well as the bond between |0'> and |2>. For the cases to be discussed in Section 4.B.5 it is not possible to cast Ψ_B in such a form because, in those cases, the Hund's-rule triplet-singlet effect in the central atom is stronger than the weak π-bonding effects so that the triplet effect dominates. Here, in allene, the strong covalent π-bonding effects dominate over the Hund's-rule effect at the central carbon. Ψ_B contributes 53% to the wavefunction.

Table 4.B.6. Occupation numbers and bond orders for the reactive quasiatomic FORS MO's of Linear and Bent Allene

A. Density matrix elements p_{ij} of Product (Linear Allene)

p_{ij}	|0>	|0'>	|1>	|2>
|0>	0.94821	0	0.88684	0
|0'>	0	0.94821	0	0.88684
|1>	0.88684	0	1.05179	0
|2>	0	0.88684	0	1.05179

B. Density matrix elements p_{ij} of Bent Allene

p_{ij}	|0>	|0'>	|1>	|2>
|0>	1.00000	0	0	0
|0'>	0	0.97708	0.59743	0.59743
|1>	0	0.59743	1.01146	0.01146
|2>	0	0.59743	0.01146	1.01146

Table 4.B.7. Natural FORS MO's for Linear and Bent Allene

A. Linear Allene

	$\vert 01b\rangle$	$\vert 01c\rangle$	$\vert 0'2b\rangle$	$\vert 0'2c\rangle$
$\vert 0\rangle$	0.686185	0.727427	0	0
$\vert 0'\rangle$	0	0	0.686185	0.727427
$\vert 1\rangle$	0.727427	-0.686185	0	0
$\vert 2\rangle$	0	0	0.727427	-0.686185
N_n	1.888351	0.111649	1.888351	0.111649
Sum	2.000000		2.000000	

B. Bent Allene

	$\vert 1p\rangle$	$\vert 12n\rangle$	$\vert 10'2b\rangle$	$\vert 10'2c\rangle$
$\vert 0\rangle$	1	0	0	0
$\vert 0'\rangle$	0	0	0.697454	0.716629
$\vert 1\rangle$	0	0.707107	0.506733	-0.493175
$\vert 2\rangle$	0	-0.707107	0.506733	-0.493175
N_n	1.000000	1.000000	1.845206	0.154794
Sum			2.000000	

Table 4.B.8. FORS population Analysis for Linear and Bent Allene

A. Linear Allene

		Natural FORS MO's					
		|01b>	|01c>	|0'2b>	|0'2c>	p_{ii}	Atoms
Quasi-	|0>	0.88913	0.05908	0	0	0.94821	1.89642
atomic	|0'>	0	0	0.88913	0.05908	0.94821	
FORS	|1>	0.99922	0.05257	0	0	1.05179	1.05179
MO's	|2>	0	0	0.99922	0.05257	1.05179	1.05179
	N_n	1.88835	0.11165	1.88835	0.11165		
	Sum	2.00000		2.00000		4	4

B. Bent Allene

		Natural FORS MO's					
		|1p>	|12n>	|10'2b>	|10'2c>	p_{ii}	Atoms
Quasi-	|0>	1.00000	0	0	0	1.00000	1.97709
atomic	|0'>	0	0	0.89759	0.07950	0.97709	
FORS	|1>	0	0.5	0.47381	0.03765	1.01146	1.01146
MO's	|2>	0	0.5	0.47381	0.03765	1.01146	1.01146
	N_n	1.00000	1.00000	1.84521	0.15479		
	Sum			2.00000		4	4

Table 4.B.9. FORS Bond Order Analysis for Linear and Bent Allene

A. Linear Allene

		Natural FORS MO's				
		|01b>	|01c>	|0'2b>	|0'2c>	p_{ij}
Quasi-	(00')	0	0	0	0	0
atomic	(01)	0.94257	-0.05573	0	0	0.88684
FORS	(02)	0	0	0	0	0
MO	(0'1)	0	0	0	0	0
pairs	(0'2)	0	0	0.94257	-0.05573	0.88684
	(12)	0	0	0	0	0

B. Bent Allene

		Natural FORS MO's				
		|1p>	|12n>	|10'2b>	|10'2c>	p_{ij}
Quasi-	(00')	0	0	0	0	0
atomic	(01)	0	0	0	0	0
FORS	(02)	0	0	0	0	0
MO	(0'1)	0	0	0.65214	-0.05471	0.59743
pairs	(0'2)	0	0	0.65214	-0.05471	0.59743
	(12)	0	-0.5	0.47381	0.03765	0.01146

Table 4.B.10 also confirms that covalent bonding is due to electron sharing between the orbitals $|1\rangle$ and $|0\rangle$ and between the orbitals $|2\rangle$ and $|0'\rangle$ as is established by the SAAPs generated from Ψ_B by the electron-hopping replacements $R_{1\to0}$, $R_{0\to1}$, $R_{2\to0'}$, $R_{0'\to2}$ namely:

$$R_{1\to0}\Psi_B = |0^2 20'\rangle \qquad R_{2\to0'}\Psi_B = |0'^2 01\rangle$$

$$R_{0\to1}\Psi_B = |1^2 20'\rangle \qquad R_{0'\to2}\Psi_B = |2^2 01\rangle$$

$$R_{1\to0}R_{2\to0'}\Psi_B = |0^2 0'^2\rangle \qquad R_{1\to0}R_{0'\to2}\Psi_B = |0^2 2^2\rangle$$

$$R_{0\to1}R_{0'\to2}\Psi_B = |1^2 2^2\rangle \qquad R_{0\to1}R_{2\to0'}\Psi_B = |0'^2 1^2\rangle$$

4.2. Bent Planar Allent ($\phi = 133.3°$)

It is instructive to compare the electronic structure of the bent planar allene transition state ("all-T.S.") not only with the linear staggered allene conformation but also with the averaged ring opening transition state of cyclopropylidene ("cyc- T.S.") discussed in Section 4.B.3. Both conformations have the same Cs symmetry plane but they differ in two respects, viz: the all- T.S. has a ring opening angle $\phi = 133.3°$ and both CH_2 groups lie in the CCC plane so that the molecule has C_{2v} symmetry, whereas the cyc-T.S. has $\phi = 84°$ and the CH_2 groups are tilted against the CCC plane so that the symmetry is only C_s.

The population-bond order matrix is listed in Table 4.B.6B, the expansions of the natural orbitals in terms of the quasiatomic orbitals are listed in Table 4.B.7B, the population analysis is given by Table 4.B.8B and the bond order analysis is given by Table 4.B.9B. The corresponding data for the cyc-T.S. were given in Tables 4.B.1B, 4.B.2B, 4.B.3B and 4.B.4B. A synoptic examination of the four tables for each of the two

Table 4.B.10. Expansion coefficients of wavefunction for linear and bent allene in terms of configurations generated from quasiatomic FORS MO's

SAAPS		Linear Allene	Bent Allene
Covalent :	$\|0^{2}12>$	0.0	0.0
	$\|0'^{2}12>$	0.0	0.0
	$\|010'2S>$	0.723744	0.722086
	$\|010'2T>$	0.050349	-0.416897
$C_1^{-}C_2^{+}$:	$\|0^{2}1^{2}>$	-0.005680	0.0
	$\|0'^{2}1^{2}>$	0.145391	0.0
	$\|00'1^{2}>$	0.0	0.096605
$C_1^{+}C_2^{-}$:	$\|0^{2}2^{2}>$	0.145391	0.0
	$\|0'^{2}2^{2}>$	-0.005680	0.0
	$\|00'2^{2}>$	0.0	-0.096605
$C_0^{-}C_1^{+}$:	$\|0^{2}0'^{2}>$	0.282896	0.0
	$\|0'^{2}0^{2}>$	0.0	0.256518
$C_0^{+}C_1^{-}$:	$\|1^{2}02>$	0.0	0.277958
	$\|1^{2}0'^{2}>$	0.344264	0.0
$C_0^{-}C_2^{+}$:	$\|0^{2}0'1>$	0.0	0.0
	$\|0'^{2}01>$	0.282896	-0.256518
$C_0^{+}C_2^{-}$:	$\|2^{2}01>$	0.344264	-0.277958
	$\|2^{2}0'1>$	0.0	0.0
$C_0^{2-}C_1^{+}C_2^{+}$:	$\|0^{2}0'^{2}>$	0.102271	0.0
$C_0^{2+}C_1^{-}C_2^{-}$:	$\|1^{2}2^{2}>$	0.154157	0.0

transition states leads to the following comparative inferences.

The four natural orbitals are similar for the two transition states, namely (see Tables 4.B.2 and 4.B.7):

$|a_1\rangle = |1p\rangle \approx |0\rangle$ is essentially a non-interacting lone orbital on the central carbon;

$|1b_1\rangle = |10'2b\rangle$ is a delocalized bonding orbital with positive contributions from $|1\rangle$, $|0'\rangle$ and $|2\rangle$;

$|2b_1\rangle = |10'2c\rangle$ in the all-T.S. and $\approx|1pc\rangle$ in the cyc-T.S., is a delocalized antibonding orbital with a node between $|1\rangle$ and $|0'\rangle$ and another node between $|0'\rangle$ and $|2\rangle$;

$|a_2\rangle = (|1\rangle - |2\rangle)/\sqrt{2}$ has one node and no contribution from the cental carbon.

The labels a_1, b_1, a_2 correspond to the respective C_{2v} irreps in the allene transition state. The increase of the CCC angle ϕ from 84° to 133.3° has the following consequences regarding these molecular orbitals:

(i) The $|a_1\rangle$ orbital loses s-character and its orbital energy increases correspondingly;

(ii) Since the increase in the distance of the end carbons decreases the steric repulsions between the hydrogens, they turn into the plane, allowing for greater π-overlap by lining up the orbitals $|1\rangle$, $|0'\rangle$ and $|2\rangle$. This lowers the orbital energy of $|1b_1\rangle$;

(iii) The increase in distance between $|1\rangle$ and $|2\rangle$ also lowers the antibonding effect between them, thereby lowering the orbital energy of $|a_2\rangle$. In the cyc-T.S. $|a_2\rangle$ is antibonding, but in the all-T.S. $|a_2\rangle$ is nonbonding with diradical character.

Because of these energy changes, the opening from 84° to 133.3° under preservation of C_s symmetry leads to an essential population shift (see Tables 4.B.3 and 4.B.8). Since the energy of $|a_1>$ increases whereas that of $|a_2>$ decreases to a nonbonding level, the occupations change from 1.95 for $|a_1>$ and 0.14 for $|a_2>$ in the cyc-T.S. to unity for both orbitals in the all-T.S., giving it diradical character.

This occupation shift, in turn, changes the character of the $|1b_1> = |10'2b>$ bonding orbital (see Tables 4.B.3 and 4.B.8). In the cyc-T.S., its major contributions (0.77 each) are on $|1>$ and $|2>$ with only a small contribution to $|0'>$ representing an electron donation of 0.29 electrons to the center carbon. By contrast, in the all-T.S. the occupation of $|0'>$ does not represent an electron donation, because $|a1> \approx |0>$ holds only one electron. Consequently, the orbital $|0'>$ contributes 0.90 to $|10'2b>$ whereas $|1>$ and $|2>$ contribute only 0.47 each. Moreover, because of the occupancy of $|a_2>$ with one electron there still results a slight charge transfer of 0.01 to the end carbons. This is however less than the similar transfer of 0.05 in linear allene.

This population analysis explains the bond order changes shown in Tables 4.B.4 and 4.B.9. The bonding effects are essentially between $|0'>$ and $|1>$ and between $|0'>$ and $|2>$ since the distance between $|1>$ and $|2>$ is large enough so that the (12) bond order probably multiplies a relatively small energy integral in both cases. The bond orders (01) and (02) in the cyc-T.S. are however lower (0.46 each) than those in the all-T.S. (0.60 each) because the latter is more delocalized over $|0'>-|1>-|2>$, as is apparent from the populations. This increase in p-type bond order from the cyc-T.S. to the all-T.S. parallels the corresponding downhill change in the potential energy surface. In both T.S.'s we have one bonding electron pair covering two atom linkages (01 and 02).

In linear allene, by contrast, the lone pair orbital $|1p\rangle \approx |0\rangle$ has expanded to cover also the twisted end orbital $|1\rangle$ while the bonding orbital $|10'b\rangle$ has contracted to cover only the end orbital $|2\rangle$ (see Table 4.B.8). For each of the two linkages there exists therefore a bond, with bond order 0.89 (Table 4.B.9). This increase in the total bond order accounts for the energy drop to linear allene.

The configurational expansion of the bent allene wavefunction in terms of SAAPs based on quasiatomic orbitals is given in the last column of Table 4.B.10. It is readily seen that the neutral base function without electron sharing is

$$\Psi_B = (\sqrt{3}|010'2S\rangle - |010'2T\rangle)/2 = |00'12T\rangle \,, \qquad (4.B.10)$$

because

$$A\{|0\rangle|0'\rangle|1\rangle|2\rangle\theta_1\} = -A\{|0\rangle|1\rangle|0'\rangle|2\rangle\, P_{23}\theta_1\}$$

and

$$P_{23}\theta_1 = (-\sqrt{3}\theta_0 - \theta_1)/2 \,,$$

where θ_0, θ_1 are the singlet and triplet coupled spinfunctions defined in Section 4.A.2.3 and P_{23} denotes a permutation between spin coordinates. Equation (4.B.10) shows again that, in contrast to the ring opening transition state, the orbitals $|0\rangle$ and $|0'\rangle$ are here both singly occupied. Ψ_B has a weight of 69.5% in the total wavefunction. Electron sharing is established by the electron hopping replacements

$$R_{1\rightarrow 0'}\ \Psi_B = |00'0'2T\rangle = -\sqrt{3}/2\ |0'^2 0^2\rangle$$

$$R_{0'\rightarrow 1}\ \Psi_B = |0112T\rangle = -\sqrt{3}/2\ |1^2 02\rangle$$

$$R_{2\rightarrow 0'}\ \Psi_B = |00'10'T\rangle = \sqrt{3}/2\ |0'^2 10\rangle = -\sqrt{3}/2\ |0'^2 01\rangle$$

$$R_{0'\rightarrow 2}\ \Psi_B = |0212T\rangle = \sqrt{3}/2\ |2^2 10\rangle = -\sqrt{3}/2\ |2^2 01\rangle$$

confirming the delocalized covalent p-bonding between |1>, |0'> and |2>. These four terms essentially account for the remaining 30.5% of the wavefunction.

The form of the base function QB is a consequence of the spatial symmetry. From Table 4.B.7 it can be inferred that, in terms of the symmetry adapted natural orbitals, the dominant SAAP is:

$$\Psi_0 = |(10'2b)^2(1p)(12n)\rangle = |(1b1)^2 a_1 a_2\rangle \qquad (4.B.11)$$

and it is apparent that this function belongs to the irreducible representation A_2. So does therefore the total wavefunction and, hence, also Ψ_B. In particular, Ψ_B must therefore satisfy $\sigma\Psi_B = -\Psi_B$ for σ being the mirror plane perpendicular to the molecule. Substituting for Ψ_B the expression (4.B.10), we find

$$\sigma\ \Psi_B = |00'21T\rangle = A\ \{(P'_{34}\ 00'12)\ \theta_1\} \qquad (4.B.12)$$

where P'_{34} is the transposition of the spatial coordinates of electrons 3 and 4. From Eq. (4.B.12) one deduces

$$\sigma\ \Psi_B = -A\ \{00'12\ P'_{34}\theta_1\} = -A\ \{00'12\ \theta_1\}$$

$$\sigma \Psi_B = - \Psi_B ,$$

which is indeed the required relationship. On the other hand, |00'12S> is unacceptable because σ |00'12S> = + |00'12S>.

4.3. Symmetry Considerations, Conical Intersection between the two Transition States.

The average ring-opening transition state at 84.25° and the allene isomerization transition state at 133.3° both have C_s symmetry. Hoever, the following reasoning shows that the ground state wavefunctions at the two transition states belong to different irreducible representations of C_s. From Table 4.B.2 it can be seen that, at the ring-opening transition state, the dominant configuration must be one in which the lone pair orbital |1p> and the three-center bonding orbital |10'2b> are both doubly occupied. Since both have A' symmetry in C_s, the dominant configuration and, hence, the wave function itself belong to the irreducible representation A' at this geometry. On the other hand, Table 4.B.7 shows that, at the allene isomerization transition state (bent allene), the dominant configuration is one in which the three-center bonding orbital |10'2b> is doubly occupied whereas the lone pair orbital |1p> and the non-bonding orbital |12n> between C_1 and C_2 are both singly occupied. Since these three orbitals belong to the irreducible representations A', A' and A" respectively, the dominant configuration and, hence, the entire wavefunction belong to the irreducible representation A" in C_s at this geometry.

From this change in irreducible representations, it can be inferred that, on a path leading from one of these transition states to the other under preservation of C_s symmetry, there exist two states, of A' and A" symmetry respectively, which cross somewhere between $\phi = 85°$ and $\phi = 133.3°$. Within the context of the full potential energy surface, this implies the existence of two surfaces which exhibit a conical intersection. The implications of this feature are discussed in detail in Section 4.A.5.

5. The free internal cogwheel motion

It stands to reason that, for values of ϕ which are not much smaller than 180°, motions along lines $\delta_1+\delta_2$=constant have a similar meaning as they do for allene, i.e. they represent approximate rigid rotations around an axis which goes approximately through the three carbon atoms and it is for this reason that such motions are approximately free. Such an interpretation breaks down however when ϕ becomes sufficiently small. Indeed, as Valtazanos et al. (1990) suggest, for $\phi=140°$ (Figure 14 of this reference) it is seen that a free motion exists only along the valleys $\delta_1+\delta_2\approx 90°$, but not anymore along the ridges $\delta_1+\delta_2\approx 0°$. The free motion along the valleys persists for ϕ values all the way back almost to the transition state (see Figures 9 to 15 by Valtazanos et al., 1990). These motions along the valleys correspond to cogwheel-like synchronized disrotatory rotations of the two CH_2 groups with a phase lag of 90°. This result could not have been foreseen without an explicit ab-initio calculation of the entire surface.

How can this isoenergetic shelf be explained? In order to answer this question we resort again to an analysis in terms of localized FORS

MOs. We consider three geometries along the valley floor on the panel for ϕ=100° (Figure 4.A.8 of Section 4.A.6), namely (δ_1,δ_2)=(90° ,0}, (45° ,45} and (0° ,90}.

5.1. Quasiatomic FORS MO's

(δ_1,δ_2) = (90° 0}

For the geometry (δ_1=90°, δ_2=0°) the right CH_2 group lies in the CCC plane and the left CH_2 group stands perpendicular to it, as illustrated in Figure 4.B.3A. The molecule has C_s symmetry with respect to the CCC plane and there are two reaction orbitals of A' symmetry and two of A" symmetry. Localization of the former yields the in-plane orbitals |0> on atom C_0 and |1> on atom C_1. Localization of the latter yields the perpendicular orbitals |2> on atom C_2 and |0'> on atom C_0 (see Figure 4.B.1). The unit vectors of the directions in which these four quasi-atomic FORS MO's point are indicated in Figure 4.B.3A. Contours of the two quasi-atomic FORS MO's of A" symmetry are exhibited in Figure 4.B.4A; they are drawn in the plane perpendicular to the CCC plane and containing the atoms C_0 and C_2. The bold contours depict orbital |0'>, the weaker contours represent orbital |2>. It is apparent that these two quasiatomic FORS MO's correspond to two p-orbitals on atoms C_0 and C_2 whose overlap is sufficient for the formation of a π-bond. Contours of the quasiatomic FORS MO's of A' symmetry are exhibited in Figure 4.B.4B. They are drawn in the CCC plane, the bold contours corresponding to |0> and the lighter contours corresponding to |1>. The overlap between these two orbitals is noticeably weaker so that they are in a less favorable position for π-bonding. (Note that the meaning of solid and dashed contours is different in Figures 4.B.4A and B).

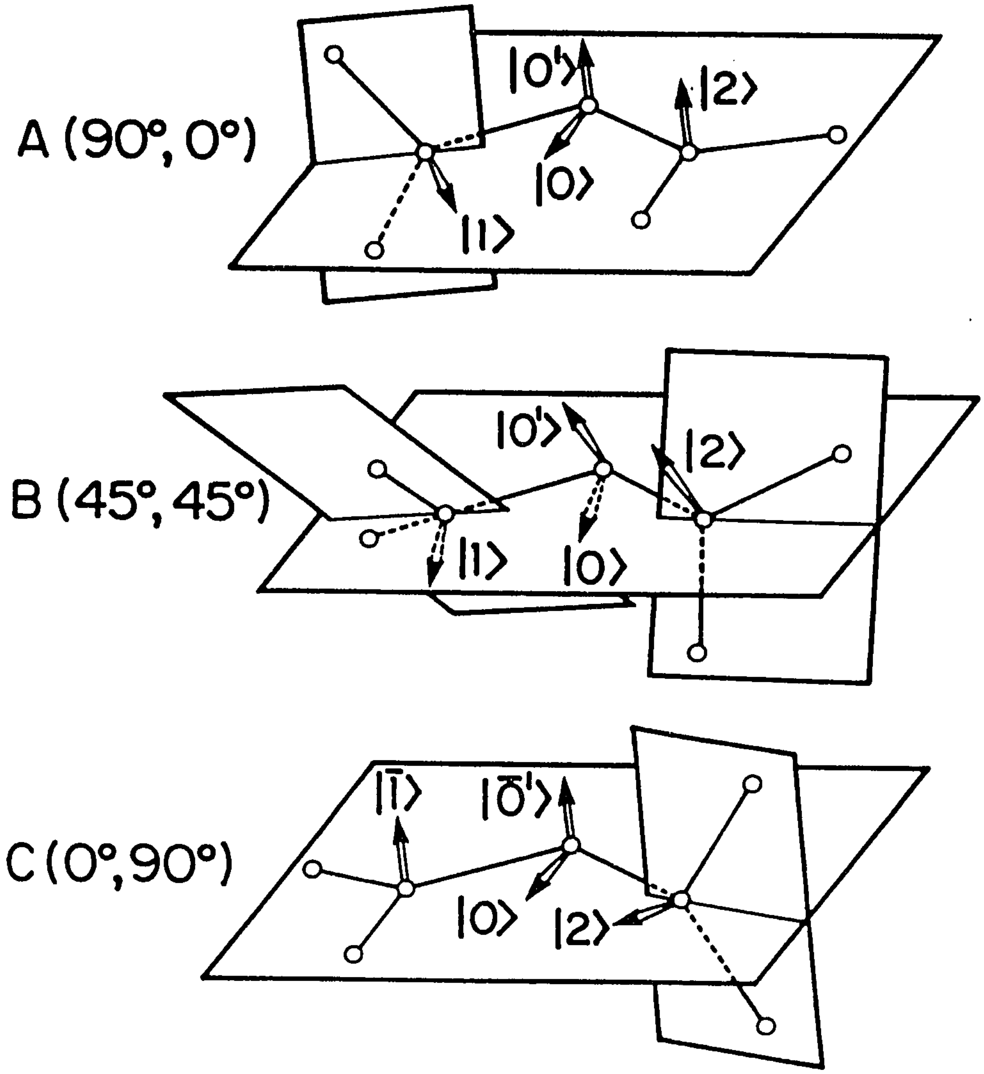

Figure 4.B.3. Positions of atoms and directions of quasiatomic reactive FORS MO's in the valley $\delta_1+\delta_2=90^\circ$ for $\Phi=100^\circ$. Direction of reactive orbitals indicated by arrows representing unit vectors. Dotted lines imply objects behind or below the CCC or CHH planes. Numbers next to A, B, C indicate (δ_1, δ_2). In Figure 4C, the labels |0'>, |1> indicate that these orbitals point in directions opposite to those of the arrows

($\delta_1 = \delta_2 = 45^\circ$)

The intermediate geometry $\delta_1 = \delta_2 = 45^\circ$, which has C_2 symmetry is shown in Figure 4.B.3B. Here the localization was performed simultaneously on all four reaction orbitals. The quasiatomic FORS MO's on the central atom are chosen as two equivalent hybrid-type orbitals rather than σ and π. Nonetheless we still denote them as |0> and |0'>. The directions of the quasi-atomic FORS MOs are again indicated by unit vectors in Figure 4.B.3B. The geometry of Figure 4.B.4B can be imagined to result from that of Figure 4.B.4A as follows: The right-hand CH_2 group rotates in such a manner that orbital |2> tilts towards the viewer and the CH_2 group on the left rotates so that orbital |1> tilts its head below the CCC plane. Simultaneously, the orbitals |0> and |0'> on the central carbon rigidly rotate together in such a manner that |0'> tilts towards the viewer and |0> tilts below the CCC plane. A remarkable result is that the two unit vectors marking the directions of |2> and |0'> as well as the bond vector C_0C_2 almost lie in one plane. In fact the plane spanned by |2> and C_2C_0 forms an angle of 2° with the plane spanned by |0'> and C_0C_2. We therefore choose the plane halfway in between these two planes for drawing the contours of the quasi-atomic FORS MO's |0'> and |2>. They are shown in Figure 4.B.5A. The situation is entirely analogous for the orbitals |1> and |0>. The contours for these orbitals are shown in Figure 4.B.5B. It is apparent that both orbital pairs exhibit a sizable overlap so that bonding interactions can develop between the partners of each pair. As before, the orbitals |0> and |0'> are given by bold contours.

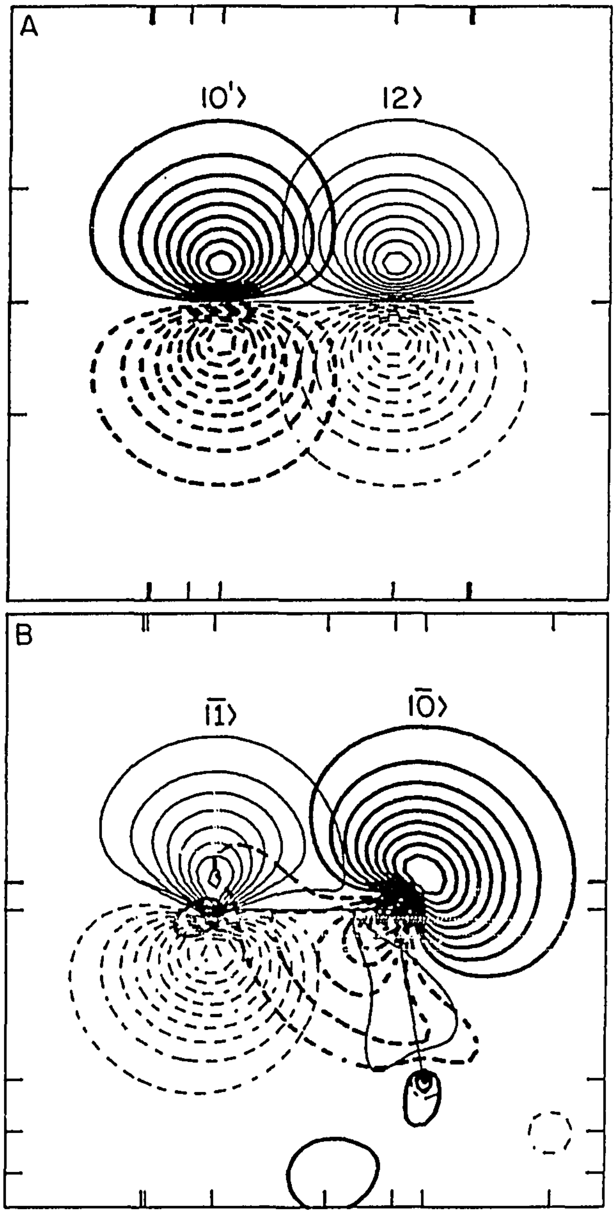

FIgure 4.B.4. Quasiatomic reactive FORS MOs for $\Phi=100^\circ$ and $(\delta_1,\delta_2)=(90^\circ,0^\circ)$. A: Drawing plane perpendicular to CCC plane, solid lines = positive, dashed lines = negative. B: Drawing plane in CCC plane, dashed lines = positive, solid lines = negative

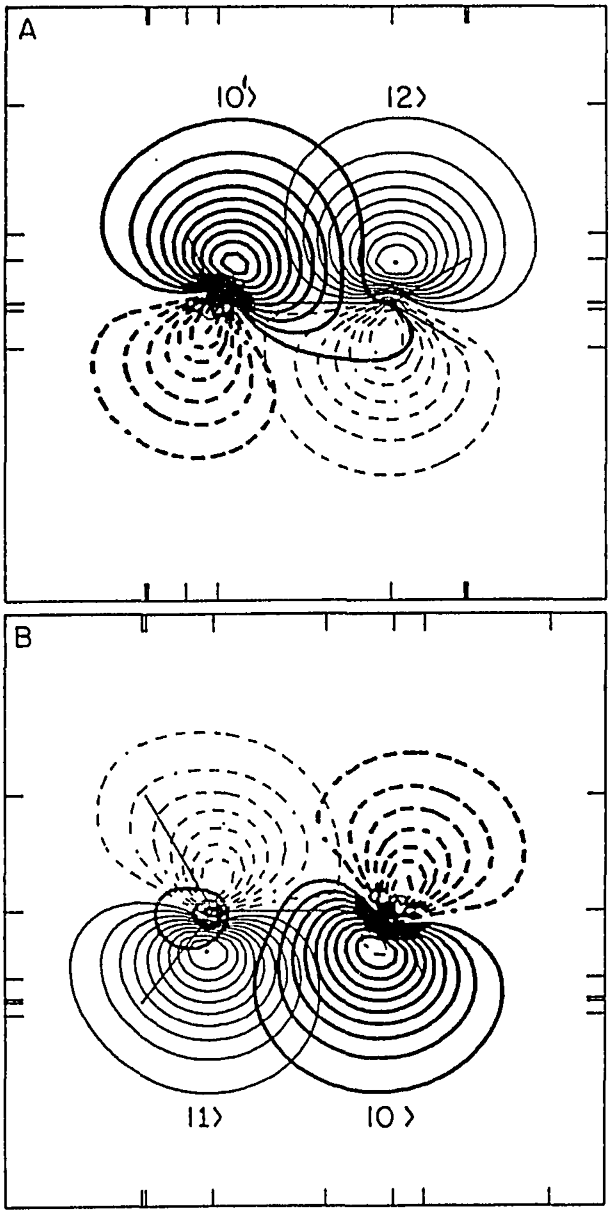

Figure 4.B.5. Quasiatomic reactive FORS MOs for $\Phi = 100°$ and $(\delta_1, \delta_2) = (45°, 45°)$. For explanation of drawing planes see text. Solid lines - positive, dashed lines - negative

$(\delta_1,\delta_2)=(0^\circ, 90^\circ)$

The positions of the atoms for the geometry $(\delta_1=0^\circ,\ \delta_2=90^\circ)$ are shown in Figure 4.B.3C. The directions of the quasiatomic FORS MO's are again indicated by unit vectors. The geometry of Figure 4.B.4C can be imagined to result from that of Figure 4.B.4B by continuing the rotations which led from 4.B.4A to 4.B.4B. Thereby orbitals |2> and |0'> should end up lying in the CCC plane whereas orbitals |1> and |0'> should end up perpendicular to the CCC plane pointing below that plane. In Figure 4.B.4C, we have however exchanged the labelling for the orbitals |0>, |0'> so that as was the case for $(\delta_1=90^\circ,\ \delta_2=0^\circ)$, |0> denotes again the in-plane orbital and |0'> denotes again the perpendicular orbital. Hence |0> of Figure 4.B.4B rotates into |0'> of Figure 4.B.4C and |0'> of Figure 4.B.4B rotates into |0> of Figure 4.B.4C. (Note also that the arrows drawn correspond to the orbitals -|1> and -|0'>, pointing upward, and are therefore labelled as |1>=-|1> and |0>=-|0'>). It is apparent that the roles of the orbitals |1> and |2> are now reversed in that the arrangement is favorable for a π-bond between |1> and |0'>, perpendicular to the CCC plane, while a weaker π-bond will be formed between |2> and |0> in the CCC plane.

5.2. Analysis for $(\delta_1,\delta_2)=(90^\circ\ 0^\circ)$ and $(\delta_1,\delta_2)=(0^\circ\ 90^\circ)$

Population and Bond-order Analysis

The density matrices in terms of these quasi-atomic orbitals are given in Table 4.B.11A and C. The occupation numbers of all four orbitals |0>, |0'>, |1>, |2> are close to one. In the case $(\delta_1,\delta_2)=(90^\circ,0^\circ)$ of Table 4.B.11A, positive bond orders exist for the orbital pair |0>, |1> and for the orbital pair |0'>, |2>. The fact that bonding can occur in both of

Table 4.B.11. Occupation numbers and bond orders of quasi-atomic orbitals along the isoenergetic valley for $\phi=100°$

A. Density matrix coefficients p_{ij} for $(\delta_1,\delta_2)=(90°,0°)$

	|0>	|0'>	|1>	|2>
|0>	1.06711	0	0.68621	0
|0'>	0	0.96612	0	0.84087
|1>	0.68621	0	0.93259	0
|2>	0	0.84087	0	1.03421

B. Density matrix coefficients p_{ij} for $(\delta_1,\delta_2)=(45°,45°)$

	|0>	|0'>	|1>	|2>
|0>	1.02020	0.11118	0.74928	-0.03815
|0'>	0.11118	1.02020	-0.03815	0.74928
|1>	0.74928	-0.03815	0.97981	-0.07665
|2>	-0.03815	0.74928	-0.07665	0.97981

C. Density matrix coefficients p_{ij} for $(\delta_1,\delta_2)=(0°,90°)$

	|0>	|0'>	|1>	|2>
|0>	1.06711	0	0	0.68621
|0'>	0	0.96612	0.84087	0
|1>	0	0.84087	1.03421	0
|2>	0.68621	0	0	0.93259

these pairs accounts for almost an entire electron having been promoted from the σ orbital $|0\rangle$ to the π orbital $|0'\rangle$ at the central carbon. It is however apparent, that the electron attraction power of $|0\rangle$ is still larger than that of $|0'\rangle$ because, taking a unit occupation of all four orbitals as reference, a charge of 0.068 electrons has moved from $|1\rangle$ to $|0\rangle$ whereas a charge of 0.034 has moved in the opposite direction, viz. from $|0'\rangle$ to $|2\rangle$. In total, a charge in the amount of 0.034 electron has been transferred to the central carbon. The bond $|0\rangle$-$|1\rangle$ has a considerably weaker bond order than the bond $|0'\rangle$-$|2\rangle$, as we expected from the overlaps inferred from Figure 4.B.4. The roles of the orbitals $|1\rangle$ and $|2\rangle$ are manifestly reversed in the density matrix for the geometry $(\delta_1,\delta_2)=(0°,90°)$ shown in Figure 4.B.3C.

The expansions of the natural FORS MO's in terms of the quasiatomic FORS MO's are listed in Table 4.B.12A for $(\delta_1,\delta_2)=(90°,0°)$ and illuminate the foregoing conclusions from a somewhat different angle. It is apparent that there exists one bonding MO $|01b\rangle$ between the quasi-atomic orbitals $|0\rangle$ and $|1\rangle$ (first column) and another another bonding MO $|0'2b\rangle$ between the quasi-atomic orbitals $|0'\rangle$ and $|2\rangle$ (third column). To each of them there exists a correlating orbital (columns two and four) and each correlated bond embodies exactly two electrons. In agreement with the preceding charge transfer observation, the bond involving $|0\rangle$ is polarized towards C_0 whereas the bond involving $|0'\rangle$ is polarized away from C_0 towards C_2. Furthermore the relative occupations of the bonding and antibonding orbitals imply that the in-plane bond involving $|0\rangle$ is weaker than the out-of-plane bond involving $|0'\rangle$. Table 4.B.12C shows the analogous results for $(\delta_1,\delta_2)=(0°,90°)$ with the roles of $|1\rangle$ and $|2\rangle$

Table 4.B.12. Natural and chemically localized FORS MO's for $\phi=100°$

A. $\delta_1=90°$, $\delta_2=0°$:

	|01b>	|01c>	|0'2b>	|0'2c>
|0>	0.740793	-0.671733	0	0
|0'>	0	0	0.692656	0.721268
|1>	0.671733	0.740793	0	0
|2>	0	0	0.721268	-0.692656
Nn	1.689348	0.310352	1.841724	0.158606
Sum	1.99970		2.00033	

B. $\delta_1=\delta_2=45°$, Natural MO's:

	|A-bond>	|A-corr>	|B-bond>	|B-corr>
|0>	0.538153	-0.458684	-0.476127	0.522784
|0'>	0.538153	-0.458684	0.476127	-0.522784
|1>	0.458684	0.538153	-0.522784	-0.476127
|2>	0.458684	0.538153	0.522784	0.476127
Nn	1.737490	0.297050	1.773617	0.191863
Sum	2.03454		1.965480	

Table 4.B.12. (continued)

B'. $\delta_1=\delta_2=45°$; Chemically localized MO's:

	|01b>	|01c>	|0'2b>	|0'2c>
|0>	0.717204	-0.694003	0.043859	0.045326
|0'>	0.043859	0.045326	0.717204	-0.694003
|1>	0.694003	0.717204	-0.045326	0.043859
|2>	-0.045326	0.043859	0.694003	0.717204
Nn	1.755554	0.244457	1.755554	0.244457
Sum	2.000011		2.000011	

C. $\delta_1=0°$; $\delta_2=90°$:

	|02b>	|02c>	|0'1b>	|0'1c>
|0>	0.740793	-0.671733	0	0
|0'>	0	0	0.692656	0.721268
|1>	0	0	0.721268	-0.692656
|2>	0.671733	0.740793	0	0
Nn	1.689348	0.310352	1.841724	0.158606
Sum	1.99970		2.00033	

Table 4.B.13. FORS population analysis for $\phi = 100^\circ$

		Natural FORS MO's					
A.(90°,0°)		$\vert 01b\rangle$	$\vert 01c\rangle$	$\vert 0'2b\rangle$	$\vert 0'2c\rangle$	P_{ii}	Atoms
Quasi-	$\vert 0\rangle$	0.92707	0.14004	0	0	1.06711	2.03323
atomic	$\vert 0'\rangle$	0	0	0.88361	0.08251	0.96612	
FORS	$\vert 1\rangle$	0.76228	0.17031	0	0	0.93259	1.96680
MO's	$\vert 2\rangle$	0	0	0.95812	0.07609	1.03421	
	N_n	1.68935	0.31035	1.84172	0.15861		
	Sum	1.99970		2.00033		4	4

		Natural FORS MO's					
B.(45°,45°)		$\vert A\text{-bond}\rangle$	$\vert A\text{-corr}\rangle$	$\vert B\text{-bond}\rangle$	$\vert B\text{-corr}\rangle$	P_{ii}	Atoms
Quasi-	$\vert 0\rangle$	0.50319	0.06250	0.40207	0.05244	1.02020	2.04040
atomic	$\vert 0'\rangle$	0.50319	0.06250	0.40207	0.05244	1.02020	
FORS	$\vert 1\rangle$	0.36555	0.08603	0.48474	0.04349	0.97981	1.95962
MO's	$\vert 2\rangle$	0.36555	0.08603	0.48474	0.04349	0.97981	
	N_n	1.73749	0.29705	1.77362	0.19186		
	Sum	2.03454		1.96548		4	4

Table 4.B.13. (continued)

B'.(45°,45°)		|01b>	|01c>	|0'2b>	|0'2c>	|b>|b'>	|c>|c'>	P_{ii}	Atoms
		Chemically localized FORS MO's							
Quasi-atomic FORS MO's	|0>	0.90303	0.11774	0.00338	0.00050	-0.00059	-0.00165	1.02241	2.04481
	|0'>	0.00338	0.00050	0.90303	0.11774	-0.00059	-0.00165	1.02241	
	|1>	0.84555	0.12574	0.00361	0.00047	0.00059	0.00165	0.97761	0.97761
	|2>	0.00361	0.00047	0.84555	0.12574	0.00059	0.00165	0.97761	0.97761
	Nn	1.75555	0.24446	1.75555	0.24446	0	0		
	Sum	2.00001		2.00001				4	4

C.(0°,90°)		|02b>	|02c>	|0'1b>	|0'1c>	P_{ii}	Atoms
		Natural FORS MO's					
Quasi-atomic FORS MO's	|0>	0.92707	0.14004	0	0	1.06711	2.03323
	|0'>	0	0	0.88361	0.08251	0.96612	
	|1>	0	0	0.95812	0.07609	1.03421	1.96680
	|2>	0.76228	0.17031	0	0	0.93259	
	N_n	1.68935	0.31035	1.84172	0.15861		
	Sum	1.99970		2.00033		4	4

Table 4.B.14. FORS Bond Order Analysis for ϕ=100°

		Natural FORS MO's				
A. (90°,0°)		|01b>	|01c>	|0'2b>	|0'2c>	p_{ii}
Quasi-atomic FORS MO pairs	(00')	0	0	0	0	0
	(01)	0.84065	-0.15444	0	0	0.68621
	(02)	0	0	0	0	0
	(0'1)	0	0	0	0	0
	(0'2)	0	0	0.92011	-0.07924	0.84087
	(12)	0	0	0	0	0

		Natural FORS MO's				
B. (45°,45°)		|A-bond>	|A-corr>	|B-bond>	|B-corr>	p_{ii}
Quasi-atomic FORS MO pairs	(00')	0.50319	0.06250	-0.40207	-0.05244	0.11118
	(01)	0.42889	-0.07332	0.44147	-0.04776	0.74928
	(02)	0.42889	-0.07332	-0.44147	0.04776	-0.03814
	(0'1)	0.42889	-0.07332	-0.44147	0.04776	-0.03814
	(0'2)	0.42889	-0.07332	0.44147	-0.04776	0.74928
	(12)	0.36555	0.08603	-0.48474	-0.04349	-0.07665

Table 4.B.14. (continued)

		Chemically localized FORS MO's						
B'.(45°,45°)		$\vert 01b\rangle$	$\vert 01c\rangle$	$\vert 0'2b\rangle$	$\vert 0'2c\rangle$	$\vert b\rangle\vert b'\rangle$	$\vert c\rangle\vert c'\rangle$	p_{ii}
Quasi-atomic FORS MO pairs	(00')	0.05522	-0.00769	0.05522	-0.00769	-0.00960	0.02544	0.11090
	(01)	0.87381	-0.12168	-0.00349	0.00049	0.00004	0.00011	0.74928
	(02)	-0.05707	-0.00744	0.05344	0.00795	-0.00922	-0.02607	-0.03841
	(0'1)	0.05344	0.00795	-0.05707	-0.00744	-0.00922	-0.02607	-0.03841
	(0'2)	-0.00349	0.00049	0.87381	-0.12168	0.00004	0.00011	0.74928
	(12)	-0.05522	0.00077	-0.05522	0.00769	-0.00900	0.02715	-0.08383

		Natural FORS MO's				
C. (0°,90°)		$\vert 02b\rangle$	$\vert 02c\rangle$	$\vert 0'1b\rangle$	$\vert 0'1c\rangle$	p_{ii}
Quasi-atomic FORS MO pairs	(00')	0	0	0	0	0
	(01)	0	0	0	0	0
	(02)	0.84065	-0.15444	0	0	0.68621
	(0'1)	0	0	0.92011	-0.07924	0.84087
	(0'2)	0	0	0	0	0
	(12)	0	0	0	0	0

Table 4.B.15. Expansion coefficients of wavefunctions for three species in the isoenergetic valley for ϕ=100° in terms of configurations generated from quasiatomic FORS MOs

SAAPS		90°,0°	0°,90°	45°,45°
$C_0^0C_1^0C_2^0$:	$\|0^2 12\rangle$	-0.006216	0.006216	-0.073841
	$\|0'^2 12\rangle$	0.002979	-0.002979	-0.073841
	$\|00'12S\rangle$	-0.286549	-0.286549	-0.327543
	$\|00'12T\rangle$	0.752690	-0.752690	0.745284
$C_1^-C_2^+$:	$\|0^2 1^2\rangle$	-0.005821	0.152381	-0.010228
	$\|0'^2 1^2\rangle$	0.080091	-0.014741	0.105977
	$\|00'1^2\rangle$	-0.003956	-0.003289	0.021182
$C_1^+C_2^-$:	$\|0^2 2^2\rangle$	0.152381	-0.005821	0.105977
	$\|0'^2 2^2\rangle$	-0.014741	0.080091	-0.010228
	$\|00'2^2\rangle$	0.003289	0.003956	0.021182
$C_0^-C_1^+$:	$\|0^2 0'2\rangle$	0.279601	-0.004490	0.284827
	$\|0'^2 02\rangle$	-0.001292	0.299058	-0.008997
$C_0^+C_1^-$:	$\|021^2\rangle$	0.001785	0.332512	0.064810
	$\|0'21^2\rangle$	0.177873	0.002625	0.246137
$C_0^-C_2^+$:	$\|0^2 0'1\rangle$	0.004490	0.279601	-0.008997
	$\|0'^2 01\rangle$	0.299058	0.001292	0.284827
$C_0^+C_2^-$:	$\|012^2\rangle$	0.332512	-0.001785	0.246137
	$\|0'12^2\rangle$	-0.002625	0.177873	0.064810
$C_0^{2-}C_1^+C_2^-$:	$\|0^2 0'^2\rangle$	0.087876	0.087876	0.085405
$C_0^{2+}C_1^-C_2^-$:	$\|1^2 2^2\rangle$	0.061851	0.061851	0.059333

reversed.

The integrated and compacted representation in form of the population and bond order analysis, given in Tables 4.B.13A, 13C, 14A and 14C confirms these conclusions.

Configurational Analysis

Table 4.B.15 lists the expansion coefficients of the FORS wavefunctions in terms of the configurations formed from quasiatomic FORS MO's for the geometries under discussion. The first column applies to the case $(\delta_1,\delta_2)=(90^\circ,0^\circ)$. Here the normalized neutral base function without electron sharing is

$$\Psi_B = 0.934|00'12T\rangle - 0.355|00'12S\rangle$$

and it has a weight of 65% in the total wavefunction. This expression for Ψ_B shows that for a CCC opening angle of 100° the orbitals $|0\rangle$ and $|0'\rangle$ on the central carbon are energetically competitive.

As mentioned before, the predominance of the triplet coupled term (T) over the singlet coupled term (S) is presumably due to an approximate "local Hund's rule". As emphasised above, this base function yields no covalent bonding, in the present case no π-bonding between C_0 and C_1 or C_2. Such bonding is the result of electron sharing resulting from the admixture of SAAPs providing for the appropriate electron jumps. Indeed the SAAPs with the larger coefficients in the first column of Table 4.B.15 provide just the right terms:

For electron sharing between $|0'\rangle$ and $|2\rangle$:

$$R_{0'\to 2}\Psi_B = |2^2 01>, \qquad R_{2\to 0'}\Psi_B = |0'^2 01>,$$

and for electron sharing between |0> and |1>:

$$R_{0\to 1}\Psi_B = |1^2 0'2>, \qquad R_{1\to 0}\Psi_B = |0^2 0'2>.$$

All other SAAPs contribute very little, except for $|0^2 2^2>$ which can be understood as $R_{1\to 0}R_{0'\to 2}\Psi_B$. From the magnitude of the coefficients, it is also seen that, in accordance with our expectations, the interaction between |0'> and |2> is stronger than that between |0> and |1>.

The case $(\delta_1,\delta_2)=(0°,90°)$ is shown in the second column. It is apparent that this column of coefficients can be obtained from the first column by (i) changing the sign of |0'> and |2>, (ii) interchanging |1> and |2>, (iii) taking into account that |00'21T> = -|00'12T>.

5.3. Analysis for $\delta_1=\delta_2=45°$

Population and Bond Order Analysis

The density matrix for this case is listed in Table 4.B.11B. It is apparent that there exists perfect symmetry with respect to the end carbons. Orbital |0> has a bonding interaction with orbital |1> and a slight non-bonded repulsion with respect to orbital |2>. Conversely orbital |0'> has a bonding interaction with orbital |2> and a slight non-bonded repulsion with respect to orbital |1>. An electronic charge in the amount of 0.020 electrons is transferred from orbital |1> to orbital |0> and equally from orbital |2> to orbital |0'>, giving the central carbon an extra electronic charge of 0.040 quite similar to the total charge transfer of 0.034 to the central carbon for the cases $(\delta_1,\delta_2)=(90°,0°)$ and $(0°,90°)$. It is also noteworthy that the two identical bond orders in this case, viz. 0.75, are approximately equal to the average of the two different bond orders for the previously considered case $(\delta_1=90°,\ \delta_2=0°)$:

$$(0.8407 + 0.6854)/2 \approx (0.8407\ K\ 0.6854)^{1/2} \approx 0.76.$$

This similarity fits in well with the near iso-energeticity of the three geometries.

Since the molecule has C_2 symmetry in this conformation, the natural orbitals have A and B symmetry. Their expansion in terms of the quasiatomic orbitals, displayed in Table 4.B.12C, shows that, because of the symmetry adaption, they mix up the two bonds. Greater clarity is therefore obtained by going over to the chemically localized FORS MO's discussed as the end of Section 4.B.2.2. In the present case, the separate localizations of the strongly and the weakly occupied natural orbitals $|\text{A-bond}\rangle$ and $|\text{B-bond}\rangle$ is readily accomplished by inspection, viz.,

$$|01b\rangle = (|\text{A-bond}\rangle - |\text{B-bond}\rangle) / \sqrt{2},$$

$$|01c\rangle = (|\text{A-corr}\rangle - |\text{B-corr}\rangle) / \sqrt{2},$$

$$|0'2b\rangle = (|\text{A-bond}\rangle + |\text{B-bond}\rangle) / \sqrt{2},$$

$$|0'2c\rangle = (|\text{A-corr}\rangle + |\text{B-corr}\rangle) / \sqrt{2},$$

From their expansions in terms of the quasiatomic orbitals, listed in Table 4.B.12B', it is apparent that the first two describe bonding and correlation between $|0\rangle$ and $|1\rangle$ whereas the last two do so between $|0'\rangle$ and

Table 4.B.16. Density matrix in terms of chemically adapted orbitals for ϕ=100° and δ_1=δ_2=45°

	|01b>	|01c>	|0'2b>	|0'2c>
|01b>	1.75555	0	-0.01860	0
|01c>	0	0.24446	0	0.05259
|0'2b>	-0.01860	0	1.75555	0
|0'2c>	0	0.05259	0	0.24446

$|2\rangle$. The density matrix between these orbitals, given by Table 4.B.16, shows that they are still near-natural. Tables 4.B.13B' and 4.B.14B' display the population and bond order analysis in terms of these chemically adapted orbitals. Since they are not exactly natural orbitals, small crossterms must be listed for them. These tables confirm our conclusions regarding populations and bonding.

Configurational Analysis

These conclusions are also reflected in the expansion coefficients for the wavefunction which are listed in the last column of Table 4.B.15. In this case the neutral base function without electron sharing is

$$\Psi_B = 0.915|00'12T\rangle - 0.402|00'12S\rangle$$

and it represents 66% of the wavefunction. It is readily seen that the remaining major contributors to this wavefunction are SAAPs which establish electron sharing between the orbitals $|0\rangle$ and $|2\rangle$ and between the orbitals $|0'\rangle$ and $|1\rangle$, namely

$$R_{0\to1}\Psi_B = |1^2 0'2\rangle, \qquad R_{1\to0}\Psi_B = |0^2 0'2\rangle$$
$$R_{0'\to2}\Psi_B = |2^2 01\rangle, \qquad R_{2\to0'}\Psi_B = |0'^2 01\rangle$$

and to a lesser extent

$$R_{0'\to2}R_{1\to0}\Psi_B = |0^2 2^2\rangle, \qquad R_{2\to0'}R_{0\to1}\Psi_B = |0'^2 1^2\rangle.$$

It is apparent that the CI expansions of all three columns are very similar.

In summary, we infer that the binding energy generated by each of the twisted π-bonds in the (45°,45°) geometry is about the average of the binding energies of the two different π-bonds found for the (0°,90°) and the (90°,0°) geometries and that this accounts for the isoenergetic shelf which corresponds to the free synchronized CH_2 rotations.

6. Population and Configuration Analysis for the Extended Basis Set Calculations

The analyses in Sections 4.B.3 through 4.B.5 were based on the calculations performed with the STO-3G basis set. Since they were carried out with a minimal basis set, the question arises whether the interpretability in terms of atomic building blocks is a consequence of this restriction. In order to show that the atomic interpretability is in fact basis-set independent, we present in this section analogous analyses of calculations made with considerably higher accuracy. While we maintain th 20 dimensional FORS space spanned by four reactive orbitals, we expand the molecular orbitals in terms of an extended contracted basis with polarization functions, viz., the Dunning-Hay basis (9s5p1d/3s2p1d) for carbon and (4s/2s) for hydrogen. The details of these calculations and of the consequences for the energy surface are already discussed in Section 4.A.3. Here we report the results of the analyses for the reactant cyclopropylidene, the product allene, the ring opening transition state and the allene isomerization transition state.

6.1. Quasi-atomic Character of Localized MO's

The first question is whether it is possible to localize the four FORS molecular orbitals, obtained from the extended basis set calculations, sufficiently strongly so that they still have quasiatomic character. Rather than drawing more contour plots of localized molecular orbitals, we examine here a more quantitative measure of their atomic character, namely: the projection of each of these orbitals on the basis of the optimal five free-atom orbitals 1s, 2s, $2p_x$, $2p_y$ and $2p_z$ of the atom on which the quasiatomic MO is allegedly concentrated. If the orthonormal orbitals of that free atom are denoted by χ_1, χ_2, χ_3, χ_4, χ_5, then the projection of a quasiatomic molecular orbital ϕ is given by

$$proj(\phi) = \sqrt{\sum_{j=1}^{5} \langle \chi_j | \phi \rangle^2} \ .$$

The optimal free-atom orbitals of the carbon atom were determined by a two-configuration MCSCF calculation of the $^3P(m_l=0,\ m_s=1)$ groundstate wavefunction

$$c_1\ A(1s^2 2s^2 2p_x 2p_y\ ) + \ c_2\ A(1s^2 2p_z{}^2 2p_x 2p_z)$$

in the same contracted basis of the carbon atom which formed part of the basis for the molecular calculations (i.e. 9s5p1d/3s2p1d).

Table 4.B.17 lists the projections of each of the four quasiatomic molecular orbitals on the respective carbon free-atom basis at the four

Table 4.B.17. Projection of Quasiatomic FORS MO's onto their Respective Free-Atom Bases (Extended plus polarization basis calculation

Critical point	$\|0>$ on C_0	$\|0'>$ on C_0	$\|1>$ on C_1	$\|2>$ on C_2
Cyclopropylidene	0.9876	0.9590	0.9466	0.9466
Ring Opening Transition State	0.9777	0.9585	0.9666	0.9666
Allene	0.9534	0.9534	0.9855	0.9855
Allene isomerization TS	0.9327	0.9780	0.9850	0.9850

critical points of the energy surface. All of them lie between 0.93 and 0.99. It is clearly possible to find a transformation among the FORS molecular orbital such that all resulting molecular orbitals have strong quasiatomic character. In view of this result, it stands to reason that maximizing these projections would yield very similar orbitals.

It may be noted that the quasiatomic molecular orbitals are mutually orthogonal. It is obviously possible to determine non-orthogonal molecular orbitals with even greater atomic projections while still spanning the same space of FORS MO's.

6.2. Population Analysis

The population analysis is entirely determined by the population-bond-order matrices between the quasiatomic orbitals characterized by the projections of Table 4.B.17. These density matrices are listed in Table 4.B.18. They should be compared to the analogous matrices listed in Tables 4.B.1 and 4.B.6, as indicated in Table 4.B.18. It is evident that the results for the accurate calculation are very similar to those for the minimal-basis-set calculations. The quantitative differences are extremely small.

Alternatively, one can compare the spectral representations of these matrices, i.e., the natural orbitals and their occupation numbers. They are listed in Table 4.B.19 which corresponds to Tables 4.B.2 and 4.B.7. This comparison reconfirms the conclusion that the analyses of the minimal-basis-set calculations and of the more accurate calculations lead to essentially identical results.

Table 4.B.18. Population-Bond-Order Matrices For Extended-plus-Polarization Basis Calculations

Cyclopropylidene (compare Table 4.B.1A)

	$\lvert 0\rangle$	$\lvert 0'\rangle$	$\lvert 1\rangle$	$\lvert 2\rangle$
$\lvert 0\rangle$	1.92959	0	-0.00311	-0.00311
$\lvert 0'\rangle$	0	0.07041	0	0.97649
$\lvert 1\rangle$	-0.00311	0	1.00001	0.97649
$\lvert 2\rangle$	-0.00311	0	0.97649	1.00001

Ring Opening Transition State (compare Table 4.B.1B)

	$\lvert 0\rangle$	$\lvert 0'\rangle$	$\lvert 1\rangle$	$\lvert 2\rangle$
$\lvert 0\rangle$	1.96027	0	-0.00334	-0.00334
$\lvert 0'\rangle$	0	0.26250	0.42708	0.42708
$\lvert 1\rangle$	-0.00334	0.42708	0.88862	0.80832
$\lvert 2\rangle$	-0.00334	0.42708	0.80832	0.88862

Allene (compare Table 4.B.6A)

	$\lvert 0\rangle$	$\lvert 0'\rangle$	$\lvert 1\rangle$	$\lvert 2\rangle$
$\lvert 0\rangle$	0.95372	0	0.91900	0
$\lvert 0'\rangle$	0	0.95372	0	0.91900
$\lvert 1\rangle$	0.91900	0	1.04628	0
$\lvert 2\rangle$	0	0.91900	0	1.04628

Allene Isomerization Transition State (compare Table 4.B.6B)

	$\lvert 0\rangle$	$\lvert 0'\rangle$	$\lvert 1\rangle$	$\lvert 2\rangle$
$\lvert 0\rangle$	1	0	0	0
$\lvert 0'\rangle$	0	0.98321	0.62642	0.62642
$\lvert 1\rangle$	0	0.62642	1.00840	0.00840
$\lvert 2\rangle$	0	0.62642	0.00840	1.00840

Table 4.B.19. Natural Orbitals and Occupation Numbers for Extended-plus-Polarization Basis Calculations

Cyclopropylidene (compare to Table 4.B.2A)

	|1p>	|1pc>	|12b>	|12c>
|0>	0.99572	0	-0.09245	0
|0'>	0	1	0.70408	0
|1>	0.06537	0	0.70408	0.70711
|2>	0.06537	0	0.70408	-0.70711
N_n	1.92918	0.07041	1.97690	0.02352
Sum	1.99959		2.00042	

Ring Opening Transition State (compare to Table 4.B.2B)

	|1p>	|1pc>	|10'2b>	|10'2c>
|0>	0.99480	-0.00084	0.10182	0
|0'>	0.03412	0.93939	0.34115	0
|1>	-0.06784	-0.24243	0.66078	0.70711
|2>	-0.06784	-0.24243	0.66078	-0.70711
N_n	1.96073	0.04206	1.91692	0.08030
Sum	2.00279		1.99721	

Table 4.B.19. (continued)

Allene (compare to Table 4.B.7A)

	$\|01b\rangle$	$\|01c\rangle$	$\|0'2b\rangle$	$\|0'2c\rangle$
$\|0\rangle$	0.68910	0.72467	0	0
$\|0'\rangle$	0	0	0.68910	0.72467
$\|1\rangle$	0.72467	-0.68910	0	0
$\|2\rangle$	0	0	0.72467	-0.68910
N_n	1.92026	0.07984	1.92016	0.07984
Sum	2.00000		2.00000	

Allene Isomerization Transition State (compare to Table 4.B.7B)

	$\|1p\rangle$	$\|12n\rangle$	$\|10'2b\rangle$	$\|10'2c\rangle$
$\|0\rangle$	1	0	0	0
$\|0'\rangle$	0	0	0.70037	0.71378
$\|1\rangle$	0	0.70711	0.50472	-0.49524
$\|2\rangle$	0	-0.70711	0.50472	-0.49524
N_n	1.00000	1.00000	1.88605	0.11395
Sum	2.00000		2.00000	

6.3. Configurational Analysis

The expansions of the FORS wavefunctions in terms of the configurations generated by the quasiatomic FORS MO's are listed in Table 4.B.20. The analogous expansions for the minimal basis set calculations were given in Tables 4.B.5 and 4.B.10. As expected (in view of the population analysis), the simpler and the more accurate calculations also agree closely in the CI coefficients of the wavefunctions, so that all inferences reached in the earlier sections regarding the interpretation of the wavefunctions and the energy changes remain valid.

The quantitative results of Tables 4.B.17 to 4.B.20 show that the analysis in terms of quasiatomic orbitals is independent of the working orbital basis. We feel therefore justified to conclude that, in fact, it is independent of how the orbitals are expressed.

7. Summary and Conclusions

FORS wavefunctions (which are unambigously defined) yield molecule-intrinsic FORS MO's among which arbitrary non-singular transformations are permissible. This freedom can be used to localize these molecular orbitals.

The maximally localized FORS MO's are thus basis-set-independent, intrinsic orbitals of such wavefunctions.

These maximmaly localized FORS MO's have the character of slightly deformed free-atom SCF or MCSCF orbitals, i.e., they are quasiatomic MO's. They form an effective basis for rigorously and unambigously achieving the objective of Mulliken's population analysis. The expansion coefficients in

Table 4.B.20. Expansion coefficients for FORS wavefunctions determined with the Extended-plus-Polarization Basis in terms of configurations generated from Quasiatomic FORS MO's

SAAPS	Cyclopropylidene Reactant[a]	Ring Opening Trans. State[a]	Allene Product[b]	Allene Isomerization T.S.[b]
$\|0^{2}12>$	0.765408	0.740695	0	0
$\|0'^{2}12>$	-0.145899	-0.120286	0	0
$\|00'12S>$	0	0.006387	0.691221	0.698631
$\|00'12T>$	0	0	0.038554	-0.403355
$\|0^{2}1^{2}>$	0.435218	0.327408	-0.005663	0
$\|0'^{2}1^{2}>$	-0.083085	-0.050827	0.163483	0
$\|00'1^{2}>$	0	0.004634	0	0.114835
$\|0^{2}2^{2}>$	0.435218	0.327408	0.163483	0
$\|0'^{2}2^{2}>$	-0.083085	-0.050827	-0.005663	0
$\|00'2^{2}>$	0	0.004634	0	-0.114835
$\|0^{2}0'2>$	0	0.324581	0.299135	0
$\|0'^{2}02>$	0.007356	-0.002941	0	0.276610
$\|021^{2}>$	0.007614	0.012779	0	0.291393
$\|0'21^{2}>$	0	0.002704	0.350872	0
$\|0^{2}0'1>$	0	0.324581	0	0
$\|0'^{2}01>$	0.007356	-0.002941	0	0
$\|012^{2}>$	0.007614	0.012779	0.350872	-0.291393
$\|0'12^{2}>$	0	0.002704	0	0
$\|0^{2}0'^{2}>$	-0.001141	0.078708	0.121189	0
$\|1^{2}2^{2}>$	-0.001141	-0.000890	0.165338	0

[a]: Compare to Table 4.B.5 [b]: Compare to Table 4.B.10

terms of configurations generated by the quasiatomic MO's can be related to chemical bonding. Energy changes along paths on the potential energy surfaces governing the discussed reactions can be elucidated through analyses in terms of the quasiatomic FORS MO's. The conclusions obtained by such analyses are basis-set independent. In many cases, the analyses of minimal-basis-set calculations will be very similar to those of the corresponding extended basis set calculations. The essential difference between the two approximations is the difference in magnitude of the projection of the quasiatomic FORS MO's on the space of the free atom MCSCF orbitals. This projection is very large (above 90% in our case) for both types of calculations. For the intrinsic quasiatomic FORS MO's (which are better approximated by the extended basis calculations) the projections are however somewhat smaller than for the minimal-basis calculations. While these orbital adjustments of the intrinsic quasiatomic MO's are essential for insuring the chemical usefulness of the predicted energy changes, they do not significantly diminish the quasi-atomic character. It can therefore be concluded that very good molecular wavefunctions can usually be formed by superimposing configurations generated from orthogonal molecular orbitals which differ from the MCSCF orbitals of free atoms only by small deformations.

In the reported sequence of investigations, insight in the cyclopropylidene-allene ring-opening has been gained on the basis of the potential energy surface governing this reaction.

The global overall features of this surface as well as the specific topographies of its key regions have been established. The changes in molecular geometry along the reaction paths and the critical energy differences have been related to the electronic rearrangements through a bonding analysis in terms of intrinsic quasiatomic molecular orbitals.

In order to be able to deal with an energy surface of such an extent, the appropriate formulation and separation of primary and secondary internal coordinates is essential. The surface turned out to exhibit a variety of nontrivial features requiring specific analyses: a bifurcation near a transition state, a valley-ridge inflection point as well as a conical intersection on the steepest descent path, and an isoenergetic shelf corresponding to a synchronized free internal motion.

We believe that such a richiness of features is not peculiar to the surface considered here. Rather, this is the first extensive ab-initio exploration of a surface involving more than three atoms. A similar variety of features is probably fairly common among potential energy surfaces governing chemical reactions.

V. REFERENCES

Bevan P. L. T. and Johnson G. R. A., J. Chem. Soc. Far. Trans. I 69, 216 (1973).

Born M. and Oppenheimer J. R., Ann. Physik 84, 457 (1927).

Brown W., Bass A. M., Davis D. D. and Simmons J. D., Proc. Roy. Soc. A 312, 417 (1969).

Burton P. G., J. Chem. Phys. 71, 961 (1979).

Burton P. G. and Harvey M. D., Nature 226, 826 (1977).

Clementi E. in "Proceedings of the Robert A. Welch Foundation Conference on Chemical Research. XVI. Theoretical Chemistry", Robert A. Welch Foundation, Houston, 117 (1973).

Davidson J. A., Schiff H. I., Brown T. J. and Howard C. J., J. Chem. Phys. 69, 1216 (1978).

Dirac P. A. M., Proc. Roy. Soc. London A 123, 713-733 (1929).

Donovan R. J. and Husain D., Chem. Rev. 70, 493 (1970).

Dubrin J., MacKay C., Pandlow M. L. and Wolfgang R., J. Inorg. Nucl. Chem. 26, 2113 (1964).

Dunning Jr. T. H. and Hay P. J. in "Methods of Electronic Structure Theory", Vol. III, H. F. Schaefer. Ed., Plenum Press, New York, 1 (1977).

Dupuis M., Spangler D. and Wendoloski J. J., Nat. Resour. Comput. Chem. Software Cat. 1, Prog. # QG01 (GAMESS), (1980). A version of the original program heavily modified mainly by S. T. Elbert and M. W. Schmidt was used.

Dykstra C. E. and Schaefer III H. F. in "The Chemistry of Ketenes, Aldehydes and Related Compounds", edited by S. Patai (J. Wiley, Interscience, NY, 1980), p. 1 and references therein.

Edmiston C. and Ruedenberg K., Rev. Mod. Phys. 35, 457 (1963).

Elbert S. T., Cheung L. M. and Ruedenberg K., Nat. Resour. Comput. Chem. Software Cat. 1, Prog. No. QM01 (ALIS), (1980).

England W. B., Chem. Phys. Lett. 78, 607 (1981).

England W. B., Rosenberg B. J., Fortune P. J. and Wahl A. C., J. Chem. Phys. 65, 684 (1976).

England W., Salmon L. S., Ruedenberg K., Topics in Current Chemistry 23, 31

(1971) and papers referenced therein.

Feller D., Katriel J. and Davidson E. R., J. Chem. Phys. 73, 4517 (1980).

Harding L. B. and Goddard III W. A., J. Chem. Phys. 67, 2377 (1977).

Harding D. R., Weston Jr. R. E. and Flynn G. W., J. Chem. Phys. 88, 3590 (1988).

Hay P. J., Dunning Jr. T. H. and Goddard III W. A., Chem. Phys. Lett. 23, 457 (1973).

Hay P. J., Dunning Jr. T. H. and Goddard III W. A., J. Chem. Phys. 62, 3912 (1975).

Hay P. J. and Goddard III W. A., Chem. Phys. Lett. 14, 46 (1972).

Hayes E. F. and Pfeiffer G. V., J. Am. Chem. Soc. 90, 4773 (1968).

Herzberg G. in "Molecular Spectra and Molecular Structure: III.Electronic Structure of Polyatomic Molecules", D. Van Nostrand, New York, (1966); (a) p. 640; (b) ibid. p. 589.

Herzberg G. and Longuet-Higgins H. C., Discuss. Faraday Soc. 35, 77 (1963).

Hochanadel C. J., Ghormley J. A. and Boyle J. W., J. Chem. Phys. 48, 2416 (1968).

Hoytnik G. J., Chem. Phys. Lett. 34, 414 (1975).

Hund F., Z. Physik 40, 742 (1927).

Husain D. and Kirsch L. J., Trans. Faraday Soc. 67, 2886 (1971).

Husain D. and Young A. N., J. Chem. Soc. Faraday Trans. II 71, 525 (1975).

Illies A. J., McKee M. L. and Schlegel H. B., J. Phys. Chem. 91, 3489 (1987).

Jones R. O., J. Chem. Phys. 82, 325 (1985).

Kalström G., Engström S. and Jönsson B., Chem. Phys. Lett. 57, 390 (1978).

Knowles P. J., Rosmus P. and Werner H.-J., Chem. Phys. Lett. 146, 230 (1988).

Kombs L. L. and Lunell S., Int. J. Quant. Chem. XXIII, 465 (1983).

Krauss M. and Neumann D., Chem. Phys. Lett. 14, 26 (1972).

Landau L. D. and Lifshitz E., "Quantum Mechanics: Non Relativistic Theory", Addison-Wesley, Reading Mass., 2nd edition, 279-282 (1965).

Lathan W. A., Radom L., Hariharan P. C., Hehre W. J. and Pople J. A., Fortschr. Chem. Forsch. 40, 1, (1973).

Lee T. J., to be published (1990).

Longuet-Higgins H. C., Proc. Roy. Soc. London A 344, 147-156 (1975).

Löwdin P.O., Phys. Rev. 97, 1474, (1955).

Lucchese R. R. and Schaefer III H. F., J. Chem. Phys. 67, 848 (1977).

Mead C. A., J. Chem. Phys. 70, 2276 (1979).

Moore C. E., Ed., National Bureau of Standards, Circular 467, "Atomic Energy Levels", Vol. I-III, U.S. Goverment Printing Office, Washington, D.C. (1958).

Morokuma T. and George T. F., J. Chem. Phys. 59, 1959 (1973).

Moscardo F., Andarias R. and San-Fabian E., Int. J. Quant. Chem. 34, 375 (1988).

Mulliken R. S., (a) J. Chem. Phys. 23, 1833, 1841, 2338, 2343 (1955). (b) A review is given in Section II.E. of R. S. Mulliken and W. C. Ermler, Diatomic Molecules (Academic Press, 1977).

Murrell J. N., Sorbie K. S. and Varandas A. J. C., Mol. Phys. 32, 1359 (1976).

Naqvi K. R., Chem. Phys. Lett. 15, 634 (1972).

Naqvi K. R. and Brown W. B., Int. J. Quant. Chem. VI, 271-279 (1972).

Okabe H. in "Photochemistry of small molecules", J. Wiley and Sons, (1978).

Pacansky J., Wahlgren U. and Bagus P. S., J. Chem. Phys. 62, 2740 (1975).

Pariseau M. A., Suzuki I. and Overend J., J. Chem. Phys. 42, 2335 (1965).

Pauling L., "The Nature of Chemical Bond", Cornell Univ. Press, Ithaca, (1960).

Riley J. F. and Cahill R. W., J. Chem. Phys. 52, 3297, (1970).

Ruedenberg K. in "Proceedings of the 1978 NRCC Workshop on the Post Hartree-Fock and Configuration Interaction Methods", Report LBL 8233, UC4, CONF 780883, Lawrence Berkeley Laboratory, University of California, p.46.

Ruedenberg K., Schmidt M. W., Gilbert M. M. and Elbert S. T., Chem. Phys.

71, 41 (1982); ibid. 71, 51 (1982); ibid. 71, 65 (1982).

Ruedenberg K. and Sundberg K. R. in "Quantum Science" (J. L. Calais, O. Goscinski, J. Linderberg, Y. Ohrn, Eds., Plenum Press, N.Y., 1976), p.505.

Shevlin P. B. in "Reactive Intermediates", Vol. 1, R. A. Abramovitek Ed., Plenum, New York, 29 (1980).

Shih S., Buenker R. J. and Peyerimhoff S. D., Chem. Phys. Lett. 28, 463 (1974).

Shortridge R. G. and Lin M. C., J. Chem. Phys. 64, 4076 (1976).

Teller E., J. Phys. Chem. 41, 109 (1937).

Tully J. C., J. Chem. Phys. 62, 1893 (1975).

Valtazanos P., Elbert S. T., Xantheas S. and Ruedenberg K., Theor. Chim. Acta.

Valtazanos P. and Ruedenberg K., Theor. Chim. Acta 69, 281 (1986).

Von Neumann I. and Wigner E., Physik Z. 30, 467 (1929).

Von Rosenberg Jr. C. W. and Trainor D. W., J. Chem. Phys. 61, 2442 (1974).

Warner P., private communication (1988).

Werner H.-J. and Knowles P. J., J. Chem. Phys. 82, 5053 (1985); Chem. Phys. Lett. 115, 259 (1985).

Wigner E. and Whitmer E. E., Z. Phys. 51, 859 (1928).

Wilson Jr. C. W. and Hopper D. G., J. Chem. Phys. 74, 595 (1981).

Wright J. S., Can. J. Chem. 51, 139 (1973).

Xantheas S. S., Elbert S. T. and Ruedenberg K., Chem. Phys. Lett. 166. 39 (1990).

Xantheas S. and Ruedenberg K., Theor. Chim. Acta.

Zhu Y.-F. and Gordon R. G. to be published (1990).

VI. ACKNOWLEDGEMENTS

A number of people have contributed either directly or indirectly in the successful completion of this dissertation.

First and foremost Professor Dr. Klaus Ruedenberg whose continuous support and encouragement made this study possible. I would like to thank him for providing me with a friendly working environment in which he was always eager to answer my numerous questions and guide my research. I consider it my priviledge that he was willing to share his thoughts with me in numerous scientific discussions.

I would also like to thank Dr. Stephen T. Elbert for his willingness to share with me his expertise of computer programming and help me overcome the various computational difficulties I encountered.

The Soukoulis family have made my stay in Ames pleasant and my wife Annmari provided a loving and caring environment at home the last one year of my graduate studies. But it was the continuous support and care of my parents Efi and Stavros back in Greece that started this effort. As a small recognition of their help I dedicate this dissertation to them.